TECHNISCHE UNIVERSITÄT MÜNCHEN
Lehrstuhl für Physikalische Chemie

Circular Dichroism Investigations of Chiral Molecules in the Gas Phase with a Laser-Mass Spectrometer

Jörn Hendryk Thore Lepelmeier

Vollständiger Abdruck der von der Fakultät für Chemie der Technischen Universität München zur Erlangung des akademischen Grades eines

Doktors der Naturwissenschaften

genehmigten Dissertation.

Vorsitzender:	Prof. Dr. Sebastian Günther
Prüfer der Dissertation:	1. Prof. Dr. Ulrich K. Heiz
	2. apl. Prof. Dr. Christoph Haisch

Die Dissertation wurde am 21.11.2018 bei der Technischen Universität München eingereicht und durch die Fakultät für Chemie am 04.02.2019 angenommen.

„For-thí loke thow lovye,
As longe as thow durest;
For ís no science under sonne
So sovereyn for the soule."

– William Langland –

CREDIT: UNIVERSITY OF NOTTINGHAM[1]

„So long as you live,
see that you love,
For no science under the sun
can so heal the soul."

– modern translation by Terrence Tiller –

Table of Content

A. Abstract ..... - 1 -

1. Introduction ..... - 5 -

1.1. Chirality - A Fundamental Component of Life ..... - 6 -

1.2. Analyzing of Chiral Molecules ..... - 9 -

1.2.1. Optical Techniques ..... - 9 -

1.2.1.1. Polarization of Light ..... - 10 -

1.2.1.2. Optical Rotatory Dispersion (ORD) ..... - 14 -

1.2.1.3. Circular Dichroism (CD) ..... - 16 -

1.2.2. Methods Based on Interaction with Chiral Systems ..... - 20 -

1.3. Heterogeneous Asymmetric Catalysis ..... - 23 -

1.4. Circular Dichroism - Resonance-Enhanced Multiphoton Ionization - Mass Spectrometry ..... - 25 -

1.4.1. Measurement Principle ..... - 25 -

1.4.2. Previous Experimental Progress ..... - 28 -

1.4.3. Comparison between Quarter-Wave Plate and PhotoElastic Modulator (PEM) ..... - 33 -

2. Results ..... - 39 -

2.1. Mass-selected Circular Dichroism of Supersonic Beam-Cooled d_4-(R)-(+)-3-Methylcyclopentanone ..... - 39 -

2.1.1. Summary and Author Contribution ..... - 39 -

2.1.2. Discussion and Conclusion ..... - 49 -

2.2. Experimental and Data Analyzing Improvements ..... - 51 -

2.2.1. Combination of Supersonic Beam and Twin-Peak Technique ..... - 51 -

2.2.2. Automatic Single Laser Pulse Evaluation ..... - 54 -

2.3. Chiroptical Inversion for Isolated Vibronic Transitions of Supersonic Beam-Cooled Molecules ..... - 58 -

2.3.1. Summary and Author Contribution ..... - 58 -

2.3.2. Discussion and Conclusion ..... - 68 -

3. Outlook ..... - 71 -

B. Bibliography ..... - 74 -

C. Appendix ..... - 80 -

Acknowledgement: ..... - 93 -

A. Abstract

During the last decades, the importance of chiral molecules for the industry and thus the significance of enantio sensitive analyzing methods has grown rapidly. Especially in the food industry and pharmacy many enantioselective (asymmetric) synthesizing methods evolved with a high priority on preferably enantiopure products. In this regard, heterogeneous asymmetric catalysis seems to be a good way for the synthesis of chiral molecules in the near future. Depending on the product of interest, the catalyst enables high enantioselectivity during the synthesis, similar to the more common homogeneous asymmetric catalytic reactions. An advantage of heterogeneous compared to homogeneous catalytic reactions is the easier separation of reactants, catalyst and products. Therefore, the search for novel or improved heterogeneous asymmetric catalyst systems is of special interest for the industry. This increased the necessity for enantio sensitive analytic methods that allow for fast and precise in situ enantiomeric excess measurements of chiral product molecules often in the gas phase under vacuum conditions.

The Circular Dichroism - Resonance-enhanced Multiphoton Ionization with a Time Of Flight - Mass Spectrometer (CD-REMPI-MS) fulfills all criteria for such CD investigations in the gas phase. CD-REMPI-MS provides enantiosensitivity due to CD and a high wavelength selectivity due to the REMPI excitation process. The additional mass selectivity of the TOF-MS allows for chiral molecule analysis within mixtures of different chiral and achiral sample molecules without any previous sample preparation. Furthermore, the spectral resolution of CD-REMPI-MS can be improved by utilizing the supersonic beam-cooling technique, which enables CD investigations of single vibronic transitions. The measured anisotropy factors for those isolated vibrational modes could thereby vary significantly from each other and especially from results under room temperature conditions (effusive beam inlet system). The huge influence of single vibronic transitions on the anisotropy factor has been confirmed by CD investigations on d_4-(R)-(+)-3-Methylcyclopetanon and resulted in a first publication for this thesis.

The main motivation of this thesis was the experimental development of the CD-REMPI-MS technique as a precise and fast analyzing method for chiral molecules in the gas phase, e.g. for product analysis of heterogeneous asymmetric catalysis. To achieve this, the already existing experimental setup was modified to allow for a combination of the supersonic beam-cooling technique and the twin-peak method. In addition, new automatic single laser pulse evaluation programs were implemented, which led to a significant improvement of the experimental precision especially in combination with the advantages of the twin-peak method. The improved precision of the CD-REMPI-MS method allowed for CD measurements on isolated vibronic transitions of supersonic beam-cooled (R)-(+)-1-Phenylethanol, which is a

common asymmetric catalytic product. The effect of various vibrational modes on the anisotropy factor of (R)-(+)-1-Phenylethanol has thereby been proven and revealed the possibility of chiroptical inversion due to different vibrations within the same electronic transition. These results were summarized in a second publication during this thesis and give an outlook on the possibilities of future CD-REMPI-MS measurements.

A. Kurzzusammenfassung

Die Wichtigkeit chiraler Moleküle für die Industrie hat über die letzten Jahrzehnte stark zugenommen und dadurch auch die Bedeutung enantio-sensitiver Analysemethoden. Vor allem in der der Lebensmittel- und Pharmaindustrie wurden viele neue enantio-selektive (asymmetrische) Synthesen entwickelt mit dem Ziel besonders enantiomerenreiner Produktherstellung. In diesem Zusammenhang werden heterogene asymmetrische Katalysen in naher Zukunft eine gute Möglichkeit zur Synthese chiraler Moleküle bieten. Abhängig vom gewünschten Produkt kann die Nutzung eines Katalysators nämlich hohe Enantioselektivität bei der Synthese liefern, so wie es in bereits häufiger genutzten homogenen asymmetrischen Katalysen der Fall ist. Ein großer Vorteil der heterogenen Katalyse im Vergleich zur homogenen Variante ist dabei die wesentlich leichtere Trennung von Edukten, Katalysator und Produkten nach der Reaktion. Daher ist die Suche nach neuen oder verbesserten heterogenen asymmetrischen Katalysesystemen von besonderer Bedeutung für die Industrie. Dies wiederum erhöht den Bedarf nach enantio-sensitiven Analysemethoden, die es erlauben schnelle in situ Messungen des Enantiomerenüberschusses chiraler Produkte vor allem in der Gasphase unter Vakuumbedingungen durchzuführen.

Die Zirkular-Dichroismus sensitive resonanzverstärkte Mehrphotonenionisation mit einem Flugzeitmassenspektrometer (CD-REMPI-MS) erfüllt alle Kriterien für solche CD Untersuchungen in der Gasphase. CD-REMPI-MS bietet neben Enantiosensitivität durch die Nutzung des CD Effekts auch eine hohe Wellenlängenselektivität durch den REMPI Anregungsprozess. Die zusätzliche Massenselektivität des TOF-MS erlaubt sogar CD Analysen einer chiralen Molekülart in einem Gemisch aus verschiedenen chiralen und achiralen Molekülen ohne irgendeine vorherige Probenvorbereitung. Mit Hilfe eines Überschallstrahl Einlasssystems als Probenzufuhr können die zu untersuchenden Moleküle effektiv gekühlt und so die spektrale Auflösung von CD-REMPI-MS deutlich erhöht werden. Dadurch werden selbst CD Untersuchungen an separaten vibronischen Übergängen möglich. Die gemessenen Anisotropiefaktoren für solche isolierten vibronischen Übergänge können dabei stark voneinander und im Besonderen von Messungen unter Raumtemperaturbedingungen (effusiver Molekularstrahl) abweichen. Der große Einfluss solch einzelner vibronischer Übergänge auf den Anisotropiefaktor konnte bei CD Messungen an d_4-(R)-(+)-3-methylcyclopetanon bestätigt werden und die Resultate führten zur ersten Publikation, die Bestandteil dieser kumulativen Dissertation ist.

Die Hauptmotivation für diese Dissertation war die Weiterentwicklung der CD-REMPI-MS Methode für ihren Einsatz als präzise und schnelle Analysemethode für chirale Moleküle in der Gasphase, wie sie bei der Produktanalyse heterogener asymmetrischer Katalysen

vorkommen. Deshalb wurde der bereits existierende experimentelle Aufbau dahingehend modifiziert, dass er eine Kombination der Überschallstrahl Technik mit der Twin-Peak Methode erlaubt. Zusätzlich wurden neue automatische Programme zur Auswertung von einzelnen Laserpulsen implementiert und so die experimentelle Präzision vor allem in Kombination mit den Vorteilen der Twin-Peak Methode deutlich erhöht. Diese erhöhte Präzision der CD-REMPI-MS Technik erlaubte erste CD Messungen an separaten vibronischen Übergängen von (R)-(+)-1-phenylethanol, welches ein gutes Beispiel für ein chirales Produkt einer asymmetrischen Katalyse ist. Dabei konnte der Effekt verschiedener Vibrationsmoden auf den Anisotropiefaktor von (R)-(+)-1-phenylethanol bewiesen werden. Außerdem konnte erstmals eine chiroptische Inversion durch die Anregung verschiedene Vibrationen innerhalb eines elektronischen Übergangs gezeigt werden. Diese Resultate wurden innerhalb dieser Dissertation in einer zweiten Publikation zusammengefasst und bieten gleichzeitig einen Ausblick auf die zukünftigen Möglichkeiten von CD-REMPI-MS Messungen.

1. Introduction

The appearance of chirality in all size scales - from the rotation of spiral galaxies over the winding direction of snail houses and the helicity of DNA down to the handedness of photons - shows its importance for nature in general (see section 1.1). A system or structure is thereby defined as chiral, if a mirror image of it exists that cannot be brought into overlap with its origin by any translation or rotation. These two mirror images of a chiral system, which have the same components and structures but an opposite handedness, are called enantiomers. In smaller scales (e.g. molecular size) chirality becomes a significant property due to the difference in interactions of the different enantiomers of two chiral systems with each other. This aspect is especially interesting for biochemistry, from food industry till pharmacy, because many chiral systems exist within the human body. However, the total similar structure and thus the physical properties of the enantiomers of a chiral molecule does not allow standard analyzing methods to distinguish between them (see section 1.2). Beside their difference in interaction with other chiral systems, chiral molecules are optically active. Thus, enantiomers differ in their interaction with photons which leads to various optical analyzing methods dependent on the polarization of the used light and combinations with other techniques. Those combined techniques are optimized for certain situations, e.g. for specially prepared samples, high precision or measurement speed. In case of heterogeneous asymmetric catalytic reactions (see section 1.3) an ideal analyzing method for the chiral product molecules has to allow for fast and precise measurements in the gas phase under vacuum conditions. In addition, without the possibility of any sample preparation the technique has to be highly selective due to an expectable mixture of the chiral product of interest with other chiral or achiral educts and products. The Circular Dichroism – Resonance-Enhanced Multiphoton Ionization - Mass Spectrometry (CD-REMPI-MS) technique (see section 1.4) fulfills all necessary criteria for those purposes. Utilizing the absorption difference of circular polarized light (circular dichroism) from a pulsed laser system for a multiphoton absorption and ionization via a resonant intermediate state (Resonance-Enhanced Multiphoton Ionization) already provides enentio sensitivity and wavelength selectivity. The combination with a Time Of Flight - Mass Spectrometer (TOF-MS) additionally provides mass selectivity. Thus, CD-REMPI-MS allows for a high selectivity even within mixtures of molecules and enables precise measurements of chiral product molecules in the gas phase with an analyzing speed restriction dependent on the repetition rate of the used laser system.

1.1. Chirality - A Fundamental Component of Life

The fundamental motivation for the basic research and experimental developments presented in this thesis arises from the importance of chirality for life in general. “Chirality” derives from the Greek word “χειρ” [kheir] which means “hand” and already hints to the most common example for chirality itself. The left and right hand of a human body consist of the same components: four fingers plus a thumb, and the same amount of bones and muscles. However, they are asymmetric mirror images of each other that cannot be overlapped by any translation, rotation or reflection (on any plane inside of it).[2] Objects that fulfill this definition are “chiral”, while objects which can be superimposed onto their mirror image are called “achiral”. The human body already consists of other obvious parts like feet and ears that are chiral, but in nature chiral objects also exist in all other scales. Any object that contains a spiral or helix form like spiral galaxies, snail houses or screws are chiral due to their two possible rotation handedness. While in the case of spiral galaxies no significant asymmetry between the amount of left or right rotating galaxies can be assumed, human made chiral objects can exist generally as one form like standard clockwise orientated screws. But also in nature asymmetries between the two handedness of a chiral object are common especially for biochemical based structures. For example, garden snails have in general right-handed (dextral, clockwise) houses and the left-handed (sinistral, anticlockwise) form exists today only as a genetic mutation for about one in a million snails.[1] A reason for the rarity of left-handed garden snails arises from their opposite sided sex organs compared to their right-handed counterparts. Thus, reproduction is only possible for snails with mates of similar winded housing, and due to small asymmetries during snail evolution the already more dominant clockwise winding direction led over generations to a nearly extinction of the other. This quite obvious biological induced asymmetric evolution can also be seen as an example for the “survival of the fittest” argumentation by C. Darwin.[3]

In the case of molecules, chirality is a special form of stereoisomerism (molecules with identical chemical formula but different spatial configuration).[4] If the stereoisomers are two non-superimposable mirror images of each other, the molecule is chiral and the two stereoisomers are called enantiomers (with prefix D and L, mainly for amino acids and sugars, or R and S for other molecules). A surplus of one over the other enantiomer is an enantiomeric excess (ee), while a 1:1 mixture of both enantiomers is titled as racemate. The origins of molecular chirality can thereby be divided into three main groups. Inherent chirality of molecules is a two dimensional phenomenon and it derives on the one hand from two pairs of two different substituents that are arranged out-of-plane around a chiral axis, which can result in a helical macrostructure (axial chirality). On the other hand, inherent chirality can be found for out-of-plane substituents relative to a defined plane like a ring structure (planar chirality). However,

the largest group of chiral molecules has a stereogenic center, usually due to a carbon atom with four different substituents (point chirality). If a molecule has more than one stereogenic center, it is still chiral but a diastereomer. Thereby, the term enantiomer can only be used for a pair of two diastereomers which have an opposite handedness for all of their stereogenic centers.

A common and important example for point chirality are the amino acids. Comparable to the biological evolution of snails - due to the asymmetric biochemical evolution of those amino acids, which are fundamental for the existence of life itself, only one handedness (enantiomer) can naturally be found nowadays. The occurrence of only one enantiomer as special case of a very high enantiomeric excess is thereby titled as homochirality[5] (enantiopurity). The currently most probable hypothesis for the homochirality of natural amino acids, which mainly appear on earth as L-amino acids (left-handed), while the D-amino acids (right-handed) only occur in some bacterial envelopes,[6] is based on a small ee of several percent found for meteoritic L-amino acids.[7-8] This finding can be combined with the additional idea that enantiopurity of amino acids is advantageous for the formation of more complex molecules (e.g. proteins) due to a lower entropy barrier.[9] Thus, a small ee of one amino acid enantiomer leads to a slightly but growing preference of life forms based on it and those lifeforms produce more of the already preferred enantiomer. Under the assumption that the first amino acids on earth have their origin in impacts of meteorites with more L-amino acids, this ee at early stage of the earth history would have evolved over billions of years to the nowadays visible homochirality. Due to a favored L-amino acid-catalyzed production of D-sugars,[10] the homochirality of the amino acids also resulted in a homochirality for natural sugar molecules. This in turn induced during evolution of higher life forms that deoxyribonucleic acid (DNA) with 2-deoxy-D-ribose (a D-sugar) as backbone of the double helix exists solely as right-handed helical structure in case of the common A- and B-DNA, while Z-DNA solely exists as left-handed helix.[11]

Those are just examples of some chiral structures, but they emphasize the importance of chirality for life on earth due to the fact that the interaction of two different chiral molecules depends on their enantiomers. Like a left shoe solely fits to a left foot, one enantiomer of a chiral molecule could have a total different behavior than the other, if it interacts or reacts with another chiral structure or molecule. Thus, the homochirality of amino acids and sugars as the base of more complex biochemical molecules (e.g. proteins and enzymes) has huge consequences for our life. Nearly all human body systems, like receptor systems, are therefore also chiral and have different reactions with chiral molecules. For example, S-carvone gives caraway its taste, while R-carvone is part of spearmint,[12] and S-limonene smells like turpentine, while R-limonene has an orange flavor.[13] Such differences are important for food industry,

where nowadays many of those natural flavors are synthesized. However, these chiral-chiral molecule interactions are even more important for the pharma industry. While for example D-DOPA, which is not produced naturally in human body, can have a negative agranulocytosis (reduction of white blood cell amount) effect,[14] L-DOPA has a positive effect in the treatment of the Parkinson's disease.[15] Another example that gained notoriety due to the drug Contergan[16-18], that was in use around 1960, are the two enantiomers of thalidomide. The drug was sold based on the positive effect of R-thalidomide as sedative,[19] but at that time the impact of S-thalidomide was unknown. Therefore, the drug was a racemate of both enantiomers and S-thalidomide revealed its dramatic teratogenic effect unfortunately while it was already in use for pregnant women. This historical chapter of pharmacy showed the huge importance of enantiopure production and enentio-sensitive analytical methods especially for the pharma industry[14] but also for other biochemical fields in general.

1.2. Analyzing of Chiral Molecules

The analysis of diastereomers, which are not enantiomers of each other, is comparable to the analysis of achiral molecules due to the fact that they vary in their physical properties (e.g. polarity, melting and boiling point, etc.). Thus, conventional physical based techniques can be used to distinguish between (or separate) those molecules. In comparison, analyzing enantiomers (both stereoisomers and diastereomers) is more complicated because their same but mirrored spatial distribution of the identical constituents give them total similar physical properties. Therefore, methods which are based on those physical differences are non-enantio sensitive.

Already in 1811 (for crystals) and in 1815 (for liquids), long before the term chirality was first defined by W. T. Kelvin in 1894, respectively F. Arago and J.-B. Biot found out that some structures and chemicals can rotate the plane of polarized light.[2, 20-21] Based on this optical activity as a common property for all chiral molecules, the first enantio sensitive analyzing method was realized with polarimeters. For several decades this technique was the only possibility to distinguish between enantiomers until C. E. Dalgliesh invented in 1952 the chiral chromatography.[22] This was the first technique related to the varying interaction of two enantiomers of two different chiral structures, as already mentioned in the previous chapter. Nowadays, the most common used enantio selective analyzing method is based on these interactions, and realized with chiral columns as stationary phase for gas chromatography (GC)[23] or high-performance liquid chromatography (HPLC).[24] However, this method only allows for the separation of the enantiomers depending on the used chiral column. Therefore, a new combination of a chiral sample with a chiral column has to be previously characterized by techniques based on optical activity.

1.2.1. Optical Techniques

As already mentioned, optical analyzing methods for chiral molecules can be ascribed to the findings of optical activity by F. Arago for crystals (solid) and J.-B. Biot for liquids.[20-21] Chiral molecules have different refraction indices for left- and right-circular polarized light (circular birefringence). This leads to a different speed of light for these two polarizations of light and this effect is opposed for the two enantiomers. Due to the fact that linear polarized light can be seen as the superposition of a left- and right-circular polarized light component the circular birefringence results in a phase shift of them, which consequently rotates the plane of their superimposed linear light. Thereby, the rotation depends on the thickness of the sample as well as the used wavelength (dispersion), which is the fundament for optical rotary dispersion (ORD) techniques.

However, beside their different refraction indices chiral molecule have different extinction coefficients for left- and right-circular polarized light.[25] Thus, an enantiomer absorbs either more left- or more right-circular polarized light while the other enantiomer does the contrary. This effect is called circular dichroism (CD) and leads e.g. to an elliptical polarization of incident linear light after passing a chiral sample. At this point it should be mentioned that the strength of the measurable ORD and CD effect is always related to the ee of the sample.[26] While an enantiopure sample has a maximized ORD or CD effect, a racemic mixture has no optical activity at all due to the fact that the opposing effects of the two enantiomers cancel each other totally.

1.2.1.1. Polarization of Light

The wave-particle duality of matter was first postulated for light by A. Einstein in 1909 to explain theoretically the experimental observations of the photoelectric effect.[27] Thereby, he invented photons (light quants) as light particles with a quantified energy $h\nu$ related to the Planck constant h and the frequency ν. His postulation, based on Planck's hypothesis of energy quantification for radiation (1900), laid the fundament for the broad field of quantum mechanics.[28] Thus, in 1921 A. Einstein was awarded with the Nobel Prize for his theoretical work regarding the photoelectric effect and the resulting consequences for modern physics.[29]

The dual character of light as electromagnetic wave and particle is nowadays commonly known, as well as the properties of photons which are massless, uncharged and elementary particles that carry electromagnetic force interactions as gauge bosons with a spin (intrinsic angular momentum) of 1.[30] Their spin usually would give them as bosons three possible eigenvalues, but due to the fact that photons have no rest mass only the two eigenvalues $\pm\hbar$ persist.[31] These two spin eigenvalues represent two possible polarizations of the photon and define its helicity which is positive (right-handed), if the spin vector points in the propagation direction of the photon, or negative (left-handed), if it points in the contrary direction. Related to the terms of positive or negative helicity, the polarization of the photon is respectively defined as right- or left-circular as it describes a clockwise of counterclockwise rotation seen from the receiver point of view.

Other light polarizations than the fundamental two circular polarizations solely exist as a superposition of certain mixtures of left- and right-circular polarized photons. While elliptical polarization results from a mixture of different amounts of left- and right-circular polarized photons, linear polarization is a special case for a similar amount of both photon polarizations. However, even if the particle behavior of light shows that the two circular polarizations are the fundamental states of light polarization, the other polarization states become clearer if light is seen as an electromagnetic wave.

1.2. Analyzing of Chiral Molecules

As an electromagnetic wave light is defined by the Maxwell-Equations as a superposition of an electric field component $\vec{E}$ and a magnetic field component $\vec{B}$ which are perpendicular to each other and in phase.[32-33] They propagate with the speed of light c as transversal waves in a direction $\vec{k}$ perpendicular to both field vectors (see figure 1a). Due to the fact that $\vec{E}$ and $\vec{B}$ are always perpendicular and in phase, the wave function for a plane electromagnetic wave can be described by the electric field propagation alone

$$\vec{E} = \vec{E}_0 \cdot e^{i(\vec{k}\vec{r}-\omega t)} \quad [1]$$

with position vector $\vec{r}$, time t and the angular frequency ω which is related to the frequency f or the wavelength λ of the light by

$$\omega = 2\pi f = 2\pi \frac{c}{\lambda}\,. \quad [2]$$

Equation [1] can be rewritten as a superposition of two orthogonal linear components to allow an easier discussion of the different light polarizations

$$\vec{E} = E_{01} \cdot e^{i(\vec{k}\vec{r}-\omega t)} + E_{02} \cdot e^{i(\vec{k}\vec{r}-\omega t+\varphi)} \quad [3]$$

with an additional phase shift φ between the two wave components. In the simplest case the perpendicular components of the electric field have similar strength $E_{01} = E_{02}$ and they are in phase with $\varphi = [0; \pm \mathrm{n} 2\pi]$ (with n as a natural number). Thus, they superimpose to an $\vec{E}$ that oscillates in a plane which represents linear polarized light. Also for phase shifts of $\varphi = \pm(2\mathrm{n}+1)\pi$ the resulting polarization stays linear but the plane of polarization flips by $90°$ from horizontal to vertical linear polarization or vice versa. In the case of $E_{01} \neq E_{02}$, the polarization is still linear but the plane rotates depending on the relative strength of both electric field components. If the two electric field components are equal ($E_{01} = E_{02}$) but have a phase shift of $\varphi = \pm\left(\mathrm{n}+\frac{1}{2}\right)\pi$, the resulting $\vec{E}$ rotates over time on a circle in a plane perpendicular to the propagation direction (see figure 1b). Due to the propagation in space this rotation describes a helical path over time which can be either left- or right-handed. The assignment of left- or right-circular polarization to a certain rotation direction of $\vec{E}$ is a matter of the point of view definition. From receiver point of view a clockwise rotation of $\vec{E}$ is related to right-circular or -handed polarization while counterclockwise rotation is referred to left-circular or -handed polarization.[34] For different electric field strengths ($E_{01} \neq E_{02}$) in the case of $\varphi = \left(\mathrm{n}+\frac{1}{2}\right)\pi$ or all other phase shifts beside the already mentioned special cases, the resulting $\vec{E}$ describes an elliptical curve during propagation which is related to elliptical polarized light.

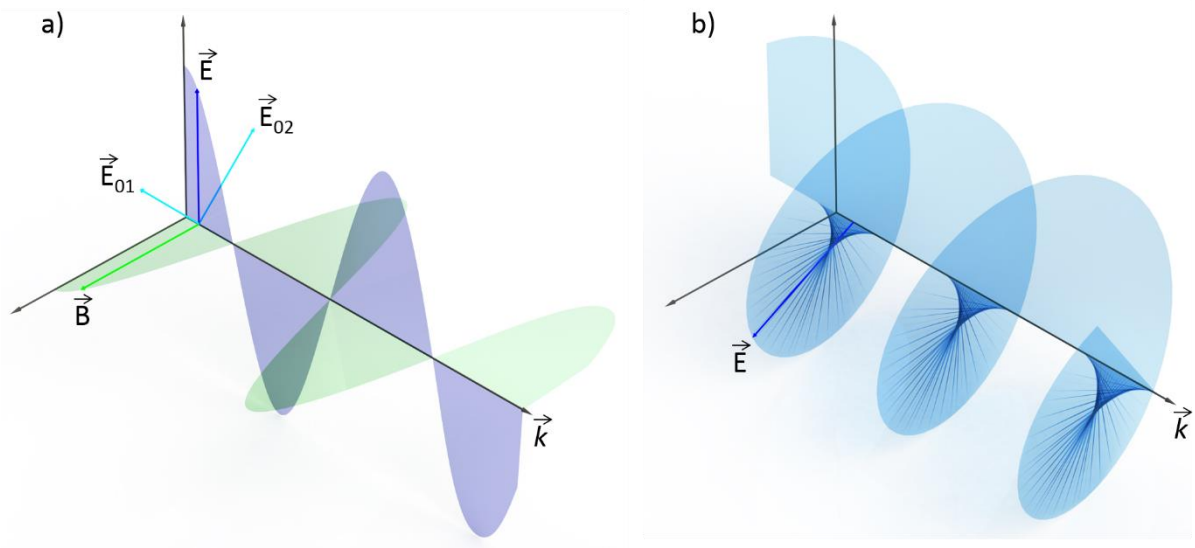

figure 1: a) Linear polarized light with perpendicular electric $\vec{E}$ and magnetic $\vec{B}$ field in propagation direction $\vec{k}$. The electric field $\vec{E}$ can be described by the superposition of two perpendicular vectors $\vec{E}_{01}$ and $\vec{E}_{02}$. b) Left-circular polarized light due to a phase shift of $\varphi = \frac{\pi}{2}$ of $\vec{E}_{02}$ relative to $\vec{E}_{01}$ which leads to a rotation of the superimposed $\vec{E}$ on a left-circular path (counterclockwise; from receiver point of view).

The polarization of light can be changed in several ways like the reflection on surfaces, scattering in different materials, with the help of polarizers or last but not least due to optical active materials. However, in the following only the principle of linear birefringence will be briefly explained, as it occurs in a quarter-wave plate or a PhotoElastic Modulator (PEM), which were both used during this thesis for the light polarization in the experimental setup. Linear birefringence is a property of anisotropic matter which is e.g. common for crystals that have non-cubic and thus an asymmetric crystal structure.[32] Due to an asymmetry between different directions within such a crystal, it can have different refraction indices n_i and thus propagation speeds $c_i = \frac{c_0}{n_i}$ for light in those directions. In the case of biaxial crystals (e.g. borax or topaz), all three symmetry axis have various refraction indices (n_a, n_b, n_c), while uniaxial crystals (e.g. barium borate or quartz) have just one extraordinary direction with a different refraction index n_e compared to all other ordinary directions n_o. Light that propagates through such crystals can experience a polarization change depending on the polarization and propagation direction relative to the e.g. extraordinary direction of a uniaxial crystal, which is also called optical axis. As long as the incident light is linear polarized, parallel or perpendicular to this optical axis, or the light propagation direction is parallel to it no polarization change will occur. In all other cases the electromagnetic wave can always be seen as a superposition of two orthogonal components, as described by equation [3], one parallel to the optical axis and one perpendicular to it. Those two components travel with different speed through the crystal relative to the refraction index difference $\Delta n = n_o - n_e$ of the ordinary and extraordinary direction. This results in a phase shift

$$\varphi_{eo} = \frac{2\pi}{\lambda} d \cdot \Delta n \qquad [4]$$

which depends on the thickness d of the crystal and on the wavelength λ of the incident light. If the phase shift of the crystal is equal to $\varphi_{eo} = \frac{\pi}{2}$, which is true for

$$d = \frac{\lambda}{4\Delta n}\,, \qquad [5]$$

incident linear polarized light in a $\pm 45°$ angle relative to the optical axis becomes circular polarized. Those crystals are called quarter-wave or $\frac{\lambda}{4}$ - retardation plates. They are commonly used for the circular polarization of light, but they have the disadvantage that each single quarter-wave plate solely can be used for a limited wavelength range depending on its material and thickness.

Another possibility to circular polarize an incident linear polarized electromagnetic wave is the usage of a PhotoElastic Modulator (PEM).[35] A PEM consists of a transparent birefringent fused silica crystal glued onto a piezoelectric transducer crystal. With a sinusoidal electric signal with a frequency ($\sim 50\ kHz$) matching for the transducer, a resonant vibration (period $\sim 20\ \mu s$) of the

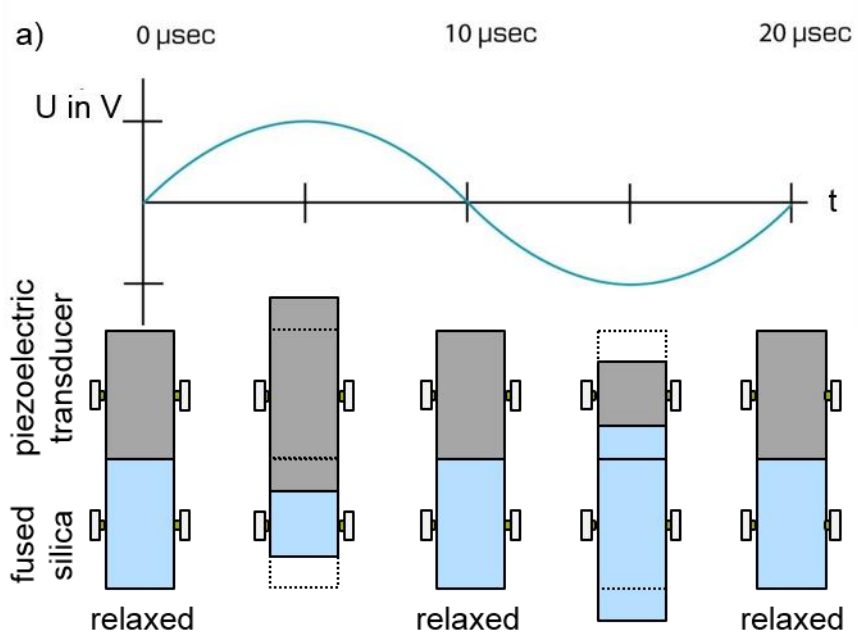

figure 2: a) The sinusoidal voltage U applied to the piezoelectric transducer crystal of the PEM stretches or compresses the crystal periodically. The frequency of this applied voltage matches thereby the resonance frequency of the crystal (in this example $50\ kHz$) which leads to a period of $20\ \mu s$ in which the fused silica crystal follows the piezoelectric crystal by opposing its deformation. The birefringence of the fused silica crystal changes thereby alongside the deformation axis (optical axis) changes periodically as well. b) The periodic refraction index variation due to the deformation of the fused silica crystal can alternate the polarization of incident light. If the incident light is linear polarized in a plane with a relative angle of $\pm 45°$ to the optical axis of the fused silica crystal and the maximum birefringence of the fully compressed and stretched crystal combined with the crystal thickness matches for the wavelength of the light (see equation 4), the resulting light polarization becomes either right- or left-circular depending on the incident polarization angle sign. Thus, during a single period three times the linear polarized light passes the PEM unchanged (relaxed position), while for two times it becomes circular polarized once right-circular and once left-circular (times of full compression and extension depending on the incident polarization angle sign).

piezoelectric crystal is induced (see figure 2a). Due to the fixed connection between both crystals, the fused silica crystal follows this vibration. Thereby, the stretching and compressing

of the fused silica crystal changes periodically the refraction index parallel to the direction of the induced vibration, while the refraction index perpendicular to that motion stays unchanged. If pulsed linear polarized light crosses in a $\pm 45°$ angle the PEM at the moments of full extension or compression of the crystal, and the thickness and refraction index difference are correctly chosen (by more or less maximum extension/compression of the crystal) to fulfill equation [5], the PEM retardation is similar to a quarter-wave plate and the resulting light becomes circular polarized (see figure 2b).

1.2.1.2. Optical Rotatory Dispersion (ORD)

Optical Rotatory Dispersion is based on the circular birefringence effect of chiral structures or molecules. Similar to the previously explained linear birefringence, circular birefringence is also related to a refraction index difference and thus to a light propagation speed variation.[36] While linear birefringence reduces or accelerates a light component alongside an optical axis (in uniaxial crystals) which has another refraction index, circular birefringence leads independent from any fixed axis to a speed variation for the two circular polarization handedness of light due to a refraction index difference between them. Linear light, that can analogously to equation [3] be described as a superposition of two circular polarized components with opposite handedness, experiences a phase shift of one of these components relative to the other due to circular birefringence. This results in a rotation of the polarization plane relative to the incident linear polarization plane (see figure 3). The optical rotation α depends thereby similar to the phase shift for linear birefringence on the thickness d of the sample but also on the used wavelength (dispersion) as well as the density, temperature and ee of the chiral sample. Those dependences influence the refraction index difference $\Delta n(\lambda, \rho, T) = n_l - n_r$ between the left-circular (n_l) and right-circular (n_r) light component. This leads to a definition of the optical rotation analogous to equation [4]

$$\alpha = \frac{\pi}{\lambda} d \cdot \Delta n(\lambda, \rho, T) \ . \qquad [6]$$

However, due to the several dependencies of $\Delta n(\lambda, \rho, T)$ this definition does not allow an easy comparison between different chiral samples or ee measurements. Thus, it is more common to define a specific rotation as follows[25]

$$[\alpha]_\lambda^T = \frac{\alpha}{d \cdot \rho} = \frac{100\alpha}{d \cdot c_p} \qquad [7]$$

with the measureable rotation angle α, thickness d and density ρ or concentration c_p (for historical reasons in $\frac{g}{100\ ml}$) of the sample. Thereby, the specific rotation can e.g. be determined at room temperature at a common wavelength to obtain reproducibility and comparability

between different ee of a chiral sample or different chiral samples at all. The ee in ORD measurements can thus be formulated as[37]

$$ee(\%) = \frac{100 \cdot [\alpha]_{obs}}{[\alpha]_{\lambda}^{T}} \quad [8]$$

with the observed specific rotation $[\alpha]_{obs}$ relative to the specific rotation $[\alpha]_{\lambda}^{T}$ of an enantiopure version of the sample measured at the same temperature and with the same wavelength. For instance, while for an enantiopure sample with a certain temperature and density its specific rotation $[\alpha]_{obs}$ is maximized and equal to $[\alpha]_{\lambda}^{T}$, in a racemic mixture the optical rotation of both enantiomers cancel each other to $[\alpha]_{obs} = 0$ independent from temperature or wavelength.

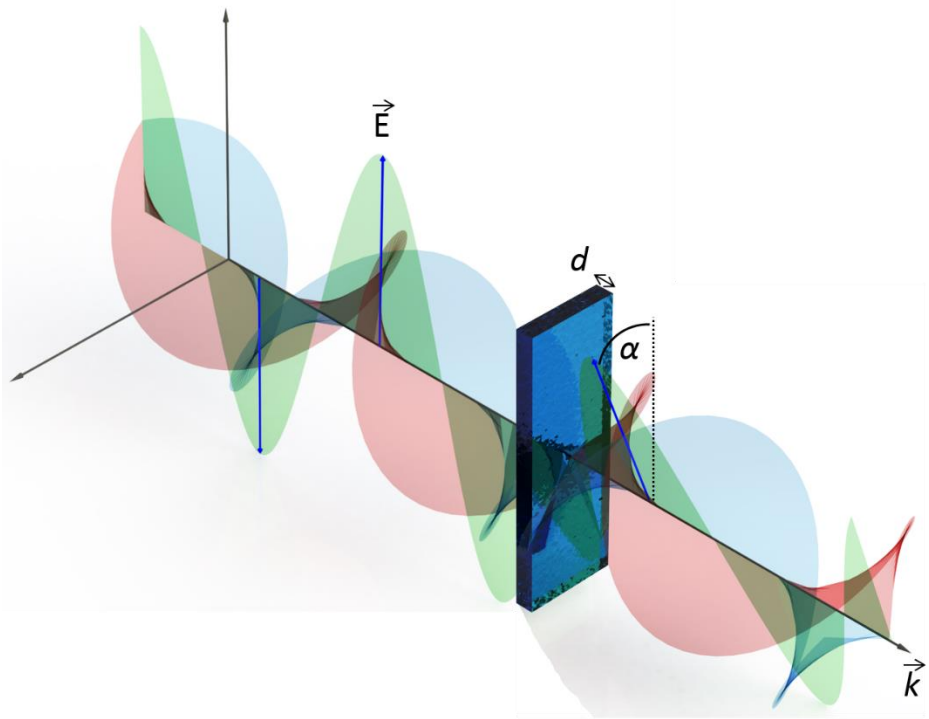

figure 3: Vertical linear polarized light as a result of two superimposed opposing handed circular polarized light components passes a chiral sample with thickness d. The circular birefringence of the sample leads to a phase shift between the two circular polarized components. Thus, the superimposed linear light out of these shifted circular components has a rotated linear oscillation plane by an angle α relative to the previous vertical alignment.

For those ee measurements or the determination of $[\alpha]_{\lambda}^{T}$ in general, the necessary measurement of the optical rotation α is usually done with the help of a polarimeter. A polarimeter consists of two polarizers that can solely be passed by linear light parallel polarized to a certain axis. The chiral sample is mounted between the two polarizers and the first polarizer is for example fixed to a position at which it can only be passed by vertical polarized light (see figure 3). The second polarizer (analyzer) behind the sample is then rotated either till the passing light shows a maximum output or totally vanishes. In the first case, the angle of the second polarizer relative to the alignment of the first polarizer is α, while in the second case the angle is perpendicular to the changed polarization plane and thus $90° - \alpha$. Those ORD polarimeter measurements were for several decades the most common methods for the

investigation of chiral samples and are still in use e.g. for the analysis of HPLC processed chiral outputs.

At this point it should be mentioned that the optical activity of chiral systems always contains an asymmetric absorption of the opposing circular light polarizations (circular dichroism), beside the circular birefringence described here. Therefore, the explained case of solely rotation of the linear polarization plane is a simplified description and in a real experiment the CD-effect leads to slightly elliptical polarized light, as it will be described in more detail in the next section.

1.2.1.3. Circular Dichroism (CD)

Another consequence of the optical activity of chiral systems or molecules is their difference in circular polarized light absorption depending on the handedness of the incident circular polarization. For the previous descriptions of linear or circular birefringence the refraction indices n_i and their differences Δn have been shown to be only real numbers but they have more correctly to be seen as complex numbers $\underline{n} = n + i\varepsilon$ with the extinction coefficient ε as imaginary part. While the real part represents the phase velocity of the light in matter as explained for linear and circular birefringence, the imaginary part represents the attenuation due to the absorption of light.[38] In the case of chiral matter, this attenuation differs for the handedness of circular polarized light due to an extinction coefficient difference $\Delta\varepsilon = \varepsilon_L - \varepsilon_R$, with respectively ε_L and ε_R for left- and right-circular polarized light.[25] This effect is called Circular Dichroism (CD) and results in an absorption difference $\Delta A = A_L - A_R$ for circular polarized light.[1],39-40 As already mentioned in the previous chapter, during ORD measurements with linear polarized light, which is a superimposition of two opposing handed circular components with similar amplitude, the CD-effect leads to slightly elliptical polarized light. Due to the absorption difference between left- and right-circular polarized light, the amplitude of the two circular handedness differs after passing a chiral sample and they superimpose to an electric field vector that rotates alongside an elliptical path. Therefore, one possibility to investigate the CD effect of a chiral sample is the measurement of the ellipticity ψ of incident linear light after passing the sample.[41] Analogous to the specific rotation $[\alpha]_\lambda^T$ (see equation 7) a specific ellipticity can be defined as[25]

$$[\psi]_\lambda^T = \frac{\psi}{d \cdot \rho} = \frac{100\psi}{d \cdot c_p} \qquad [9]$$

[1] Analogous to the existence of linear and circular birefringence for phase velocity differences due to various real parts of the refraction index, also the dichroism effect appears for linear as well as circular polarized light due to varying imaginary parts of the refraction index. Thus, linear dichroism leads similar to circular dichroism to an attenuation/absorption difference for linear polarized light depending on the polarization plane alignment relative to a certain axis with another extinction coefficient.

with the thickness d and density ρ or concentration c_p (for historical reasons in $\frac{g}{100\ ml}$) of the sample. The specific ellipticity is thereby related to the extinction coefficient difference via the relative molar mass M of the chiral sample[25]

$$[\theta]_\lambda^T = \frac{[\psi]_\lambda^T \cdot M}{100} = 3300\ \Delta\varepsilon = CD \qquad [10]$$

with the molar ellipticity $[\theta]_\lambda^T$ that is often used as CD value in $mdeg$. The ellipticity ψ can be measured with the help of two polarizers, similar to ORD measurements with a polarimeter. The first polarizer in front of the sample defines the incident linear polarization plane while the second polarizer (analyzer) is placed behind the sample. The ellipticity of the light that passed a chiral sample can be calculated by measuring the light intensity behind the second polarizer, that is once aligned parallel and once perpendicular to the first polarizer. For instance, due to the elliptical polarization, the light intensity does not vanish totally for a perpendicular alignment of both polarizers as it should for linear polarized light. However, this method is relatively uncommon compared to other CD investigation techniques.[25]

More common is the direct measurement of the left- and right-circular light absorption which is used in conventional CD spectrometers.[26] Thereby, the output of a continuous light source is first linear polarized with a polarizer and then circular polarized by a PEM (see section 1.2.1.1). At first, a reference measurement is done without a sample or, in case of a solved sample, with solely the solvent. The wavelength range of interest is scanned with the help of a monochromator in front of a PhotoMultiplier Tube (PMT) that is used as detector. For each wavelength step one measurement is performed with left-circular and one with right-circular polarized light, which should lead to equal PMT signals due to the fact that the solvent is achiral. The same scan is afterwards repeated with the (solved) chiral sample in the beamline and thus the detected intensity difference for left- and right-circular polarized light can be measured. The resulting absorption difference ΔA normalized to the mean absorption A delivers the often used anisotropy factor (*g*-value or -factor)[25]

$$g = \frac{\Delta A}{A} = \frac{\Delta\varepsilon}{\varepsilon} = \frac{CD}{3300\varepsilon}\ . \qquad [11]$$

The anisotropy factor has the advantage of comparability between CD effects of various chiral samples independent from their relative light absorption at a certain wavelength.

The CD effect can also be contemplated on a more theoretical basis compared to equation [11] to get a more general feeling for the sign and expected value of the anisotropy factor. The absorption difference between left- and right-circular polarized light in chiral molecules is a result of a coupling variation between the electromagnetic field of the electromagnetic wave and the electric ($\vec{\mu}$) and magnetic ($\vec{m}$) transition dipole moments of the absorbing molecule.[25]

1.2. Analyzing of Chiral Molecules

Due to the absorption of a photon with a matching energy for either an electronic (Electronic Circular Dichroism; ECD)[42] or a vibrational (Vibrational Circular Dichroism; VCD)[43] excitation within the molecule, either an electron of the molecule gets excited to a higher orbital shell and thus the molecule is in an electronically excited state, or the molecule starts vibrating and thus reaches another vibrational state. In both cases, the electron cloud and therefore the charge distribution changes from the previous less excited (or often ground state) to the excited state. Thereby, the new electron cloud equilibrium state can have another electric dipole moment, and for the transition an electric transition dipole moment $\vec{\mu}$ can be determined. Furthermore, the performed charge movement induces a magnetic moment analogous to the electron movements in a conductor (Biot–Savart law; via right-hand rule).[36] Charge rotations induced by an electronic quadrupole rotation during the transition induce thereby a magnetic transition dipole moment $\vec{m}$. These charge rotations and the strength of the induced $\vec{m}$ relative to $\vec{\mu}$ is of special interest due to the rotational character of the circular polarized light that couples differently depending on its handedness to those transition dipole moments resulting in an absorption difference.[25] Therefore, a dipole strength $D = |m|^2 + |\mu|^2$ and rotational strength $R = |m||\mu| * \cos\theta$ can be defined with the enclosed angle θ between $\vec{m}$ and $\vec{\mu}$. This rotational strength normalized by the dipole strength leads to another anisotropy factor definition as follows[25]

$$g = 4\frac{R}{D} = 4\frac{|m||\mu|*\cos\theta}{|m|^2+|\mu|^2}\,. \qquad [12]$$

With this definition it becomes obvious that the sign of the *g*-value solely depends on the angle θ between $\vec{m}$ and $\vec{\mu}$. If $\theta > 90°$ the *g*-value is negative, while $\theta < 90°$ results in a positive *g*-value. Furthermore, the anisotropy factor is zero either for a perpendicular alignment of $\vec{m}$ and $\vec{\mu}$ or if the excited transition has either no electric or no magnetic transition dipole moment. Consequently, a maximal anisotropy factor can be measured for a parallel (or antiparallel) alignment and an additionally equal strength (vector length) of $\vec{m}$ and $\vec{\mu}$. However, usually the electric transition dipole moment is several magnitudes larger than the magnetic transition dipole moment (as long as it is not quantum-mechanically forbidden while the magnetic transition is allowed). Therefore, ECD anisotropy factors are typically in the per mille region and for the lower effect in VCD measurements about 10 to 100 times smaller.[25] For the measurement of such small excitation or absorption differences of chiral samples, several experimental methods have been developed focusing on different resulting aspects of the CD effect or combining various techniques to allow higher enantio sensitivity even within mixtures of several different chiral and achiral molecules.

One method, which was used and further developed for the measurements presented in this thesis, is a combination of MS and REMPI with circular polarized nanosecond laser pulses for

the resonant excitation and subsequent ionization of chiral molecules in the gas phase.[44-45] The REMPI process with circular polarized light allows simultaneously for enantiosensitivity due to the CD effect and for wavelength selectivity due to the necessary wavelength that matches an electronic or vibronic resonance of the investigated chiral molecule. The subsequent ionization by absorption of an additional photon[2] enables the usage of a TOF-MS[46] and thus for separation of the produced ions depending on their mass. The measured ion yield obtained for left- (I_L) and right-circular (I_R) polarized light delivers thereby analogous to equation [11] the anisotropy factor

$$g = \frac{\Delta I}{I} = 2\frac{I_L - I_R}{I_L + I_R}\,. \qquad [13]$$

In comparison to conventional CD spectrometers which are often used for liquid phase analysis, the usage of this method on samples in the gas phase reduces the interactions of the chiral molecules of interest with other chiral or achiral molecules to a minimum. The measurement speed, which plays often an important role for analysis of dynamic processes (e.g. asymmetric catalytic reactions), depends mainly on the laser repetition rate. Therefore, the combined CD-REMPI-MS method with its three-dimensional sensitivity and selectivity allows for chiral molecule investigations in the gas phase even within mixtures with other chiral or achiral molecules. Due to the usage of CD-REMPI-MS for the measurements presented in this thesis, its fundamental principles are described in detail in section 1.4 and its reachable sensitivities are discussed in the results section 2.

Another CD based investigation method that also uses REMPI, but with pulsed femtosecond laser systems, focuses on the resulting photoelectrons instead of the ions of the REMPI process.[47-48] First theoretical predictions[49] of an asymmetry within the angular distribution of the emitted photoelectrons from ionized randomly orientated chiral molecules were already made in 1976, while experimental observations, at first with synchrotron radiation,[50] were made in 2001. The asymmetry within the angular distribution is an electric dipole dependent effect and occurs between the forward and backward emitted photoelectrons relative to the propagation direction of the used circular polarized light. Thereby, the preference direction of the asymmetry can be swapped by changing the handedness of either the enantiomer or the circular polarized light. The resulting PhotoElectron Circular Dichroism (PECD) effect is due to its solely electric dipole dependence several magnitudes higher than the ECD effect of the chiral molecule which depends additionally on the magnetic transition dipole moment.

[2] Depending on the photon energy and the ionization threshold of the sample molecule, the absorption of only one addition photon after the resonant excitation is only the simplest example for a REMPI process ((1+1)-REMPI). The REMPI processes can be arbitrary complicated with additional resonant or non-resonant intermediate states by absorption of several photons with different wavelength (see section 1.4 and 2.1).

Therefore, the enantiosensitivity of PECD enables ee measurements with error margins of below one percent.[51] If this technique is combined with an additional mass spectrometer, the coincident measurement of photoelectrons and -ions allows for determination of the absolute configuration of the chiral sample molecules.[52-53]

An experimentally quite new (2013) and different approach for the investigation of chiral molecules in the gas phase is based on microwave spectroscopy and called microwave three-wave mixing.[54] It is related to the three rotational constants A, B and C of the chiral sample molecules that necessarily need non-vanishing electric dipole moments μ_A, μ_B and μ_C to enable this investigation method. While the rotational constants as well as the dipole strengths are similar for both enantiomers of a chiral molecule, the product of $\mu_A\mu_B\mu_C$ has an opposing sign due to a sign difference in one of the three dipole moments within a fixed coordinate system. In microwave three-wave mixing, supersonic-beam cooled chiral molecules are measured by resonant excitation of an electronic c-type transition induced by an external linear electric field E_z combined with another perpendicular external electric field E_x for an induced intermediate relaxation via an a-type transition. The final relaxation of the molecule leads then to a b-type transition via emission of an electric field E_y perpendicular to E_x and E_z, which has a phase difference of π for the two enantiomers of the chiral molecule. This technique also allows for ee measurements due to the fact that the amplitude of the resulting signal E_y depends on the ee of the chiral sample.[55] However, microwave three-wave mixing is obviously not a CD related technique but anyhow has been mentioned here due to the fact that it reveals interesting perspectives for rovibronic transitions in CD-REMPI-MS measurements as they are shown in section 2.1.

1.2.2. Methods Based on Interaction with Chiral Systems

Beside their difference in optical activity, the two enantiomers of a chiral sample vary in their interaction and reactivity with other chiral systems. This interaction difference can be used as fundament for enantio sensitive separation methods based on chromatography techniques. Chromatography in general is a commonly used technique for the analysis of chemical mixtures due to the fact that it allows for a separation of a mixture into its components.[56] A chromatograph consists of a mobile and a stationary phase (or column) in a closed system. As the names imply, the mobile phase moves through the system either due to gravity or pressure, while the stationary phase is fixed at its position and passed by the mobile phase. The chemical mixture is injected into the mobile phase and flows with it through or alongside the column. The different components of the mixture switch thereby rapidly their interaction or binding partners from mobile to stationary phase and vice versa. While a component has more affinity and thus is more often bound to the stationary phase, it flows slower through the system

than a component that more often interacts with the moving mobile phase. Thus, the components of the sample mixture reach the end of the system at different times and can be either directly analyzed with the help of other techniques (UV-Vis, mass spectrometry, fluorescence, etc.) or just extracted separately.

Depending on the sample aggregation state and various separation criterions, which e.g. can be chosen to separate especially one component of interest from the others, the mobile and stationary phase differ in their composition and combination. The aggregate state of the mobile phase, that matches the aggregate state of the sample, defines thereby two main chromatography techniques: gas chromatography (GC) and liquid chromatography (LC). For GC the mobile phase could be for example helium, hydrogen or nitrogen that flows with the gaseous sample through a capillary that is coated with the stationary phase, which is either solid or a viscous liquid. The choice of the column compound depends especially on the polarity of the sample components. For example, a polar component binds more easily to a polar stationary phase, while a nonpolar component is less time bound and thus travels faster through the system. This principle works also in LC for the liquid mobile phase (e.g. polar methanol or nonpolar hexane) as well as for the stationary phase out of silica (polar) or C-18 (nonpolar). Another important factor for the selectivity and the general flow velocity especially in LC is the surface and packing of the stationary phase. A larger surface of the stationary phase due to the usage of porous membranes or compact packed granules increases the interaction rates of the sample with the stationary phase and thus its separation effect. However, a more compact packing of the column decreases the analysis speed of the technique because of an overall lower flow velocity. Therefore, HPLC was invented in the 1970s to allow for highly compact packing of the stationary phase with particle sizes around $50\ \mu m$ in average.[24] The problem of low flow rates is thereby avoided by significantly higher working pressures of some hundred bar on the mobile phase.

The described chromatography techniques are in general not enantio sensitive due to the similar interactions of the two enantiomers of a chiral molecule with achiral molecules. At this point the interaction difference of enantiomers with enantiomers of another chiral molecule can be utilized to increase or decrease the interaction rate of one or the other enantiomer of the sample with the stationary phase. Therefore, non-racemic chiral columns can be used for GC or HPLC to enable different flow velocities for the two enantiomers of the chiral sample.[23] As chiral column for such enantio sensitive GC or HPLC measurements β-cyclodextrine (a sugar ring molecule) or one of its derivatives are commonly chosen. As already mentioned, GC and HPLC with chiral columns only allow for a separation of the two enantiomers but for the characterization of the used columns as well as for the final analysis of the chiral outputs it is

still necessary to use methods based on optical activity such as polarimeters (for ORD) or conventional CD spectrometers.[57]

1.3. Heterogeneous Asymmetric Catalysis

The first concepts for asymmetric (enantioselective) synthesis were already introduced in 1894 by E. Fischer due to his investigations on sugar synthesis.[58] However, those syntheses were non-catalyzed reactions and at that time the relevance of enantiopure products was low or still unknown compared to nowadays. After this, with the upcoming modern food industry with a raising amount of synthetic flavors the importance of asymmetric synthesis increased. In case of pharmacy, especially the dramatic problems with the drug Contergan[16-18] in the 1960s revealed the critical necessity for enantiopure production of drugs (see section 1.1). A breakthrough was reached in 1968 by W. Knowles with a novel asymmetric catalysis. He reported a catalyzed asymmetric hydrogenation process which led to the first industrial asymmetric synthesis of L-DOPA[15] that is used in the Parkinson's disease treatment.[59] Based on the work of W. Knowles, R. Noyori refined in 1980 the asymmetric hydrogenation by utilizing homogeneous transition metal complexes with BINAP reaching ee's of up to 100%. In the same year, B. Sharpless described the asymmetric epoxidation of allylic alcohols, which resulted in an industrial asymmetric synthesizing process for glycidol, that is a key component for the production of β-blockers in heart medicines. For their contributions on basic research on asymmetric catalysis and the subsequent effects on modern food industry and pharmacy, W. Knowles, R. Noyori and B. Sharpless were honored with the Nobel Prize for chemistry 2001.[60]

The function of the catalyst in asymmetric catalysis is quite similar to normal catalytic reactions. In normal catalytic reactions the catalyst participates in the reaction and lowers the activation energy without being depleted in the reaction.[58] In asymmetric catalytic reactions the catalyst itself is in general chiral (e.g. a transition metal complex with a chiral ligand), while the reagents can be chiral or achiral. The interactions of the chiral catalyst either with the chiral reagent or the chiral product decrease differently the activation energy for the reaction paths resulting in various diastereomers of a chiral product. Thus, the reaction path for one enantiomer is energetically favored compared to the other and leads to a catalyzed enantioselective (asymmetric) synthesis. The ee of the chiral product depends thereby on the activation energy difference between the reaction paths which can through a Boltzmann factor mainly be influenced by the choice of the chiral catalyst as well as its ee. Beside the necessity of enantio sensitive analysis for the ee measurement of the chiral catalyst, the ee of the chiral products has also to be measured. While the catalyst can probably be investigated separately from the asymmetric reaction, the ee measurement of the chiral products can be more challenging due to the fact that they are mixed up with non-converted chiral and achiral educts as well as the chiral catalyst. Therefore, a combination of HPLC combined with a conventional CD spectrometer is commonly used for the product analysis of asymmetric catalytic reactions (see

section 1.2.1.3 and 1.2.2).[57] However, this analyzing method does not allow for in situ measurements of chiral products during the asymmetric catalytic reaction and thus does not provide a possibility for optimization of the dynamic system and its conditions during the reaction. Those properties of an analyzing technique are especially important for the research on novel combinations of educts and catalysts as well as the in situ observation and adjustment of their reaction conditions.

While homogeneous asymmetric catalysis with its advantage of high activity and selectivity is still the dominant form of industrial asymmetric catalysis, the research interests focus nowadays increasingly on heterogeneous systems.[61-63] Heterogeneous asymmetric catalysis has the potential advantage of a lower depletion of the catalyst as well as an easier separation and recycling of both the catalyst and products which could reduce the costs in industrial processes. Furthermore, heterogeneous asymmetric catalysis can have high selectivity comparable to homogeneous reactions dependent on the reactant-catalyst system. For example, the catalyst in heterogeneous reactions can thereby be a tailored metal-organic complex which is immobilized and thus it is highly ordered on a surface, while the reactants and chiral products are gaseous. In such an example, the necessity of precise and fast enantio sensitive in situ measurements in the gas phase becomes obvious especially as analyzing method during research of new reactant-catalyst systems. Furthermore, the used ee measurement technique has to be highly selective due to the still existing mixture of non-converted reactants with the chiral products. Beside PECD and probably microwave three wave-mixing (see section 1.2.1.3), CD-REMPI-MS with its high selectivity and sensitivity for CD gas phase measurements fulfills all requirements to analyze those heterogeneous asymmetric catalysis. This motivated the further development of the CD-REMPI-MS technique (see next section) within this thesis and finally let to the presented results in section 2.

1.4. Circular Dichroism - Resonance-Enhanced Multiphoton Ionization - Mass Spectrometry

One of the major motivations for the work presented in this thesis was the further development of the CD-REMPI-MS technique for its purpose as analyzing method especially for heterogeneous asymmetric catalysis in the ultra-high vacuum. Therefore, in the following sections the fundamental experimental principles of this enantio sensitive, wavelength and mass selective technique are presented in more detail. Furthermore, the experimental progresses of this method and the state of the art at the beginning of this thesis are contemplated as well as the resulting ideas for developments that led to the publications around CD-REMPI-MS presented in this thesis. Finally, a comparison between PEM and quarter-wave plate as two possibilities for the circular polarization of light is shown.

1.4.1. Measurement Principle

The CD-REMPI-MS method is especially prepared for CD measurements on small amounts of chiral samples in the gas phase under vacuum conditions ($\sim 10^{-6}\, mbar$; during measurements). In general, the sample molecules or even a mixture of different chiral and achiral molecules are introduced into a vacuum chamber via an effusive beam inlet system.[3] The sample, which is usually liquid, is thereby directly connected to the vacuum chamber by a thin needle. If the vapor pressure of the sample is high enough at the given temperature (normally room temperature but the sample and inlet system can also be heated), the molecules partly go over into the gas phase, which results in a continuous flow of molecules from the sample source into the vacuum chamber. In the vacuum chamber this molecular beam is overlapped and thus illuminated by a perpendicular aligned circular polarized laser beam (see figure 1b of the first publication[64]). For the investigations presented in this thesis, pulsed nanosecond Nd:YAG laser systems (Spitlight Hybrid by InnoLas Laser; repetition rate: $30\, Hz$) have been used as light source.[4] Laser light from solid state lasers has the advantage of a well-defined beam profile with a high collimation, a narrow spectral linewidth and high photon densities (optional by focusing the laser beam). A disadvantage of such laser systems is their fixed fundamental wavelength ($1064\, nm$ for Nd:YAG lasers) that can only be changed by nonlinear optics like second harmonic generation crystals (frequency doubling). Thus, the second, third, etc. harmonic frequency of the Nd:YAG fundamental can be generated leading

[3] The sample molecules can also be introduced via a supersonic beam inlet which is explained with its advantages and disadvantages in the next section.
[4] The light source for CD-REMPI-MS does not have to be a nanosecond laser system. For example, pico- or femtosecond laser systems have the advantage of higher repetition rates and lower laser pulse energies but high laser pulse intensities. However, those laser systems have the disadvantage of higher spectral linewidths compared to nanosecond laser systems.

to the reachable wavelengths $532\,nm$, $355\,nm$, $266\,nm$ or $216\,nm$. However, one of the Nd:YAG lasers was used as pumping laser for a dye laser system (Pulsare by Fine Adjustment) with a spectral linewidth of $0.04\,cm^{-1}$ that allowed for wavelength tuning depending on the selected dye (i.e. wavelength range of $\sim 10\,nm$ per dye). This enabled laser spectroscopy investigations of the chiral sample molecules.

As a CD based technique (see section 1.2.1.3)[25], CD-REMPI-MS utilizes the circular polarized laser light for the resonant excitation of an electronic transition (ECD) in the chiral samples. A direct measurement of the absorption difference of left- and right-circular polarized light by the detection of the light intensity after the excitation (after passing the sample) like in a conventional CD spectrometer is thereby not possible[5] but also not desired. Instead, the resonant excitation of the sample molecules is used as a first intermediate transition of a Multiphoton Ionization (MPI)[6],[44, 65] process, which means in the simplest case the absorption of one more photon for the ionization step (see figure 1a of the second publication[66]). The overlap region of molecular and laser beam (and thus the REMPI process) is placed between two stainless steel plates within the vacuum chamber. This repeller and accelerator plates are positively charged (repeller: $\sim 1800\,V$; accelerator: $\sim 1100\,V$; distance: $5\,cm$) and represent the first part of a linear TOF-MS following the design of W. Wiley and I. McLaren.[46] The also positively charged molecular ions produced in the REMPI process are accelerated in the electric field between the repeller and accelerator plate to a multi-channel plate detector. In their flight path behind the accelerator a third grounded plate (distance: $2\,cm$) represents a second acceleration stage, that allows for a second-order space focus, as described in detail in previous publications.[45, 67] After the grounded plate the ions fly through an about $120\,cm$ long field-free drift region with the detector at its end. The general principle of the TOF-MS is thereby based on the similar potential energy that the ions obtain within the two acceleration stages. This potential energy is converted into kinetic energy ($E_{kin} = \frac{1}{2}mv^2$) of the ions and results in different velocities for ions with different masses. Due to these velocity differences ions of different masses separate within the field-free drift region and thus reach the detector after different flight times. This mass separation is not only important in the case of sample mixtures but also because of a possible fragmentation of the molecular ions during or after the ionization process. Therefore, the mass selectivity of the TOF-MS allows for an independent investigation of various chiral or achiral molecular ions within a sample mixture as well as a separate investigation of their fragment ions.

[5] In the gas phase the molecular densities are too low and thus signal differences are too small for direct intensity measurements.
[6] The MPI process can also be described here as REMPI process due to the resonance-enhancement of the first excitation step.

The resulting ion yield of a chiral molecule of interest depends thereby on the absorption efficiencies and thus extinction coefficients for the resonant excitation of the chiral sample with left- or right-circular polarized light. As already mentioned in section 1.2.1.3, the anisotropy factor for CD-REMPI-MS can thus be defined by the ion yield difference for left- and right-circular polarized light (see equation [13]). The utilized REMPI process can be complicated depending on the investigated electronic transition and ionization threshold of the sample molecule as well as the wavelengths of the used laser systems. For example, additional resonant intermediate transitions can occur (see figure 1a of the first publication[64]) which have their own electric and magnetic transition dipole moments and thus measureable anisotropy factors. Such additional CD active resonant transitions accumulate their g-values to an overall anisotropy factor for the whole REMPI process.[7],[44] At this point it should be mentioned that it has been experimentally observed that the final ionization step of the REMPI process does not have any addition g-value at all and solely resonant intermediate transitions contribute to the overall g-value.[68] Furthermore, non-resonant transitions involving a virtual intermediate state, which has no defined electronic configuration and thus no conclusive electric or magnetic transition dipole moments, also do not contribute to the overall g-value (see first publication[64]).

However, for higher ordered REMPI processes there are two possibilities to avoid those g-value accumulations due to extra resonant transitions, which do not allow for direct CD measurement of one certain electronic transition.[65] On the one hand, additional laser systems with only linear polarized light can be used to excite the sample molecule to a resonant intermediate state of interest without an anisotropy factor contribution, or the wavelength of this additional laser system is tuned to allow for a direct ionization out of the investigated resonant intermediate state.[64] In the latter case, an additional advantage can be the reduction of the order of the REMPI process (i.e. the amount of overall photons for the ionization process is reduced) due to the fact that lower laser intensities are necessary for a sufficient ion yield. Those measurements with additional laser systems are called, multi-color[8] experiments because of the different wavelength that are used for the resonant excitation and the ionization step. On the other hand, the wavelength of the circular polarized laser system can be adjusted to allow for a resonant excitation of the electronic transition of interest and a subsequent ionization via additional non-resonant intermediate transitions.[68-71] However, due to the angular momentum of the photon those two-photon processes follow other quantum mechanical selection rules and thus enable other final electronic states with varying anisotropy factors compared to single-photon experiments. In addition, the excitation or ionization via a virtual

[7] For example in a (1+1+1)-REMPI process the anisotropy factors of the first and second resonant transition accumulate to an overall g-value, while the ionization step does not contribute an additional g-value.
[8] If only one laser system is used, it is a one-color experiment; for two laser systems, it is a two-color experiment; etc.

intermediate state needs significantly higher laser intensities not only due to the higher ordered MPI process but especially due to the virtual state itself, which reduces the reachable ion yields by several magnitudes.

Depending on the investigated electronic transition of the chiral sample molecule and the therefore used REMPI process each laser pulse (or two combined laser pulses in case of two-color REMPI) leads to a certain ion yield and to a current at the multi-channel plate detector at defined times depending on the ion masses. This current is recorded as voltage on an oscilloscope (WaveRunner 610Zi by LeCroy) and averaged for about 200 laser pulses with left-circular polarized light and afterwards for 200 laser pulses with right-circular polarized light. Out of these averaged ion yields one anisotropy factor for the investigated electronic transition of the chiral molecule can be calculated. Due to laser intensity and molecular beam density fluctuations this procedure has to be repeated about 100 times for statistical reasons. The corresponding standard LabVIEW program for the data acquisition and a direct CD evaluation is shown in the appendix section C.2.2.

These general principles of the CD-REMPI-MS technique can for example be modified by using a supersonic beam inlet system to improve the spectral resolution of the experiment or by utilizing the twin-peak and reference method to increase the experimental precision as it will be explained in the following section.

1.4.2. Previous Experimental Progress

The previous described CD-REMPI-MS method with an effusive beam inlet system as molecular beam source and a quarter-wave plate for the circular polarization of a pulsed nanosecond dye laser beam was mainly used during the last years by our group for CD investigations on 3-methylcyclopentanone (3-MCP).[65, 67] The molecule 3-MCP was used as sample, since its carbonyl group has the advantage of an extraordinary high anisotropy factor of several percent for ECD measurements on its electric dipole forbidden $n \rightarrow \pi^*$ transition.[72] Because of this electric dipole forbidden transition, other ketones possess in general high g-values compared to the usually sub-percent anisotropy factors of other chiral molecules. Therefore, 3-MCP is a perfect chiral test molecule for new experimental approaches, ee measurements or even investigations on molecular ion CD.[67, 73] However, the high anisotropy factor and thus the high absorption difference for left- and right-circular polarized light for 3-MCP has the disadvantage of a distinct saturation effect.[44, 65, 74] The saturation effect influences the measurable maximum anisotropy factor and depends especially on the used REMPI process. It occurs due to focusing the laser beam within the overlap region with the molecular beam, which results in very high laser pulse intensities. Thus, most of the sample molecules within the overlap region get excited to the resonant intermediate state which leads

to a beginning saturation of this state. Higher laser pulse intensities do not increase the amount of molecules excited to the resonant intermediate state as significant as it should be for a hypothetical infinite amount of excitable sample molecules. Therefore, the laser intensity dependence of the reachable ion yield decreases with increasing laser pulse intensities and respectively increasing saturation effect.[9] For example, in the case of full saturation all molecules within the overlap region get excited and ionized by the laser pulse and thus any laser intensity increase results only in the same ion yield (independent from the laser intensity). Especially for high anisotropy factors this effect is not desirable for CD-REMPI-MS due to its dependence on the absorption efficiencies for left- and right-circular polarized light. If the laser intensity increases, the ion yield of the favorable absorbed circular polarization increases less than for the other circular polarization and thus the measured g-value (see equation [13]) decreases (see figure 4). Finally, in the extreme case of full saturation for both circular polarizations the anisotropy factor vanishes totally due to a similar ion yield for both circular polarizations (all sample molecules within the overlap region become excited and ionized).[44]

Two main possibilities to avoid those saturation effects, which especially in the case of huge g-values like for 3-MCP have a high influence on the really measurable g-value, are as follows. On the one hand, one way to decrease the saturation to a minimum is the usage of lower laser intensities (less focused laser beams) for the CD measurements. However, the laser intensities that are necessary for a minimum measurable ion yield above the noise level are a limiting factor. Especially in the case of a more photon process, like a (1+1+1)-REMPI investigation of the $n \rightarrow \pi^*$ transition of 3-MCP, the first intermediate state becomes easily saturated, while the ion yield is close to the noise level due to the necessity of high laser intensity for a three photon ionization process.[44] Furthermore, such REMPI processes with more than one resonant intermediate transition lead to a cumulative effect for the individual anisotropy factors of each resonant excited transition. Thus, the overall anisotropy factor of a REMPI process with more than one resonant transition becomes a cumulated g-value of the single transition g-values that additionally might be reduced due to the saturation effect. If the anisotropy factor of all but one resonant intermediate transition is not already known, this cumulative effect decreases the significance of the measured anisotropy factor in higher ordered REMPI processes. Therefore, on the other hand the use of another REMPI process is a more favorable option to avoid saturation effects. In the case of the CD investigation of the $n \rightarrow \pi^*$ transition of 3-MCP, an (1+1')-REMPI process by absorption of a second photon coming from the fifth harmonic ($213\ \mathrm{nm}$) of another pulsed Nd:YAG nanosecond laser system (ionization laser) can be used for a direct ionization out of the first resonant intermediate state. The resonant transition is still

[9] The laser intensity dependence of the ion yields corresponds to the order of the REMPI process. Therefore, without saturation for a (1+1)-REMPI process a nearly quadratic relation can be expected, while a (1+1+1)-REMPI process has a nearly cubic relation, etc.

excited by the circular polarized laser pulse of the dye laser system, but the necessary laser intensity for this first resonant excitation alone can be significantly lower than for a three photon (1+1+1)-REMPI process (see first publication[64]). Thus, the saturation effect can be significantly reduced, but a minimum necessary ion yield above the noise level stays always as a limiting factor.

This limitation can be improved by increasing the experimental precision, which is mainly influenced by the statistical error margins due to molecular density and laser intensity fluctuations from pulse to pulse. One possibility to reduce the influence of those pulse to pulse fluctuations as well as systematic errors due to laser intensity or molecular beam density changes over the whole CD measurement (time scale of about $45\,min$) is the reference method.[44-45, 65] Thereby, an achiral reference molecule is measured parallel to the chiral analyte molecule. In case of an effusive beam inlet system, both molecule types are part of the same molecular beam and simultaneously excited and ionized by the same laser beam. The achiral reference molecule is chosen as similar as possible in its structure to the chiral analyte molecule but must have another mass. Thus, the behavior in the REMPI process of both molecule types is also similar (they have only slightly shifted absorption bands) but the TOF-MS allows for a separate CD measurement of them. For example, cyclopentanone (CP) can be used as achiral reference molecule for 3-MCP. Due to the fact that the reference molecule is achiral, its measured anisotropy factor has to be zero. If any experimental fluctuations during the measurement lead to a residual g-value for the achiral reference molecule (g_{ref}), it can be assumed that the g-value of the chiral analyte molecule (g_{ana}) is also influenced by these fluctuations. Therefore, the anisotropy factor of the chiral analyte can be corrected (g_{corr}) by the achiral reference g-value as follows

$$g_{corr} = g_{ana} - g_{ref}\ . \qquad [14]$$

This reference method especially minimizes the influence of systematic errors, e.g. due to laser or molecular beam changes over the whole measurement time.

Another way to substantially decrease statistical errors due to laser intensity fluctuations is the twin-peak technique.[45, 75] The laser beam that passes the molecular beam within the vacuum chamber is thereby aligned through a window on the opposite side of the chamber, reflected by a mirror back into the chamber and again focused into another overlap region with the molecular beam. Thus, two spatial separated ionization spots are created resulting in two time shifted ion signals of similar mass within one time of flight spectrum (twin-peak). The important point of reflecting the laser beam by nearly $180°$ is the effect on the circular polarization of the incoming laser beam. The inversion of the propagation direction without changing the phase shift between the superimposed linear polarized light components (see section 1.2.1.1) results

in a switch from left- to right-circular polarization or vice versa. Therefore, the incoming laser beam has the opposite circular polarization compared to the reflected laser beam and the ion yields for the twin-peaks represent the ion yields for opposing circular polarizations. Thus, in general the twin-peak technique provides all necessary information (I_L and I_R) for the calculation of the anisotropy factor within a single laser pulse, which makes the CD measurement independent from pulse to pulse laser fluctuations. However, the twin-peak technique suffers from additional systematic errors. On the one hand, the laser beam loses energy by passing the extra optics (chamber window, mirror and focal lens) resulting in a reduced laser intensity for the reflected beam. On the other hand, the incoming and reflected laser beam pass the molecular beam at different positions and especially in different distances to the inlet system. The molecular density at the two ionization spots is therefore also different. These two error sources can be seen as systematic errors due to the percentage loss of laser energy at each optical element as well as the percentage difference in molecular density at two fixed positions relative to the molecular beam inlet. These systematic errors can be erased by switching the circular polarization of the incoming laser beam from left- to right-circular or vice versa every 200 laser pulses and averaging over all measured g-values. This results in another definition for the anisotropy factor for twin-peak measurements as follows[66]

$$g_{TP} = \frac{g_{LR}+g_{RL}}{2} = \frac{I_{L_1}-I_{R_1}}{I_{L_1}+I_{R_1}} + \frac{I_{L_2}-I_{R_2}}{I_{L_2}+I_{R_2}} \quad [15]$$

with g_{LR} as g-value resulting from an incident left-circular (ion yield I_{L_1}) and reflected right-circular (ion yield I_{R_1}) polarized laser beam and g_{RL} for the opposing polarizations (I_{R_2} and I_{L_2} respectively for the incident and reflected laser beam). The twin-peak method becomes thereby again slightly laser intensity dependent due to laser fluctuations from the first 200 laser pulses to the second 200 laser pulses with the opposite circular polarization for the incoming laser beam. As already mentioned, those laser fluctuations on larger time scales can be identified and corrected by the reference method. Thus, a combination of both techniques results in a significant improvement of the experimental precision of CD-REMPI-MS measurements.[45]

The validity of anisotropy factor measurements with CD-REMPI-MS depends also on the existence of conformers of the sample molecule due to the fact that the structural variation of conformers leads to differences in their anisotropy factor. Under effusive beam conditions the sample molecules, that enter the gas phase depending on their vapor pressure, are in a thermal equilibrium with their surrounding environment. Therefore, the sample molecules have an internal temperature which is comparable to room temperature conditions and this results in the presence of different conformers, hot bands and an overlap of vibronic bands due to rotational broadening. For example, in the case of 3-MCP as sample molecule under room

temperature conditions an equatorial and an axial conformer exist in a relation of $0.78 : 0.22$.[76-77] Under room temperature conditions any CD measurement leads therefore to a similar related mixture of the g-values of both conformers. Furthermore, the typical rotational broadening of vibronic bands under room temperature conditions for aromatic molecules is about $200\,cm^{-1}$. These rotationally broadened vibronic bands overlap together with the additional hot bands to broad electronic transition absorption bands without an observable vibronic fine structure (see figure 2 of the second publication[66]). CD measurements on such an electronic transition provide only general information of its anisotropy factor which has to be seen as an averaged g-value of all overlapping vibronic transition and hot band g-values.

One possibility to allow for a reduced internal temperature of the investigated sample molecules and thus an increase of the spectral resolution of the CD-REMPI-MS technique is the usage of a supersonic beam instead of an effusive beam inlet system.[74, 76, 78] The chiral sample molecules are thereby seeded in a carrier gas ($\sim 2.8\,bar$ Argon) in a separated high pressure region. This high pressure region is connected to a prevacuum chamber ($\sim 5 \cdot 10^{-4}\,mbar$) via a pulsed valve with a 0.2 mm diameter nozzle (see figure 1b of the first publication[64]). The valve is pulsed simultaneously with the $30\,Hz$ laser systems. If the valve opens, the seeded chiral sample molecules expend together with the carrier gas into the prevacuum chamber and reach velocities above the speed of sound under these conditions. Due to the much larger orifice of the nozzle compared to the mean free path of the molecules, at the moment of opening the frequent collisions between the chiral sample molecules and the carrier molecules lead to a fast equalization of the translation movement in direction of the low pressure region. During the expansion the collision frequency drops rapidly and an adiabatic cooling occurs. Thereby, the internal energy of the sample molecules is transferred into translational energy. Finally, the collisions nearly stop and due to the low internal energy the energetically most stable conformer of the sample molecule persists (i.e. the equatorial conformer for 3-MCP). In addition, any vibrational excitations freeze out to the ground state (i.e. no hot bands are observable) and the rotational broadening (rotational temperature of $< 15\,K$)[74] is significantly reduced (see figure 2 of the second publication[66]). Furthermore, the prevacuum chamber is separated from the main chamber (i.e. ionization chamber with the ion source of the TOF-MS; $< 5 \cdot 10^{-6}\,mbar$) by a skimmer that can only be passed by the central part of the supersonic beam. This central part has the lowest internal temperature and residual translational degree of freedom. The supersonic beam-cooling thus allows for CD measurements on isolated vibronic transitions that can have varying and significantly higher anisotropy factors compared to effusive beam measurements due to the g-value averaging of different conformers and overlapping vibronic and hot bands under room temperature conditions.[74]

All those previous experimental improvements and observations around the CD-REMPI-MS technique gave the basis for any further developments performed during this thesis.[64, 66, 79]

1.4.3. Comparison between Quarter-Wave Plate and PhotoElastic Modulator (PEM)

As already mentioned in section 1.2.1.1, two main methods (the usage of a quarter-wave plate or a PEM) exist for the circular polarization of linear polarized laser light. An advantage of quarter-wave plates is their relative cheapness compared to a PEM. However, quarter-wave plates can only be used for a limited wavelength range of about $200\ nm$ due to their quite fixed dependence between their refraction index, thickness and resulting phase shift (see equation [4]). Therefore, a set of quarter-wave plates is necessary to allow for CD investigations on different sample molecules or measurements of varying electronic transitions of the same molecule. In addition, switching the quarter-wave plate leads always to slight alignment changes, and for the realignment new calibration measurements are required. Furthermore, the circular polarization due to the quarter-wave plate depends on the optical axis position relative to the linear polarization plane of the incident laser light, which have to be in a $\pm 45°$ angle to each other. For CD-REMPI-MS measurements a switch from left- to right-circular polarized light after each 200 laser pulses (i.e. with a laser repetition rate of $30\ Hz$ every seven seconds) is necessary and thus the quarter-wave plate has to be rotated by $90°$ ($+45°$ to $-45°$ angle relative to the incident linear polarization plane). This rotation is performed mechanically with the help of a stepper motor connected to the rotatable mounted quarter-wave plate. However, these rotations consume about half a second unused measurement time to ensure a finished mechanical movement of the quarter-wave plate. Furthermore, due to the mechanical character of the rotation the precision and reproducibility of the quarter-wave plate positioning after several CD measurements with 200 rotations each has to be tested by new calibration measurements.

In comparison to that, a PEM can cover a broad wavelength range of about $1800\ nm$. For example, the Hinds Instruments PEM-100, I/FS 50, used during this thesis works for a wavelength range of $170 - 2000\ nm$.[35, 80] Another advantage of the PEM is the periodical change from left- to right-circular polarized light and vice versa with a resonance frequency of $50\ kHz$ (i.e. a period of $20\ \mu s$). This high frequency has to be synchronized with the $30\ Hz$ repetition rate of the used pulsed laser systems and allows theoretically for a change from left- to right-circular polarization from pulse to pulse. The polarization change is thereby electronically and not time limited by any mechanical movement, which reduces the reproducibility of the circular polarization, like in the case of quarter-wave plate rotations. Thus, only one alignment and calibration measurement should be necessary for CD-REMPI-MS

measurements on various chiral sample molecules over an unlimited period of measurement intervals. Therefore, as first development of the CD-REMPI-MS technique a PEM-100, I/FS 50, by Hinds Instruments was implanted in the experimental setup to replace the previously used set of quarter-wave plates.

For the calibration measurements of the PEM (i.e. the correct synchronization of the laser pulses with the PEM phase delay for left- or right-circular polarization) or the quarter-wave plate an experimental setup comparable to a polarimeter (see section 1.2.1.2) is used in combination with a LabVIEW program (see appendix C.2.1). The incident pulsed and linear polarized laser beam is at first attenuated by a Brewster-window and aperture to allow for measurements with photodiodes which saturate if the light intensity is to high (see figure 4). Even if laser light should theoretically be linear polarized, a first Glan-Taylor(-Foucault) prism[81] is used as polarizer to determine a perfect linear polarization in a $45°$ angle relative to the deformation axis of the birefringent fused silica PEM crystal or the optical axis of the quarter-wave plate. The part of the laser beam with a slightly different polarization plane is reflected by the Glan-Taylor prism to a reference-photodiode, while the main laser beam passes the PEM or quarter-wave plate. The afterwards e.g. circular polarized laser beam has to pass a second Glan-Taylor prism that is set in a $90°$ angle relative to the first polarizer. Thus, solely light polarized perpendicular to the previous linear polarization plane defined by the first polarizer (i.e. vertical linear polarization if the first polarizer was passed solely by horizontal linear polarized light or vice versa) can pass the second polarizer. Theoretically circular polarized light can be seen as a superposition of two linear polarized light components with an equal intensity that are phase shifted by $\frac{\pi}{2}$ (see section 1.2.1.1). Thus, after passing the second polarizer the measurable laser intensity at the signal-photodiode should vanish, if the PEM or quarter-wave plate does not change the polarization of the linear polarized laser beam. If the linear polarization plane is turned by $90°$, the measurable signal should be maximized (full laser intensity) and intermediate (half laser intensity), if the laser beam is circular polarized. Finally, the laser beam intensity measured by the signal-photodiode is normalized to the reference-photodiode signal to compensate laser intensity fluctuation during the calibration measurements.

A quarter-wave plate is not able to turn the linear polarization plane[10] and thus the measurable laser intensity can only be changed from zero (the optical axis is parallel or perpendicular to the linear polarization plane and does not change the laser beam polarization) to halve the maximum laser intensity (the optical axis is in a $45°$ angle relative to the incident linear polarization plane and leads to circular polarized light). The handedness of the circular

[10] For turning the linear polarization plane of incident linear polarized light a halve-wave instead of a quarter-wave plate can be used.

polarized light can thereby not be determined by the measured laser intensity but by knowledge of the incident linear polarization plane and observation of the angle of the optical axis relative to it. For all alignments in between the laser beam polarization is elliptical and the measurable laser intensity depends on the reached ellipticity.

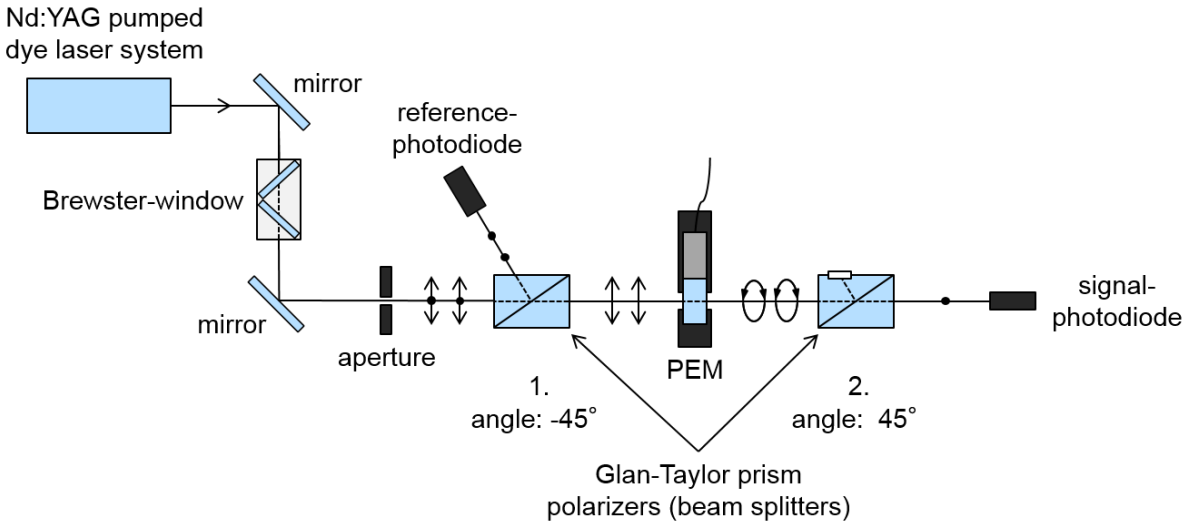

figure 4: PEM polarization test setup for a pulsed Nd:YAG pumped dye laser system. The dye laser beam is attenuated by a Brewster-window combined with an aperture to allow for measurements with beam intensities suitable for the photodiodes. The probably not totally linear polarized laser beam is filtered by a first polarizer (Glan-Taylor prism) in a $45°$ angle to the crystal axis of the PEM. The thereby reflected laser intensity is measured by a reference-photodiode to allow for reference correction of the signal-photodiode intensity relative to the absolute laser intensity. The PEM changes the laser beam polarization from linear to circular or elliptic (or does nothing while the crystal is in his relaxed state) and the polarization is analyzed by a second polarizer in a $-45°$ angle (90° relative to the first polarizer). Thus, the analyzer is solely passed by the opposing linear polarization alignment (vertical or horizontal) compared to the first polarizer. During one period of the PEM the laser intensity therefore vanishes twice (relaxed PEM crystal) and becomes twice maximal (about have the absolute laser intensity behind the first polarizer) for the two circular polarization positions (full stretched or compressed PEM crystal).

A PEM in quarter-wave retardation mode[11],[80] behaves quite similar to a quarter-wave plate with maximum laser intensity (halve of the incident laser intensity) in case of circular polarization, when the fused silica crystal is either fully stretched or compressed. The signal intensity vanishes, if the PEM crystal is relaxed and the linear polarization is not changed at all. Different from the quarter-wave plate with its angle dependence relative to the linear polarization plane of the incident laser beam, these polarization changes occur for the PEM dependent on the time at which the laser beam passes the PEM. Within the already mentioned period of $20\ \mu s$ (see figure 2) of the used PEM for this thesis two phase delays exist at which the PEM is relaxed (i.e. vanishing laser intensity at the signal-photodiode) and two phase delays result in opposing circular polarizations (i.e. half of the incident laser intensity). However, the handedness of the circular polarized light cannot be determined with this

[11] At this point it should be mentioned that the PEM is able to run in a half-wave retardation mode and thus can also be used similar to a half-wave plate. In this mode, the applied sinusoidal voltage amplitude is higher and leads to a higher full extension and compression of the fused silica crystal which is able to reach a birefringence sufficient for halve-wave retardation. This mode has also been testes during this thesis but was not relevant for the CD investigations shown in section 2.

experimental setup. Instead either a combination of the PEM plus an additional quarter-wave plate or a test CD measurement with a known chiral molecule is necessary.

A full period calibration measurement for the PEM can be seen in figure 5. The black curve (squares) shows a perfect calibration with relaxed PEM (unchanged linear polarization) at phase delays of $0.6\ \mu s$ and $10.6\ \mu s$ and fully compressed or stretched PEM crystal (left-/right-circular polarized light) at phase delays of $5.6\ \mu s$ and $15.6\ \mu s$. Especially the measured reference corrected laser intensity for both circular polarization handedness is similar as expected. If the $30\ Hz$ laser beam pulsing is synchronized to these phase delays (i.e. coincident passing of the laser beam at these phase delays), the afterwards circular polarized laser beam can be used for CD investigations by simple electronically switching the synchronization from $5.6\ \mu s$ to $15.6\ \mu s$ and vice versa. However, the red calibration curve (diamonds) shows the same measurement just three hours earlier with a laser intensity difference of $\sim 10\%$ between the two circular polarizations with opposing handedness. This effect often occurred during PEM calibration test measurements and could not be explained or actively influenced. Neither alignment changes of the PEM relative to the incident light in sense of small angle changes or repositioning of the beam path (slightly decentral pathing) nor laser intensity or temperature changes[12] enabled to control this unequal laser intensity for left- and right-circular polarization during calibration measurements. Seen from the principle of the calibration measurement method, at this point it had to be assumed that the used PEM did not function properly as a quarter-wave plate when the laser beam intensity of the two circular polarization phase delays is not equal.[13] Instead, the measured laser intensity difference hints to a slight ellipticity at the phase delays with maximum laser intensities. These non-reproducible and controllable problems during the PEM calibration could not be solved nor the reason for their appearance be identified during this thesis.

[12] The Hinds Instruments support expected either a heat up of the crystal due to the incident laser beam intensity or an uneven cooling due to air conditioning in the lab as reason for the strange calibration curve results. Furthermore, it has to be mentioned that the here shown time dependence which might hint to coincidence with a laser heat up phase could not be reproduced and contrary calibration curve behaviors were recorded (i.e. similar intensity at the beginning and different intensities after some hours).

[13] Compared to the PEM each calibration measurement performed with a quarter-wave plate (i.e. a full "period" as a full rotation of the quarter-wave plate by the stepper motor) showed similar maximal laser intensities for the two positions with circular polarization as expected.

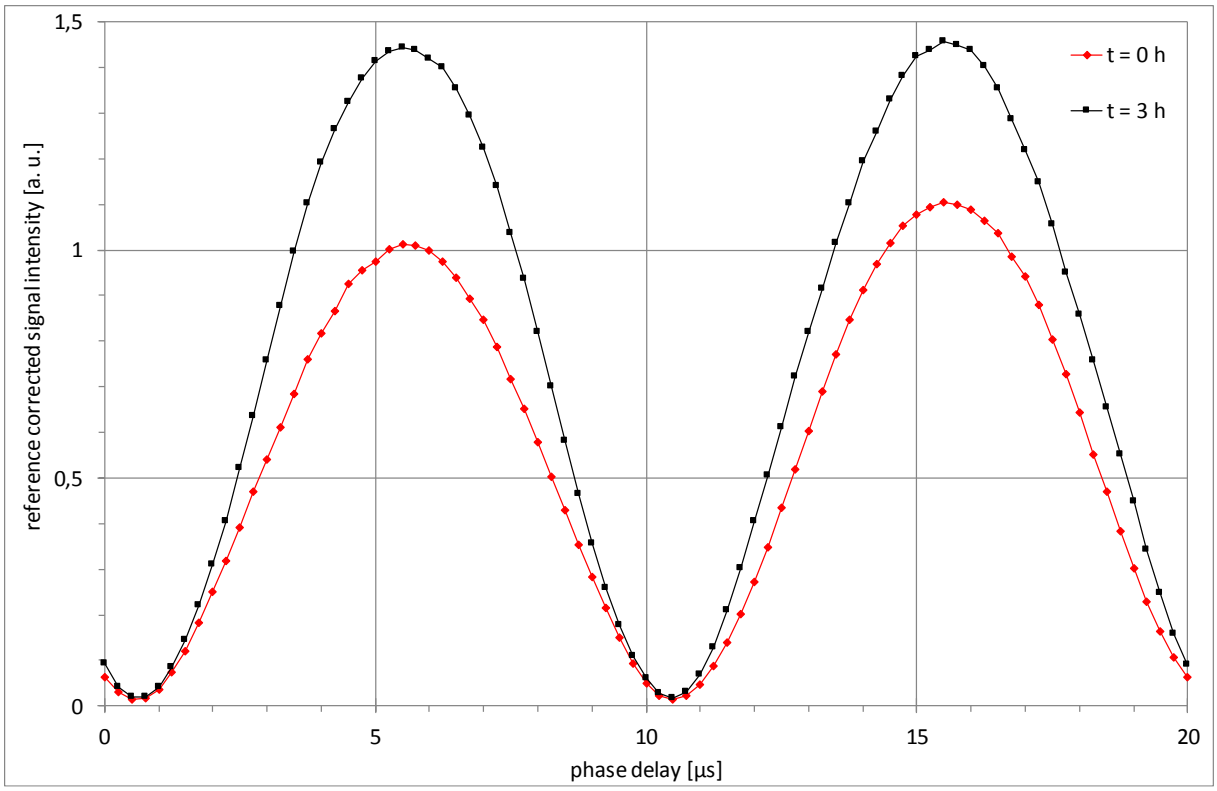

figure 5: Two PEM polarization test measurements recorded with the test setup shown in figure 4. The phase delay of one complete PEM period ($20\ \mu s$) has been once scanned before the first PEM CD investigation (see figure 6) at 01.07.2014 (red curve; $t = 0\ h$) and once after all CD measurements three hours later at the same day (black curve; $t = 3\ h$). The absolute reference corrected signal intensity measured by the signal-photodiode can solely be compared within one measurement and not between the two measurements due to alignment and aperture opening differences.

Therefore, the effect of the observed irregularities in the calibration curve was tested in real CD investigations with the CD-REMPI-MS setup (see figure 1b of the first publication[64]) by comparing quarter-wave plate and PEM results. The CD measurements have been performed on the $n \rightarrow \pi^*$ transition ($18_0^4 25_0^1$) of supersonic beam-cooled d_4-(R)-(+)-3-MCP with (1+1')-REMPI (see figure 1a of the first publication[64]). The results for two series of data measured with a PEM at two different dates as well as two series of data measured with a quarter-wave plate also at two different dates are shown in figure 6. Beside the supersonic beam-cooled d_4-(R)-(+)-3-MCP, effusive beam d_4-CP was measured to allow for a reference correction of the g-values. For an observation of an expectable saturation effect the dye laser energy ($324.454\ nm$) was varied, while the ionization laser ($213\ nm$) was fixed to an energy of $0.5\ mJ$. However, the absolute anisotropy factor or the saturation effect are not of special interest at this point,[14] but the g-values measured with a PEM in comparison to the quarter-wave plate results are similar within the error margins. The already mentioned two calibration curves (see figure 5) represent thereby the PEM calibration situation before and after the CD investigations from 01.07.2014. It can be concluded that, if the calibration curve intensity

[14] An explanation of the CD-REMPI-MS measurement principle can be found in the previous sections and a detailed description of the experimental conditions with d_4-(R)-(+)-3-MCP as sample is given in section 2.1. The results are equivalent to the measurements shown in figure 4 of the first publication.

difference has a real effect on CD measurements due to residual ellipticity, the influence is smaller than the experimental error margins. Thus, the PEM was used due to its advantages compared to a quarter-wave plate for the CD-REMPI-MS investigations that led to the two publications[64, 66] presented in this thesis.

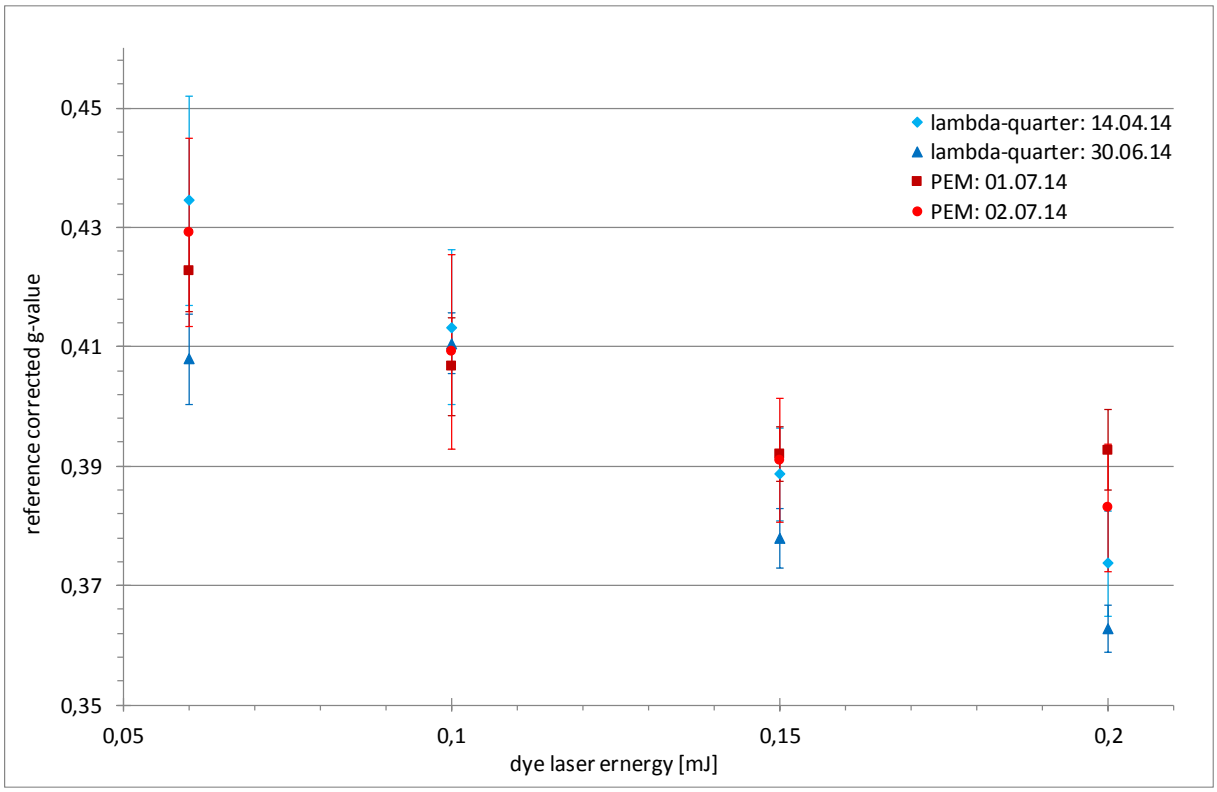

figure 6: CD investigation of the $n \rightarrow \pi^*$ transition ($18_0^4 25_0^1$) of supersonic beam-cooled d₄-(R)-(+)-3-MCP with (1+1')-REMPI. The shown g-values have been reference corrected with effusive beam d₄-CP measurements. During the CD measurements the ionization laser ($213\,nm$) had a fixed energy of $0.5\,mJ$, while the dye laser energy ($324.454\,nm$) was varied for an observation of the saturation effect. The measurements are equivalent to the results shown in figure 4 of the first publication[64]. For a comparison of quarter-wave plate and PEM for the circular polarization of the dye laser beam, each measurement has been done four times, twice with a quarter-wave plate (teal diamonds; blue triangles) and twice with a PEM (dark red squares; red circles) at two different dates.

2. Results

The overall development of the CD-REMPI-MS technique during this thesis is presented based on two publications[64, 66] which are shown and discussed in detail in the following sections. The measurements for the first publication[64] are mainly focused on the possibility to enhance the anisotropy factor by excitation of single vibronic transitions of supersonic beam-cooled d_4-(R)-(+)-3-methylcyclopentanone (d_4-(R)-(+)-3-MCP). The results led thereby to ideas for improvements of the experimental setup which were performed between the first and second publication. The focus of the second publication lays more on an increase of the experimental precision by a combination of supersonic beam and twin-peak technique with a new single laser pulse evaluation. Furthermore, the second publication shows measurements of (R)-(+)-1-phenylethanol as a common example for an asymmetric catalysis product. Those measurements represent the actual status of the experiment and thus of the CD-REMPI-MS technique in general.

2.1. Mass-selected Circular Dichroism of Supersonic Beam-Cooled d_4-(R)-(+)-3-Methylcyclopentanone

The CD-REMPI-MS setup used for this publication[64] enabled for the first time CD measurements on supersonic beam-cooled d_4-(R)-(+)-3-MCP with a PEM. Due to an enhancement of the anisotropy factor by single vibronic transition excitation, the results show the highest g-value ever measured in liquid or gas phase.

2.1.1. Summary and Author Contribution

Previous publications[74, 76] on supersonic beam-cooled (R)-(+)-3-MCP already revealed the high potential of CD-REMPI-MS measurements with nanosecond laser systems combined with supersonic beam-cooling. Due to the effective freeze-out of the at room temperature excited vibrations (resulting in hot bands) and the reduced broadening by rotations, supersonic beam-cooling allows for excitation of isolated vibronic transitions from the absolute ground state. In addition, the cold sample molecules can be expected to exist only in their most stable conformer form which prevents a mixing of anisotropy factors from various conformers during ECD measurements.[77] Depending on the excited vibrational modes, the isolated vibronic transitions can have significantly differing anisotropy factors. Thus, (1+1')-REMPI of the $n \rightarrow \pi^*$ transition of (R)-(+)-3-MCP showed for isolated vibronic transitions with an involved ring-twisting mode (ν_{18}) the highest g-values with up to $+(42.1 \pm 1.1)\%$ (for $18_0^4 25_0^1$).[74]

2.1. Mass-selected Circular Dichroism of Supersonic Beam-Cooled d4-(R)-(+)-3-Methylcyclopentanone

Based on these previous findings, the first publication[64] presented here shows CD-REMPI-MS measurements on effusive as well as supersonic beam-cooled d_4-(R)-(+)-3-MCP and thus for another but comparable molecule to (R)-(+)-3-MCP. The necessary assignment of the vibronic transitions in case of the supersonic beam measurements has been enabled by comparison of the (1+1')-REMPI supersonic beam spectra of d_4-(R)-(+)-3-MCP and d_4-CP (as achiral reference molecule) with the spectra of (R)-(+)-3-MCP and CP. The supersonic beam-cooling of d_4-(R)-(+)-3-MCP was thereby sufficient for a separation of the P, Q and R rotational branches of the corresponding $18_0^4 25_0^1$ vibrational mode of the $n \rightarrow \pi^*$ transition. Therefore, for the first time CD investigations on the rotational branches of a vibronic transition have been performed with (1+1')-REMPI. In addition to those (1+1')-REMPI measurements, (1+1+1)-REMPI measurements have been done to allow for a view on the influence of the second resonant electronic transition ($\pi^* \rightarrow 3d$) on the anisotropy factor in comparison to the previous results for (R)-(+)-3-MCP.[74] As final proof of the possible enhancement of the anisotropy factor due to single vibronic excitations of a certain vibrational mode, some (1+1')-REMPI and (1+1+1)-REMPI measurements have been made under effusive beam (room temperature) conditions.

The described measurements presented in this publication were performed in equal shares by the authors J. Lepelmeier and K. Titze.

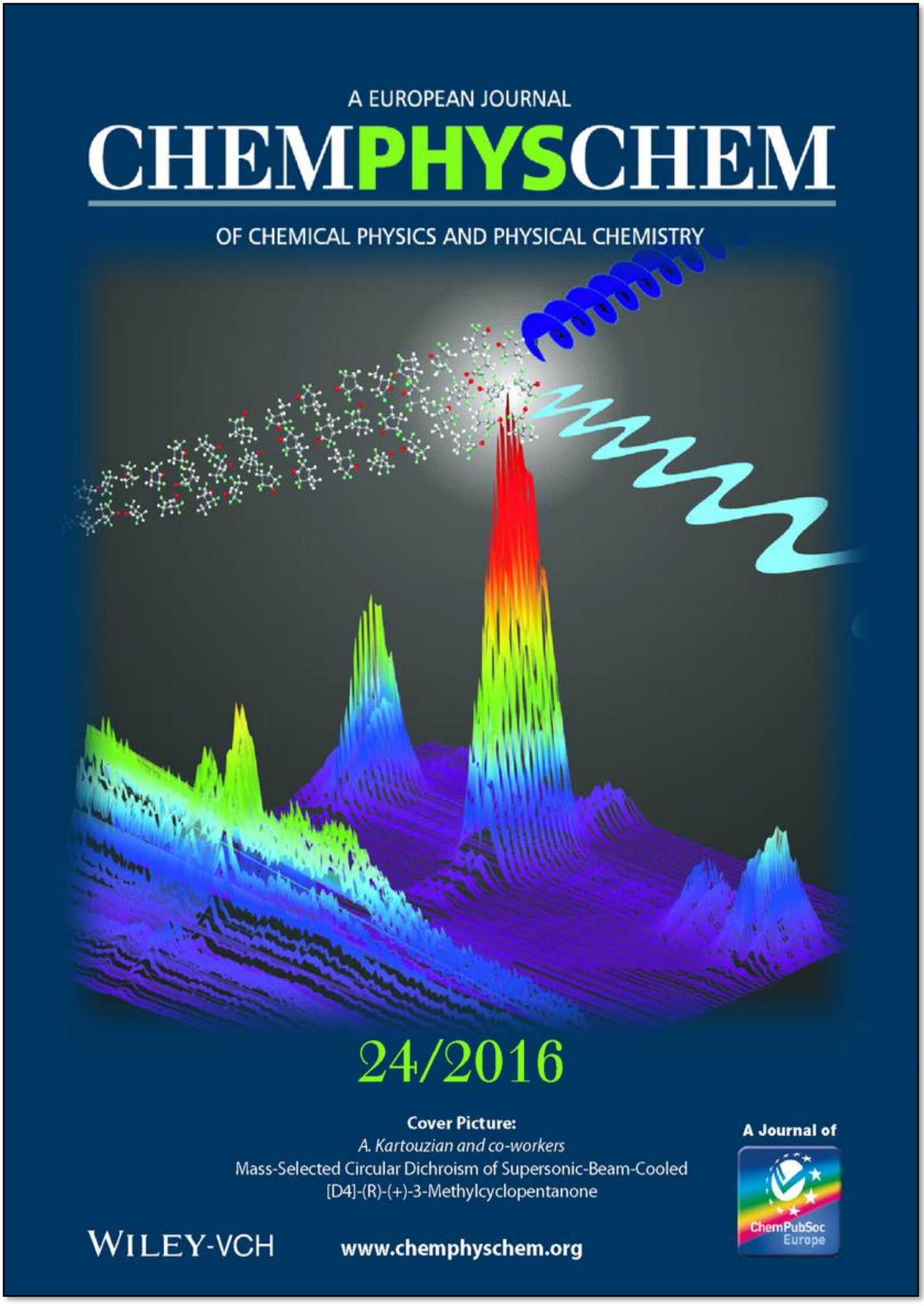
A EUROPEAN JOURNAL
CHEMPHYSCHEM
OF CHEMICAL PHYSICS AND PHYSICAL CHEMISTRY
24/2016
Cover Picture:
A. Kartouzian and co-workers
Mass-Selected Circular Dichroism of Supersonic-Beam-Cooled
[D4]-(R)-(+)-3-Methylcyclopentanone
A Journal of
ChemPubSoc
Europe
WILEY-VCH
www.chemphyschem.org

ChemPubSoc Europe

DOI: 10.1002/cphc.201600811

CHEMPHYSCHEM Articles

Mass-Selected Circular Dichroism of Supersonic-Beam-Cooled [D_4]-(*R*)-(+)-3-Methylcyclopentanone

Jörn Lepelmeier, Katharina Titze, Aras Kartouzian,* Ulrich Boesl, and Ulrich Heiz[a]

UV spectroscopy and electronic circular dichroism (ECD) experiments on supersonic-beam-cooled deuterated (*R*)-(+)-3-methylcyclopentanone ([D_4]-(*R*)-(+)-3-MCP) have been performed by using a laser mass spectrometer. The spectral resolution not only allowed excitation and CD measurements for single vibronic transitions but also for the rotational P, Q, and R branches of these transitions. The investigated $n \rightarrow \pi^*\left(18_0^4 25_0^1\right)$ transition showed the largest anisotropy factor ever observed for chiral molecules in the gas phase, which, due to residual saturation of the excited transition, represents only a lower limit for the real anisotropy factor. Furthermore, one-color (1 + 1 + 1) and two-color (1 + 1′) resonance-enhanced multiphoton ionization (REMPI) measurements were performed and the effusive-beam (room temperature) and supersonic-beam results for [D_4]-(*R*)-(+)-3-MCP were compared. These results allowed a differentiation between single-step ECD (comparable to conventional ECD) and cumulative ECD (only possible in multiphoton excitation) under supersonic-beam conditions.

1. Introduction

In several aspects of life and, therefore, in diverse fields of science from physics to chemistry, and particularly in the pharmaceutical and food industries, chiral molecules are of considerable importance. The impact of each enantiomer could be contrary, for example, one enantiomer may be an effective cure, whereas the other enantiomer is poisonous. Therefore, fast and sensitive analytical tools are necessary to provide information about the enantiomeric excess of chiral molecules under various conditions, such as different aggregate states, in mixtures with other molecules, or as products of asymmetric catalytic processes. To this end, chiroptical spectroscopy (circular dichroism (CD) and optical rotation dispersion (ORD)) are the most commonly used direct techniques.[1–3] In addition to the widespread application of chiroptical spectroscopy in the liquid phase for characterization purposes,[4–5] various methods have been developed to study chiral systems in the gas phase[6–11] and at surfaces and interfaces.[12–14] CD utilizes the absorption difference of left- and right-circularly polarized light depending on the enantiomer of a chiral molecule (CD effect). It also allows several combinations with other nonenantioselective analysis techniques, such as angular-resolved photoelectron spectroscopy,[15–16] nonlinear two-photon spectroscopy,[17–18] and mass spectrometry (MS).[17–20]

In addition to CD spectroscopy (with its enantiosensitivity) and MS (with its mass selectivity), resonance-enhanced multiphoton ionization (REMPI)[21–23] with its wavelength and, therefore, molecule-species selectivity was used in the presented experiment. The CD-REMPI-MS method provides a highly selective and sensitive analytical tool, even for mixtures of chiral and achiral molecules in the gas phase, such as in asymmetric catalysis.[24–27] This technique was combined with supersonic-beam cooling[28–30] to achieve a higher spectroscopic resolution. Benefiting from this improved spectral resolution, it was recently demonstrated by using one-color CD-REMPI-MS that single vibronic transitions can possess very different anisotropy factors[31] in accordance with theoretical predictions.[32–33] In particular, excitations of the ring-twisting mode (ν_{18}) in (*R*)-(+)-3-MCP showed a significant increase in the anisotropy factor compared with effusive-beam measurements.[31] The higher anisotropy factors of such single vibronic transitions are of special interest because they could facilitate the distinction between the enantiomers of a chiral molecule. This is advantageous, for example, for enantiomeric-excess measurements[34] by using CD-REMPI-MS. In these measurements, the ratio of enantiomers is determined by the residual *g* value of an unknown mixture, which depends greatly on the absolute measurable anisotropy factor of an enantiopure sample in comparison. Motivated by this, the dependence of the anisotropy factor on rovibronic transitions based on a ring-twisting vibration (ν_{18}) in [D_4]-(*R*)-(+)-3-MCP is investigated herein. The comparison of supersonic-beam-cooled spectra of protonated and deuterated 3-MCP and CP has, therefore, allowed the spectral assignment of [D_4]-(*R*)-(+)-3-MCP. Finally, by comparing one- and two-color CD-REMPI-MS, the partial contributions of different excitation steps in the multiphoton ionization to the anisotropy factor were evaluated to investigate the influence of subsequent excitation steps in one-color (cumulative) ECD under supersonic-beam conditions.

[a] *J. Lepelmeier, Dr. K. Titze, Dr. A. Kartouzian, Prof. U. Boesl, Prof. U. Heiz*
Technische Universität München
Lehrstuhl für Physikalische Chemie
Lichtenbergstr. 4
85748 Garching (Germany)
E-mail: aras.kartouzian@tum.de

Experimental Section

The experimental setup used here (see Figure 1b) has already been explained in detail in previous works.[6,18,31] It consists of two separately pumped vacuum chambers connected through a skimmer as the supersonic-beam inlet. Inside the smaller prevacuum chamber in front of the skimmer, a pulsed general valve with a nozzle (0.2 mm diameter) was used to create the supersonic beam. The pulsing frequency of the valve was synchronized to the 30 Hz repetition rate of the laser systems used. The backpressure of the argon carrier gas was set at 2.8 bar, which gave a pressure of 5×10^{-4} mbar within the chamber during measurements. During the experiment, the pressure within the main chamber, which contained an additional effusive-gas-beam inlet, an ion source, and a time-of-flight mass spectrometer (TOF-MS) with a multichannel plate, was 2×10^{-6} mbar (without an active gas inlet, the pressure was 2×10^{-7} mbar). The applied linear TOF-MS followed the design of Wiley and McLaren.[35] The prevacuum chamber with the skimmer, and thus the supersonic-beam inlet, was perpendicular to the axis of the ion-source optics and TOF within the main chamber, whereas the effusive-beam inlet, through a nozzle in the middle of the repeller plate, was collinear to that axis.

For the resonance excitation of the investigated molecules, [D_4]-(*R*)-(+)-3-MCP and [D_4]-CP were injected into the main chamber through the effusive- or supersonic-beam inlet, and a Nd:YAG (Spitlight Hybrid by InnoLas Laser) pumped dye laser (Pulsare by Fine Adjustment) with a spectral linewidth of 0.04 cm^{-1} was used. The wavelength range of $\lambda = 315 - 335$ nm suitable for the sample molecules was generated by using the frequency-doubled emission of DCM [4-(dicyanomethylene)-2-methyl-6-(4-dimethylamino-styryl)-4H-pyran] dissolved in DMSO ($\lambda = 630–670$ nm). To investigate the anisotropy factor of [D_4]-(*R*)-(+)-3-MCP by using CD spectroscopy, a photoelastic modulator (PEM-100 by Hinds Instruments) was employed for circular polarization of the linear laser light.[36] This optical system, tunable in wavelength and polarization, was used for excitation and ionization through the resonant absorption of three photons via two intermediate states in a one-color (1+1+1)-REMPI process (see Figure 1a). In addition, the fifth harmonic ($\lambda = 213$ nm) of a second Nd:YAG laser (Spitlight Hybrid by InnoLas Laser) was used for two-color (1+1′)-REMPI studies. In this case, the dye laser resonantly excited the sample molecules to the first intermediate state before they were ionized by consecutively absorbing a $\lambda = 213$ nm photon instead of another two dye laser photons. Ions produced in these REMPI processes were afterwards mass separated and detected by using TOF-MS.

2. Results and Discussion

As already described, CD-REMPI-MS allows the simultaneous measurement of different types of molecules, for example, a chiral molecule mixed with an achiral molecule. Because an achiral molecule has, by definition, an anisotropy factor (*g* value) of zero, it can be used as a reference to correct systematic errors in the experimental setup. This results in a definition for the reference-corrected *g* value as described in previous works:[10,18]

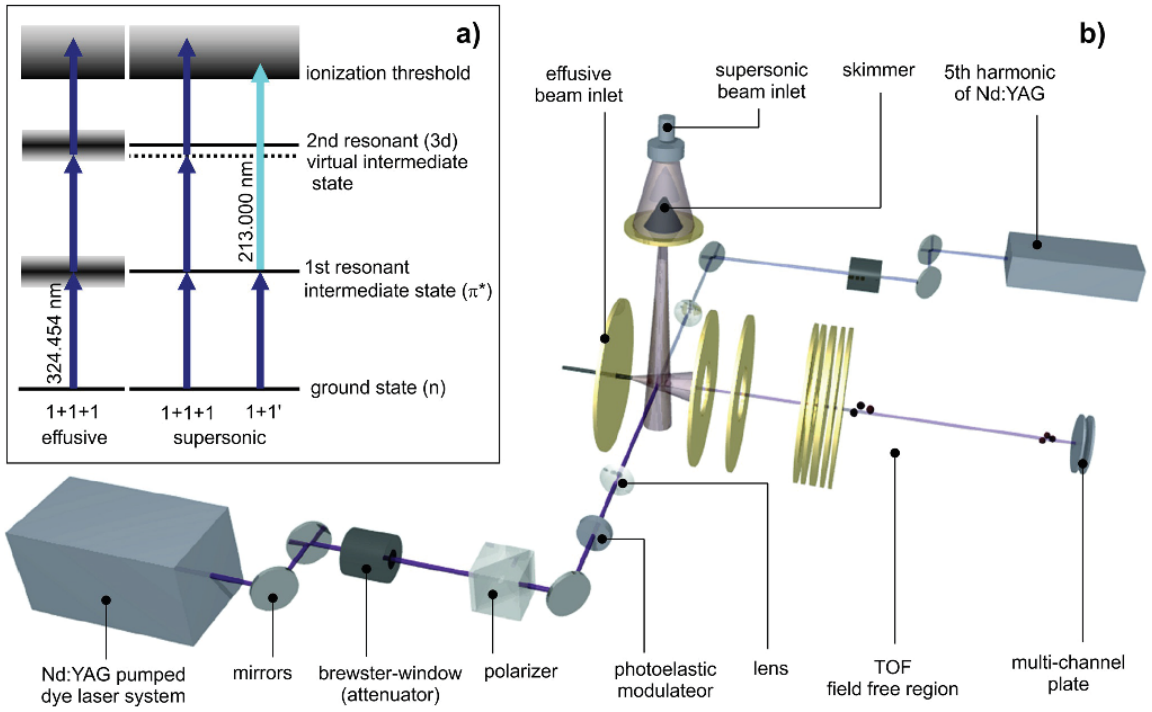

Figure 1. a) Excitation scheme for a (1+1+1)-REMPI process in effusive and supersonic beams and a (1+1′)-REMPI process in a supersonic beam are shown for [D_4]-3-MCP. b) The experimental setup is illustrated schematically with two laser systems for one- or two-color measurements and a prevacuum chamber that consists of a supersonic-beam inlet separated from the main chamber by a skimmer. The main vacuum chamber consists of an effusive-beam inlet in line with the ion-source optics (perpendicular to the supersonic beam) and TOF with a multichannel plate.

$$g = 2\frac{I_L - I_R}{I_L + I_R} \quad (1)$$

$$g_{corr} = g_{ana} - g_{ref} \quad (2)$$

in which the ion yields I_L and I_R obtained with left- or right-circularly polarized light for the resonance excitation of analyte (g_{ana}) and reference (g_{ref}) molecules. The difference between g_{ana} and g_{ref} then leads to the reference-corrected anisotropy factor (g_{corr}). One g value was achieved by averaging over 50 measurements. Each consisted of ion signals from 400 laser pulses; 200 with left-circularly polarized light and 200 with right-circularly polarized light.

Depending on the chiral analyte, an achiral reference molecule was chosen with a very similar structure, a different mass, and comparable absorption properties. Herein, [D_4]-CP was chosen as the reference for chiral analyte [D_4]-(*R*)-(+)-3-MCP. The spectra of supersonic-beam-cooled [D_4]-(*R*)-(+)-3-MCP, (*R*)-(+)-3-MCP, [D_4]-CP, and CP from resonance excitation of the $n \rightarrow \pi^*$ transition by using the dye laser, and subsequent ionization with the second Nd:YAG laser ((1 + 1′)-REMPI) are depicted in Figure 2. For the CP spectrum, the 0_0^0 transition and the most significant vibrational modes $18_0^2 25_0^1$, 25_0^2, $18_0^2 25_0^2$, and $18_0^4 25_0^1$ have been assigned with the support of theory,[37] as explained in detail in a previous work.[31] The spectrum of [D_4]-CP shows a similar pattern with a redshift of about 30 cm^{-1} (10 cm^{-1} for the 0_0^0 transition) compared with CP, which allows a confident assignment of the same vibrational modes (see Table 1). In addition to the peaks due to the methyl group, these vibrational modes can also be identified in the spectra of (*R*)-(+)-3-MCP and [D_4]-(*R*)-(+)-3-MCP. Again, a redshift of about 30 to 40 cm^{-1} (11 cm^{-1} for the 0_0^0 transition) for the spectrum of [D_4]-(*R*)-(+)-3-MCP compared with (*R*)-(+)-3-MCP can be seen. It should be noted that the equatorial-to-axial population ratio of 3-MCP is expected to be 78:28% at room temperature. At the extremely low temperatures achieved by supersonic-beam cooling, however, only the most stable (equatorial) conformer exists and thus we assume a negligible influence due to multiple conformers.

All vibrational modes marked in Figure 2 and represented in Table 1 consist of a CO out-of-plane bending mode (ν_{25}), whereas three modes are combined with a ring-twisting mode (ν_{18}). Previous (*R*)-(+)-3-MCP measurements[31] showed that the contribution of a ν_{18} mode can lead to large anisotropy factors of up to $+(42.1 \pm 1.1)\%$ ($18_0^4 25_0^1$) compared with a pure ν_{25} mode with $+(3.6 \pm 0.2)\%$ (25_0^2). Therefore, the supersonic-

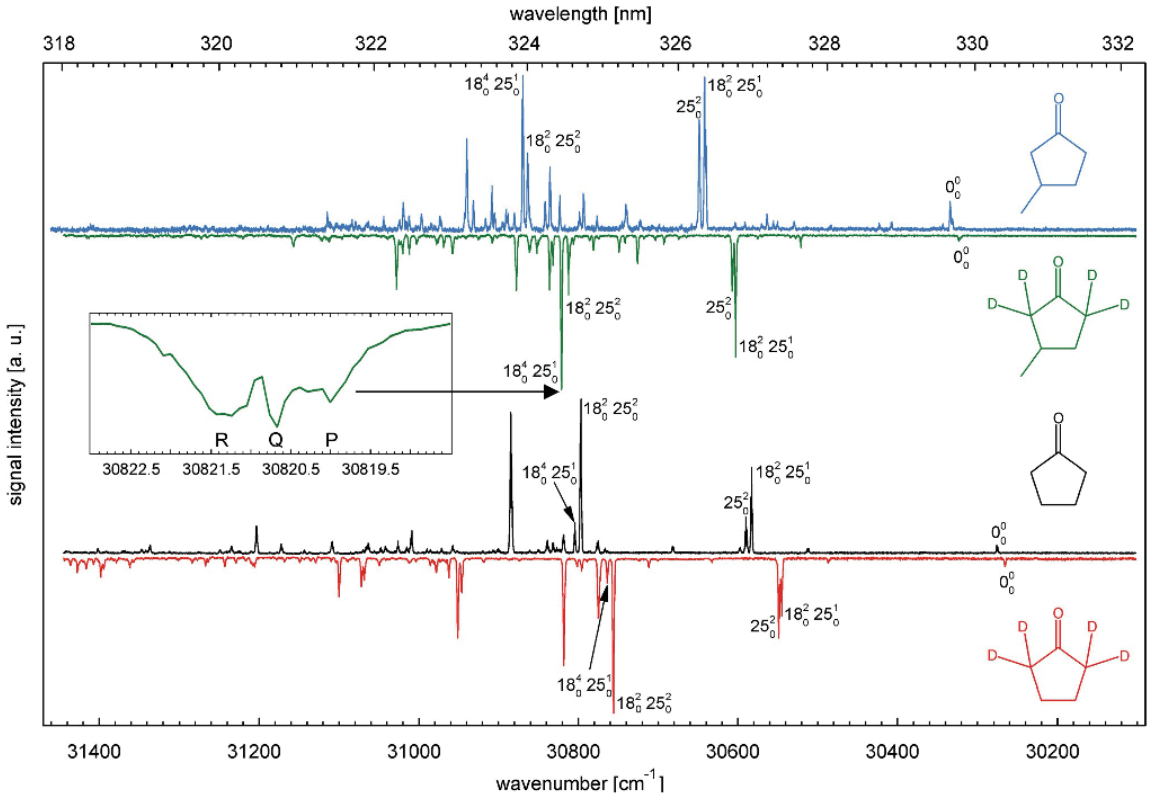

Figure 2. UV spectrum of the $n \rightarrow \pi^*$ transition of (*R*)-(+)-3-MCP (blue), [D_4]-(*R*)-(+)-3-MCP (green), CP (black), and [D_4]-CP (red) in a supersonic beam measured with (1 + 1′)-REMPI. In the shown range of 31 460–30 100 cm^{-1}, the 0_0^0 transitions and some low-frequency vibronic transitions ($18_0^2 25_0^1$, 25_0^2, $18_0^2 25_0^2$, and $18_0^4 25_0^1$) are indicated. Inset: The vibronic transition $18_0^4 25_0^1$ of [D_4]-3-MCP with its resolved P, Q, and R branches (at 30 820.0, 30 820.7, and 30 821.3 cm^{-1}, respectively).

Table 1. Measured frequencies for the 0_0^0 transition and the vibrational modes $18_0^2 25_0^1$, 25_0^2, $18_0^2 25_0^2$, and $18_0^4 25_0^1$ for CP, [D_4]-CP, (*R*)-(+)-3-MCP, and [D_4]-(*R*)-(+)-3-MCP. All vibrational modes are shown relative to their 0_0^0 transition. Furthermore, the redshift of [D_4]-CP and [D_4]-(*R*)-(+)-3-MCP relative to CP and (*R*)-(+)-3-MCP are represented by their calculated positive-frequency differences.

Vibrational mode	CP [cm^{-1}]	[D_4]-CP [cm^{-1}]	Difference [cm^{-1}]	3-MCP [cm^{-1}]	[D_4]-3-MCP [cm^{-1}]	Difference [cm^{-1}]
0_0^0	(30276)	(30266)	10	(30334)	(30323)	11
$18_0^2 25_0^1$	307	279	28	308	280	28
25_0^2	314	283	31	314	284	30
$18_0^2 25_0^2$	521	490	31	529	489	40
$18_0^4 25_0^1$	528	498	30	536	498	38

beam measurements for [D_4]-(*R*)-(+)-3-MCP presented here were performed on the $18_0^4 25_0^1$ transition with [D_4]-CP as an achiral reference molecule. It is obvious that resonance excitation of the transitions in both molecules in a supersonic beam is not possible with the same wavelength as long as their narrowed transition bands do not overlap (see Figure 2). The employed experimental setup, however, allows CD-REMPI-MS measurements of molecules injected into the vacuum chamber by a supersonic and an effusive beam at the same time. Thus, both gas inlets were used to enable the simultaneous measurement of supersonic-beam-cooled [D_4]-(*R*)-(+)-3-MCP as the chiral analyte and room-temperature [D_4]-CP as the achiral reference injected through the effusive beam. It should be noted here that because the reference molecule is provided effusively whereas the analyte is in a supersonic jet, the reference corrections described above should be handled with extra care because concentration fluctuations in the gas inlets are not necessarily correlated.

The anisotropy factors presented in Figure 3 for the (1 + 1′)-REMPI of [D_4]-(*R*)-(+)-3-MCP by resonance excitation of the $n \rightarrow \pi^*$ vibronic transition $18_0^4 25_0^1$ are reported for the three rotational branches (P, Q, and R; see Figure 2, inset). During all measurements, the intensity of the ionization laser was fixed, whereas the intensity of the dye laser was varied to monitor a decrease in the anisotropy factor due to saturation of the involved transition, as observed in previous works.[11,31] The dye-laser intensity was changed by varying the pulse energy, which was measured outside the vacuum chamber. Therefore, the absolute laser intensities, which depended on the pulse energy and the beam focus within the overlap region of the laser and molecular beam inside the vacuum chamber, were estimated.

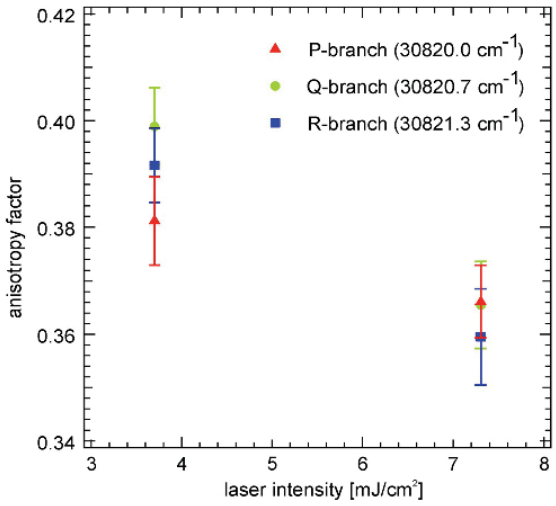

Figure 3. Measurements of the anisotropy factor of [D_4]-(*R*)-(+)-3-MCP for the three rotational branches (P, Q, R) of the vibronic transition $18_0^4 25_0^1$ with (1 + 1′)-REMPI for two different dye-laser intensities.

The results reveal that, within the error margins of our method, the anisotropy factor is not influenced by the rotational branches ($\Delta J = [-1, 0, +1]$ for the P, Q, and R branches, respectively). However, the spectroscopic resolution was not sufficient to resolve single rovibronic transitions. Therefore, the resulting anisotropy factors are averaged values over several transitions of the separately investigated rotational branches, and thus a dependence on different single rovibronic transitions cannot be excluded. Furthermore, the increase in the anisotropy factor observed as the dye-laser intensity was decreased indicates a saturation effect of the transition to the resonant intermediate state, as described previously for other vibronic transitions of (*R*)-(+)-3-MCP.[11,31] The essentially similar saturation behavior of the three branches studied here further supports the conclusion that the anisotropy factor is not altered by individual rotational branches.

Based on this conclusion of negligible rotational branch influences on the anisotropy factor, all values shown in Figure 4 are either directly measured only for the Q branch or averaged over the three branches. As mentioned before, a clearly visible saturation effect, particularly for the (1 + 1′)-REMPI measurements, can be seen. For the lowest laser intensities ($\approx 1.8\ mJ\,cm^{-2}$ within the overlap region with the molecular beam) that still generate measurable ion yields, the anisotropy factor becomes $+(46.7 \pm 1.4)\%$ but decreases with increasing laser intensity to $+(21.2 \pm 0.3)\%$ within the measured range. Due to the revealed intensity dependence that still exists at the lowest applied laser intensities, it can be assumed that the saturation effect did not vanish within the shown intensity range. The measurable anisotropy factor can, therefore, be expected to increase further with lower laser intensities and thus the value of $+46.7\%$ represents the lower limit for the real *g* value. However, to our knowledge it is already the highest known anisotropy factor measured in the liquid or gas phase and exceeds the *g* value recorded for the same vibronic transition of (*R*)-(+)-3-MCP. This large anisotropy factor can be explained by the contribution of the ring-twisting mode to the high *g* values of (*R*)-(+)-3-MCP.[31] Moreover, note that by fur-

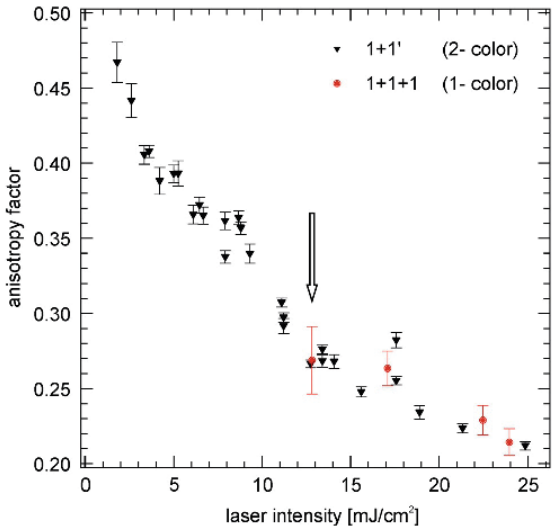

Figure 4. Anisotropy factors of the vibronic transition $18_0^4 25_0^1$ of $[D_4]$-(*R*)-(+)-3-MCP measured with (1 + 1′)- and (1 + 1 + 1)-REMPI for different dye-laser intensities.

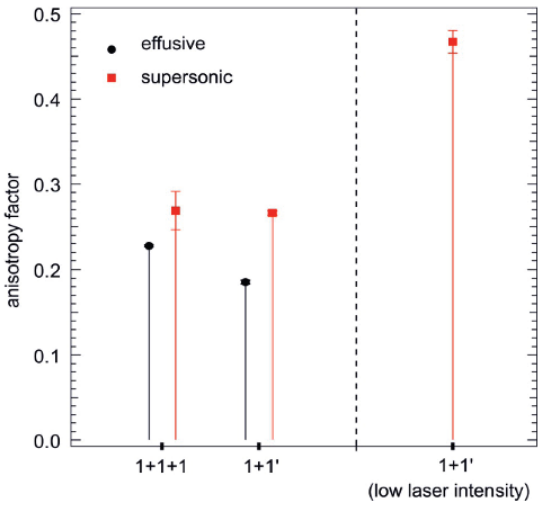

Figure 5. Comparison of the anisotropy factors of $[D_4]$-(*R*)-(+)-3-MCP measured with (1 + 1′)- and (1 + 1 + 1)-REMPI in effusive and supersonic beams with the same wavelength (324.454 nm) and laser intensity (see Figure 4) for the dye laser. The error bars for the effusive-beam and the two-color supersonic-beam measurements lie within the shown points. For comparison, the lower limit for the real anisotropy factor measured with (1 + 1′)-REMPI in a supersonic beam at lower laser intensity is shown.

ther increasing the laser intensity, a full saturation of the intermediate state and, therefore, a *g* value of 0% should be obtained at some point.[11] The observed intensity-dependent trend towards higher intensities (see Figure 4) is in accordance with this expectation.

In addition to these (1 + 1′)-REMPI measurements, anisotropy factors of the same vibronic transition recorded by using (1 + 1 + 1)-REMPI are also shown in Figure 4. For (1 + 1 + 1)-REMPI, the same dye-laser system was used as for the resonance excitation step in the (1 + 1′)-REMPI, but without an extra laser pulse from the secondary Nd:YAG laser that was used for the ionization step (see Figure 1a). Instead, the dye-laser pulse alone ionized the excited $[D_4]$-(*R*)-(+)-3-MCP molecules via a second intermediate $\pi^* \rightarrow$ 3d transition. Ion yields produced by this three-photon process are more dependent on the laser intensity than ion yields from the previously discussed (1 + 1′)-REMPI process. For this reason, low dye-laser intensities lead to a significant increase in statistical errors due to low signal-to-noise ratios compared with the (1 + 1′)-REMPI measurements with similar laser intensities (e.g., for the measurement points marked with an arrow at about 13 mJ cm^{-2}). Thus, measurements with (1 + 1 + 1)-REMPI for laser intensities below this indicated value were not feasible with our experimental setup. However, within the useable intensity range the anisotropy factors recorded by using (1 + 1 + 1)-REMPI are similar to the (1 + 1′)-REMPI values within the error margins and show the same saturation behavior. Due to the latter, the highest *g* value reached here was $+(26.9 \pm 2.3)\%$ with (1 + 1 + 1)-REMPI and again represents the lower limit for the real *g* value of this process, as previously explained.

The equality of the anisotropy factors for (1 + 1 + 1)-and (1 + 1′)-REMPI within the margins of error is of special interest here. Previous works with (*R*)-(+)-3-MCP in an effusive beam[9, 11, 18] showed that, due to the second excitation step to an additional intermediate state in the (1 + 1 + 1)-REMPI process, the resulting *g* value is the sum of the first and second excitation step *g* values (cumulative *g* value). Measurements of $[D_4]$-(*R*)-(+)-3-MCP in an effusive beam show the same behavior (see Figure 5). For the (1 + 1′)-REMPI process under effusive-beam conditions, a *g* value of $+(18.6 \pm 0.3)\%$ can be seen, whereas the (1 + 1 + 1)-REMPI process delivers a *g* value of $+(22.7 \pm 0.2)\%$. Thus, the calculated contribution of the second excitation step to the sum of the overall *g* value of (1 + 1 + 1)-REMPI is $+(4.1 \pm 0.5)\%$. Therefore, the major part of the *g* value is assigned to the first excitation step. However, the anisotropy factors measured in an effusive beam are low compared with the supersonic-beam measurements, although saturation of the first transition step occurred in the latter case. This confirms that *g* values measured in an effusive beam have to be seen as an averaged *g* value over many overlapping vibronic transitions.[31] Thus, isolated vibronic transitions that can only be investigated within a supersonic-cooled beam could have higher anisotropy factors by far than this averaged value. For the (1 + 1′)-REMPI measurements of $[D_4]$-(*R*)-(+)-3-MCP presented herein, this increase of +28.1% (supersonic +46.7%; effusive +18.6%) is more distinct than for (*R*)-(+)-3-MCP (+22.1%; supersonic +42.1%;[31] effusive +20.0%[11]).

In contrast to the effusive-beam measurements, the presented supersonic-beam results for the investigated $18_0^4 25_0^1$ transition do not reveal a difference between (1 + 1 + 1)- and (1 + 1′)-REMPI processes, at least in the medium-to-high laser-intensity range. The explanation for this behavior is the reduced broadening of the transition bands due to the supersonic-beam-cooling effect, which does not allow for an overlapping

of transitions in the first and second excitation step. Therefore, in a (1+1+1)-REMPI process, a resonance excitation of the second transition with the same wavelength as the first transition becomes unlikely (see Figure 1a). This means that most probably the second intermediate state is a virtual state and thus does not contribute to the anisotropy factor. Considering this result, under supersonic-beam conditions the (1+1+1)-REMPI process investigated herein should be more accurately denoted as a (1+2)-REMPI process. Furthermore, it has previously been shown that the ionization step does not give rise to a nonvanishing *g* value.[9] Thus, the observed anisotropy factor in the case of supersonic-beam measurements can be solely attributed to the first resonance excitation step.

3. Conclusions

The investigated $n \rightarrow \pi^*$ ($18_0^4 25_0^1$) transition) of [D_4]-(*R*)-(+)-3-MCP did not reveal, within the margins of error, a dependence of the anisotropy factor on the rotational branches excited as a resonant intermediate state in a supersonic-beam (1+1′)-REMPI process. However, our first experimental attempt with CD-REMPI-MS on rovibronic transitions might encourage future investigations into this evolving scientific field. In particular, theoretical approaches, which to our knowledge presently do not exist for rotationally resolved ECD, could be of great value. Other experimental techniques, for example, microwave three-wave mixing,[38–39] have shown that supersonic-beam cooling combined with broadband rotational (microwave) spectroscopy also enables a high enantiosensitivity for enantiomeric excess measurements. It is also known that in two-photon spectroscopy the Q branch and P or R branches show different behavior on excitation with linear or circularly polarized light.[9,40–42] Our results prove that rotational-branch-resolved ECD is possible. Thus, a subsequent fascinating question would be whether switching from left to right circularly polarized excitation exhibits differences for the enantiomers of chiral molecules in rotational-branch-resolved two-photon spectroscopy (which obeys rules similar to Raman spectroscopy).

Compared with the previous investigations on (*R*)-(+)-3-MCP, the (1+1′)- and (1+1+1)-REMPI measurements of [D_4]-(*R*)-(+)-3-MCP in effusive and supersonic beams deliver new insights. As already assumed for (*R*)-(+)-3-MCP,[31] the exceptionally high *g* value seen herein can be explained by the contribution of the ring-twisting mode ν_{18}, which can only be investigated selectively in a supersonic beam. Furthermore, under effusive-beam conditions the measured anisotropy factors were low compared with the supersonic beam results, which confirmed that *g* values investigated in an effusive beam are averaged over all overlapping transitions. The difference in the observed anisotropy factor for a single vibronic excitation compared with the effusive beam result was significantly higher for [D_4]-(*R*)-(+)-3-MCP (+28.1%) than for (*R*)-(+)-3-MCP (+22.1%). A possible explanation for this effect is that the larger mass due to the four deuterium atoms in [D_4]-(*R*)-(+)-3-MCP leads to an increased amplitude of the ring-twisting vibration around the C=O axis compared with protonated 3-MCP. It seems plausible that this higher amplitude enhances the influence of the vibration on the anisotropy factor due to the fact that the rotation of the electron density around this axis causes the large CD of 3-MCP.

Moreover, the phenomenon that *g* values due to the excitation of consecutive transitions are cumulative in the (1+1+1)-REMPI process[11] was also observed for [D_4]-(*R*)-(+)-3-MCP in an effusive beam. However, the additional (1+1′)-REMPI measurements performed here revealed that this behavior did not appear in the supersonic beam, which can be explained by a nonresonant transition to a virtual intermediate state without any *g* value at all. Thus, the high *g* values of up to $+(46.7 \pm 1.4)\%$ measured by using (1+1′)-REMPI under supersonic-beam conditions can be solely assigned to the first resonant $n \rightarrow \pi^*$ ($18_0^4 25_0^1$) transition. Such high anisotropy factors could have great impact, for example, on enantiomeric-excess measurements[34] of chiral molecules.

Furthermore, this already exceptionally high anisotropy factor has to be considered as the lower limit for the real *g* value due to the saturation of the transition to the excited intermediate state.[11,31] The problem of saturation effects with nanosecond lasers may be solved by using pico- or femtosecond lasers. The reduced ionization efficiency due to lower laser-pulse energy will be compensated by high laser-pulse intensities. In addition, the usually higher repetition rates of these laser systems will lead to a smaller statistical error. Accordingly, the corresponding short-pulse experiments on supersonic-beam-cooled chiral molecules are strongly encouraged.

Acknowledgements

The authors greatly acknowledge support by the German Research Foundation through the projects KA4166/2-1 and BO718/10 and the European Research Council through an Advanced Research Grant (246645-ASC3).

Keywords: circular dichroism · mass spectrometry · resonance-enhanced multiphoton ionization · rotational spectroscopy · supersonic beam cooling

[1] M. G. Finn, *Chirality* **2002**, *14*, 534.
[2] L. Whitmore, B. A. Wallace, *Biopolymers* **2008**, *89*, 392.
[3] N. Sreerama, R. W. Woody, *Anal. Biochem.* **2000**, *287*, 252.
[4] J. L. Alonso-Gomez, A. Navarro-Vazquez, M. M. Cid, *Chem. Eur. J.* **2009**, *15*, 6495.
[5] S. Kunz, P. Schreiber, M. Ludwig, M. M. Maturi, O. Ackermann, M. Tschurl, U. Heiz, *Phys. Chem. Chem. Phys.* **2013**, *15*, 19253.
[6] U. Boesl, A. Kartouzian, *Annu. Rev. Anal. Chem.* **2016**, *9*, 343.
[7] H. G. Breunig, G. Urbasch, P. Horsch, J. Cordes, U. Koert, K.-M. Weitzel, *ChemPhysChem* **2009**, *10*, 1199.
[8] P. Horsch, G. Urbasch, K. M. Weitzel, D. Kroner, *Phys. Chem. Chem. Phys.* **2011**, *13*, 2378.
[9] C. Loge, U. Boesl, *Phys. Chem. Chem. Phys.* **2012**, *14*, 11981.
[10] C. Logé, U. Boesl, *ChemPhysChem* **2011**, *12*, 1940.
[11] C. Logé, A. Bornschlegl, U. Boesl, *Anal. Bioanal. Chem.* **2009**, *395*, 1631.
[12] P. Heister, T. Luenskens, M. Thaemer, A. Kartouzian, S. Gerlach, T. Verbiest, U. Heiz, *Phys. Chem. Chem. Phys.* **2014**, *16*, 7299.
[13] V. K. Valev, J. J. Baumberg, C. Sibilia, T. Verbiest, *Adv. Mater.* **2013**, *25*, 2517.

[14] T. Petrallimallow, T. M. Wong, J. D. Byers, H. I. Yee, J. M. Hicks, *J. Phys. Chem.* **1993**, *97*, 1383.
[15] C. Lux, M. Wollenhaupt, C. Sarpe, T. Baumert, *ChemPhysChem* **2015**, *16*, 115.
[16] A. Kastner, C. Lux, T. Ring, S. Züllighoven, C. Sarpe, A. Senftleben, T. Baumert, *ChemPhysChem* **2016**, *17*, 1119.
[17] R. Li, R. Sullivan, W. Al-Basheer, R. M. Pagni, R. N. Compton, *J. Chem. Phys.* **2006**, *125*, 144304.
[18] U. Boesl, A. Bornschlegl, C. Logé, K. Titze, *Anal. Bioanal. Chem.* **2013**, *405*, 6913.
[19] C. Logé, U. Boesl, *ChemPhysChem* **2012**, *13*, 4218.
[20] P. Horsch, G. Urbasch, K.-M. Weitzel, *Chirality* **2012**, *24*, 684.
[21] T. J. Cornish, T. Baer, *J. Am. Chem. Soc.* **1987**, *109*, 6915.
[22] T. J. Cornish, T. Baer, *J. Am. Chem. Soc.* **1988**, *110*, 3099.
[23] K. W. D. Ledingham, R. P. Singhal, *Int. J. Mass Spectrom. Ion Processes* **1997**, *163*, 149.
[24] W. Hao-Yang, G. Yin-Long, in Chiral Recognition in the Gas Phase, CRC Press, **2010**, pp. 167.
[25] L. Ma, C. Abney, W. Lin, *Chem. Soc. Rev.* **2009**, *38*, 1248.
[26] M. S. Taylor, E. N. Jacobsen, *Angew. Chem. Int. Ed.* **2006**, *45*, 1520; *Angew. Chem.* **2006**, *118*, 1550.
[27] M. T. Reetz, K. M. Kühling, H. Hinrichs, A. Deege, *Chirality* **2000**, *12*, 479.
[28] A. Kantrowitz, J. Grey, *Rev. Sci. Instrum.* **1951**, *22*, 328.
[29] G. B. Kistiakowsky, W. P. Slichter, *Rev. Sci. Instrum.* **1951**, *22*, 333.
[30] A. Amirav, U. Even, J. Jortner, *Chem. Phys.* **1980**, *51*, 31.
[31] K. Titze, T. Zollitsch, U. Heiz, U. Boesl, *ChemPhysChem* **2014**, *15*, 2762.
[32] N. Lin, F. Santoro, X. Zhao, A. Rizzo, V. Barone, *J. Phys. Chem. A* **2008**, *112*, 12401.
[33] N. Lin, Y. Luo, F. Santoro, X. Zhao, A. Rizzo, *Chem. Phys. Lett.* **2008**, *464*, 144.
[34] U. Boesl von Grafenstein, A. Bornschlegl, *ChemPhysChem* **2006**, *7*, 2085.
[35] W. C. Wiley, I. H. McLaren, *Rev. Sci. Instrum.* **1955**, *26*, 1150.
[36] A. F. Drake, *J. Phys. E* **1986**, *19*, 170.
[37] J. Zhang, W. Y. Chiang, J. Laane, *J. Chem. Phys.* **1993**, *98*, 6129.
[38] D. Patterson, M. Schnell, J. M. Doyle, *Nature* **2013**, *497*, 475.
[39] V. A. Shubert, D. Schmitz, D. Patterson, J. M. Doyle, M. Schnell, *Angew. Chem. Int. Ed.* **2014**, *53*, 1152; *Angew. Chem.* **2014**, *126*, 1171.
[40] G. Placzek, E. Teller, *Zeitschrift für Physik* **1933**, *81*, 209.
[41] W. M. McClain, *Acc. Chem. Res.* **1974**, *7*, 129.
[42] U. Boesl, H. J. Neusser, E. W. Schlag, *Chem. Phys.* **1976**, *15*, 167.

Manuscript received: July 22, 2016
Revised: October 5, 2016
Final Article published: November 3, 2016

2.1.2. Discussion and Conclusion

Chiral molecules in general have anisotropy factors in sub-percent region, while ketones possess high g-values of several percent due to their carbonyl group, which leads to an electric dipole forbidden $n \rightarrow \pi^*$ transition.[72] In comparison, (R)-(+)-3-MCP showed in previous works exceptionally high g-values of $+20.0\%$[44] under effusive beam (room temperature) conditions. This g-value could be enhanced to $+42.1\%$[74] by excitation of single vibronic transitions with an involved ring-twisting mode ($18_0^4 25_0^1$) under supersonic beam.

The investigations on d_4-(R)-(+)-3-MCP presented here,[64] confirm those results on (R)-(+)-3-MCP. Under effusive beam conditions the $n \rightarrow \pi^*$ transition of d_4-(R)-(+)-3-MCP has a (1+1')-REMPI g-value of $+(18.6 \pm 0.3)\%$ which is increased by using (1+1+1)-REMPI to $+(22.7 \pm 0.2)\%$. The second resonant transition ($\pi^* \rightarrow 3d$) in the (1+1+1)-REMPI process (see figure 1a of the first publication[64]) results thereby in an additional g-value of $+(4.1 \pm 0.5)\%$ that cumulates with the anisotropy factor of the first resonant transition to the overall g-value of $+(22.7 \pm 0.2)\%$. This cumulative effect for subsequent resonant excitations of different transitions has already been reported for (R)-(+)-3-MCP.[44] Under supersonic beam conditions the presented (1+1')-REMPI results of d_4-(R)-(+)-3-MCP reveal the highest g-value ever measured in liquid or gas phase with $+(46.7 \pm 1.4)\%$ for the excitation of the single vibronic transition $18_0^4 25_0^1$ (see figure 4 of the first publication[64]). However, this anisotropy factor can only be assumed as the lower limit for the real g-value since saturation[44, 74] of the resonant intermediate state even with the lowest measureable laser intensities cannot be excluded. Thus, the real g-value is expected to be higher than $+46.7\%$. In any case, it is higher than for (R)-(+)-3-MCP and extraordinary enhanced in relation to the effusive beam results. While for (R)-(+)-3-MCP the difference between (1+1')-REMPI under effusive and supersonic beam conditions was $+22.1\%$, for d_4-(R)-(+)-3-MCP a difference of $+28.1\%$ can be observed. An explanation for this larger increase due to excitation of a single vibronic transition could be the higher mass of the deuterated d_4-(R)-(+)-3-MCP. The additional mass might lead to a higher amplitude of the involved ring-twisting vibration especially around the C=O axis and therefore to a higher influence of the vibration on the g-value compared to the protonated (R)-(+)-3-MCP.

Also for supersonic beam-cooled d_4-(R)-(+)-3-MCP a comparison of (1+1+1)-REMPI and (1+1')-REMPI has been done. In contrary to the already mentioned effusive beam results, the extra excitation step in (1+1+1)-REMPI does not change the anisotropy factor within the error margins (see figure 5 of the first publication[64]). A possible explanation for this behavior could be the narrow resonances of d_4-(R)-(+)-3-MCP under supersonic beam conditions (see figure 2 of the first publication[64]) which does not allow for a coincident resonant transition to a second

intermediate state. Thus, the second transition has to be seen as non-resonant excitation and the overall excitation process as (1+2)-REMPI instead of (1+1+1)-REMPI.

Furthermore, for the first time ECD measurements on separated rotational branches of a single vibronic transition have been presented on supersonic beam-cooled d_4-(R)-(+)-3-MCP. The (1+1')-REMPI results do not reveal within the error margins any g-value differences between the P, Q and R branches of the excited $n \rightarrow \pi^*$ ($18_0^4 25_0^1$) transition (see figure 3 of the first publication[64]). However, for achiral molecules two-photon spectroscopy experiments[68-71] already showed a variation regarding the excitation of the Q branch relative to the P or R branches with linear or circular polarized light. Furthermore, the microwave three-wave mixing technique[54-55] is solely based on a difference in the electric transition dipole moments of rotations (see section 1.2.1.3). Therefore, the possibility for investigations of separated rotational branches with ECD under supersonic beam conditions might encourage theoretical works on this field which do not exist at the moment. Due to the relatively high error margins of about $\pm 1\%$, a higher precision of the used technique might give new insights on the effect of different rotational branches on the anisotropy factor.

One way for a possible improvement of the statistical error could be the usage of pico- or femtosecond laser systems which have higher repetition rates. In addition, those laser systems have lower laser pulse energies but high laser pulse intensities and thus could also solve the problem of saturation effects. Especially in case of the used CD-REMPI-MS setup, another possibility is the modification of the experimental arrangement to allow twin-peak[45, 75] measurements of supersonic beam-cooled sample molecules, which is explained in the following sections.

2.2. Experimental and Data Analyzing Improvements

After the measurements which are presented in the first publication[64] of this thesis, the experimental setup was modified to allow twin-peak measurements on supersonic beam-cooled molecules. Furthermore, the data analysis has been changed from the previously mentioned oscilloscope averaging procedure, which results in one g-value for a package of 200 left- and 200 right-circular polarized laser pulses, to a new single laser pulse evaluation. By both modifications, which are explained in more detail in the following sections, the precision of the CD-REMPI-MS setup has been significantly improved leading to the investigations on supersonic beam-cooled 1-phenylethanol presented in the second publication[66].

2.2.1. Combination of Supersonic Beam and Twin-Peak Technique

The first way to improve the experimental precision of CD-REMPI-MS measurements on supersonic beam-cooled chiral molecules was the utilization of the twin-peak technique (see section 1.4.2). Previous twin-peak measurements under effusive beam conditions already showed the advantages of this technique compared to standard CD measurements (single-peak with solely one laser beam).[45] Furthermore, the improved precision due to the twin-peak technique can be combined with the reference method to reach error margins in the permille range. However, the twin-peak technique could not be utilized in the previous experimental setup (see figure 1b of the first publication[64]) for supersonic beam measurements because of geometric reasons. The alignment of the supersonic beam was perpendicular to the TOF-MS axis. Thus, the width of the supersonic molecular beam after passing the skimmer was too narrow to allow for an overlap with two laser beams (the incident and reflected beam) at different positions to generate two ionization spots with sufficient ion yield for a twin-peak measurement.[15]

Therefore, the important point to realize a combination of supersonic and twin-peak technique for CD-REMPI-MS measurements was the rearrangement of the experimental setup for an inline supersonic beam to the TOF axis. The resulting new experimental setup is shown in figure 7. In general, the prevacuum chamber is mounted inline to the TOF-MS and can still be separately pumped due to a dismountable skimmer between the prevacuum chamber and the

[15] If the supersonic molecular beam can be seen as a cone after passing the skimmer, the two ionization spots have to lay inline to and centered on the TOF axis. However, the distance between both spots has to be sufficient for a separation of peaks with similar mass after the flight time in the drift free region of the TOF. Thus, the two laser beams only pass the outer parts of the supersonic beam which have such a low molecular density (the molecular density of a supersonic beam is already in general low compared to an effusive beam) that the resulting ion yield drops below the noise level.

ion source.[16] A novel component that had to be designed for the inline supersonic beam was a repeller plate with an implanted effusive beam inlet system. Due to the inline supersonic beam the previous repeller plate which had a centered needle as effusive beam inlet could not be used anymore. The supersonic beam needs a free pathing realized as an inner cone with an opening diameter from $7\,mm$ to $9\,mm$ in TOF direction to reach the ion source nearly undisturbed (see figure 8 in this thesis and figure 1b of the second publication[66]). However, beside twin-peak measurements under supersonic beam conditions also effusive beam twin-peak measurements or simultaneous CD investigations (to allow for reference molecule measurements)[17] of molecules from both inlet systems should still be possible. Therefore, the repeller plate consists of two separate plates. The front plate has a centered cone cut with a closing diameter from $15\,mm$ to $10\,mm$ in TOF direction, while the smaller back plate has a similar outer cone shape with a diameter smaller by $0.6\,mm$ to fit into the front plate cone. Connected to a gap around this outer cone on the back plate, a pipe connection exists to up to two different effusive beam inlet sources (placed outside the vacuum chamber) to enable mixing two effusive beam samples. Inside the back plate cone the already mentioned opening cone cut allows for the undisturbed passing of the supersonic beam. The outer cones with the diameter difference of $0.6\,mm$ guide the effusive beam around the supersonic beam to the ion source as a wrapping molecular beam, that mixes softly with the supersonic beam within the ion source. Thus, sample molecules of both molecular beam sources can simultaneously be measured with the twin-peak technique inline to the TOF-MS (see figure 9). The supersonic beam is thereby still as cold as in the previous setup even with an active effusive beam and without a mounted skimmer[18] (see figure 2 of the second publication[66]).

The improvement of the experimental precision due to these setup modifications combined with the new single laser pulse evaluation is discussed on the basis of the shown CD investigations of 1-phenylethanol in the second publication[66] and thus in section 2.3.

[16] Beside the inline supersonic beam, a desorption chamber was implanted to the setup with a lock in system for sample holder and an extra window for a desorption laser beam. This desorption chamber allows for CD-REMPI-MS investigations of laser desorbed non-volatile chiral molecules (see section 3) but it was not used during this thesis.

[17] A simultaneous CD measurement of two different supersonic beam-cooled molecule types (i.e. chiral analyte and achiral reference) is nearly impossible due to the narrow absorption peaks. Thus, a resonant excitation of two molecule types with the same wavelength is very unlikely because of a missing overlap of their individual single vibronic transitions even for molecules with quite similar structure.

[18] The alignment of the pulsed valve for the supersonic beam creation together with the two laser beams for twin-peak and the mounted skimmer was quite complicated and the molecular densities were low. Therefore, the skimmer was dismounted. Test measurements showed that the supersonic beam-cooling without skimmer was sufficient for CD investigations on single vibronic transitions.

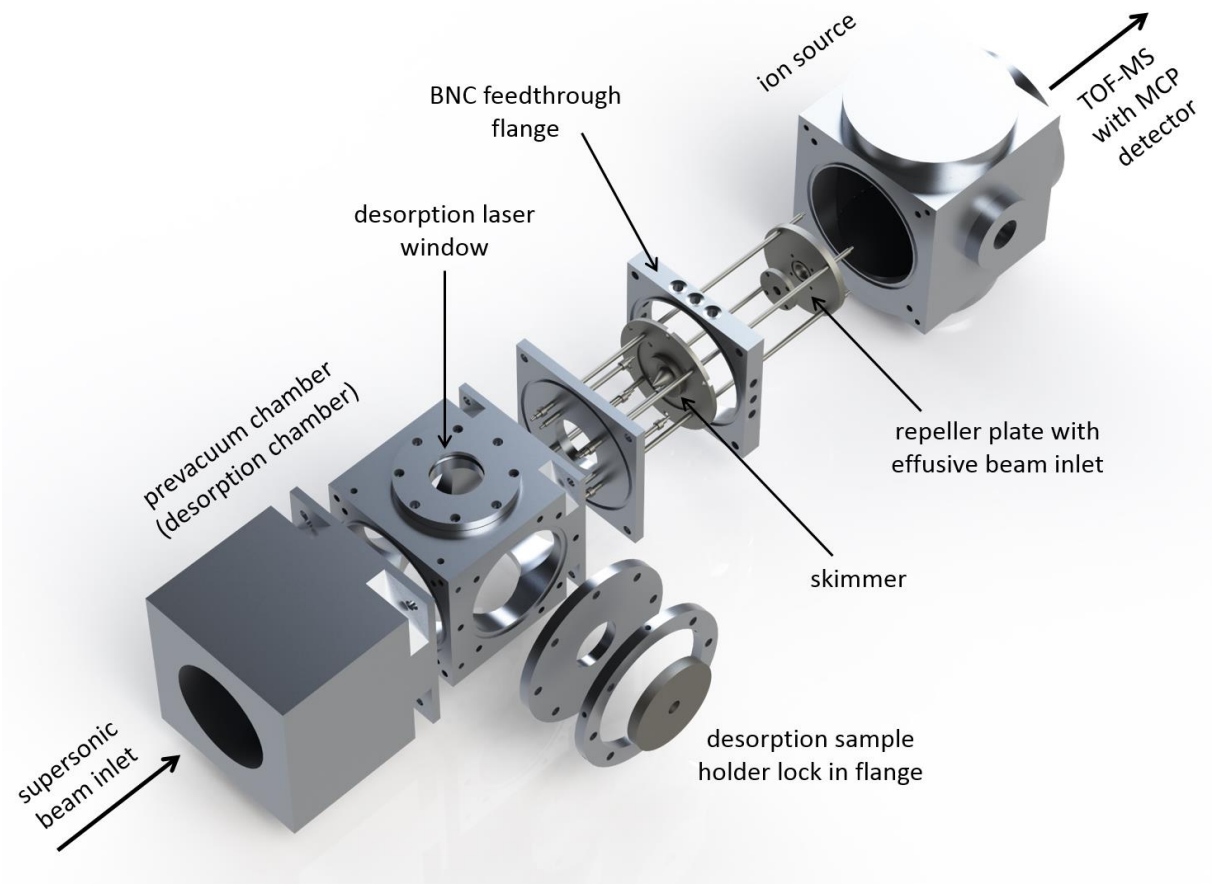

figure 7: Experimental setup modifications for supersonic beam measurements inline to the TOF-MS which allows a combination with the twin-peak technique. The supersonic beam is created by a pulsed general valve (not shown here) that is placed in a prevacuum chamber ($\sim 5 \cdot 10^{-4}\ mbar$). Within this prevacuum chamber a sample holder can be implanted for laser desorption experiments. The prevacuum chamber can be separated by a skimmer from the main chamber ($\sim 5 \cdot 10^{-6}\ mbar$) with the inline TOF-MS. For a simultaneous inline measurement of samples under effusive beam as well as supersonic beam conditions a novel repeller plate has been used that has an implanted effusive beam inlet system (see figure 8 of this thesis and figure 1b of the second publication[66]).

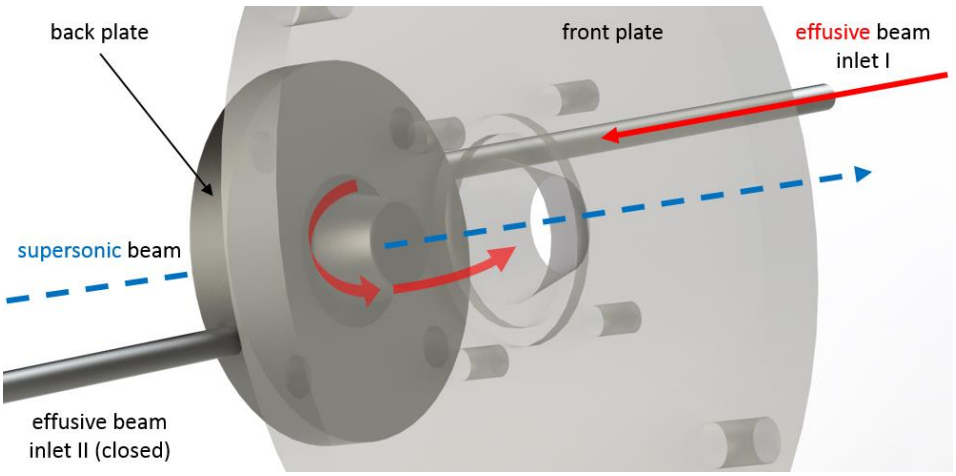

figure 8: Illustration of the repeller plate with combined effusive beam inlet system (see figure 1b of the second publication[66]). The repeller front plate (here transparent and slightly dismounted to allow for a view on the back plate) has a cone cut in the middle that closes from $15\ mm$ to an end diameter of $10\ mm$ in molecular beam direction (i.e. in TOF direction). The back plate consists of a outer cone in the middle that fits with a diameter difference of $0.6\ mm$ into the cone of the front plate. Around this back plate cone is a surrounding gap which is connected to two pipes for two different effusive beam inlets with sample reservoirs outside the vacuum chamber. Inside the back plate cone another cone cut allows for a nearly undisturbed pathing of a supersonic beam from the backside through the repeller plate. This inner cone has an opening diameter from $7\ mm$ to $9\ mm$ in TOF direction.

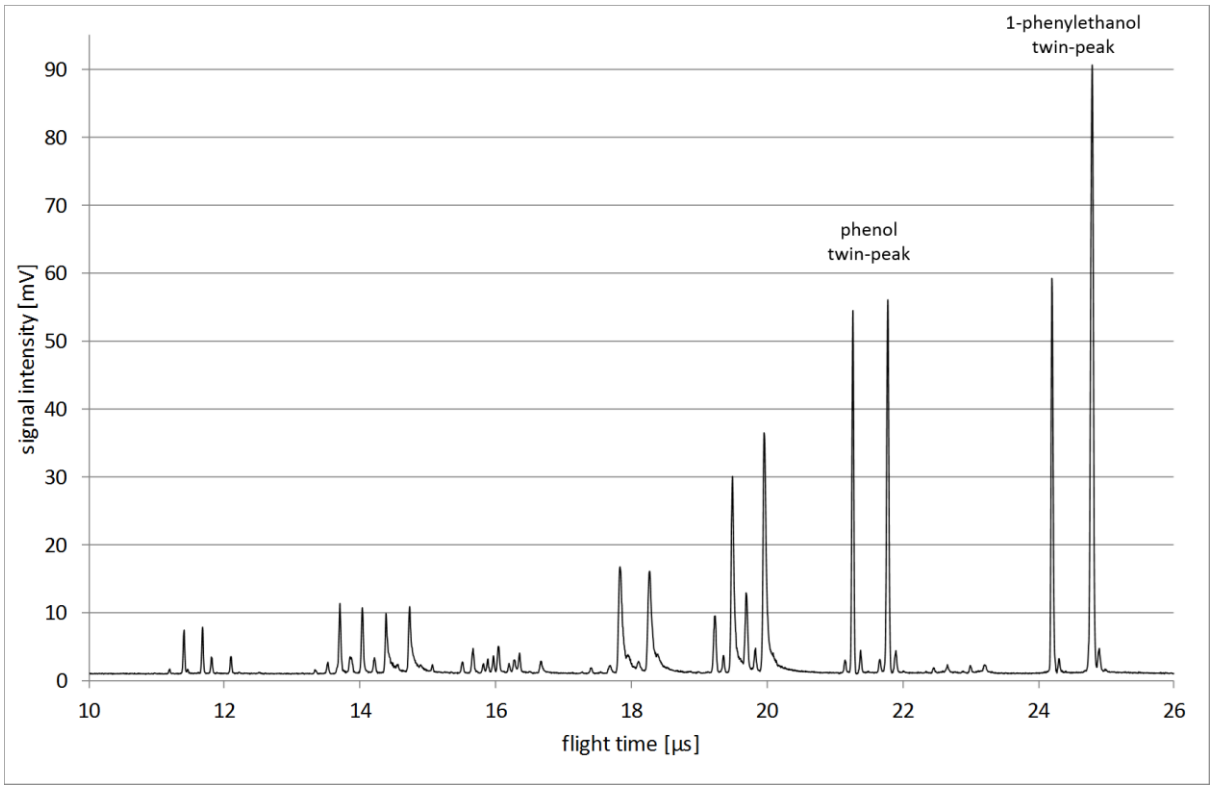

figure 9: Time of flight spectrum of supersonic beam-cooled 1-phenylethanol and effusive beam phenol as reference molecule obtained with (1+1)-REMPI at the 0_0^0-transition ($265.873\ nm$). Due to the experimental setup modifications (see figure 7) effusive beam as well as supersonic beam samples can be measured simultaneously with the twin-peak method. Thus, all mass peaks (also fragment peaks) appear twice in the shown spectrum.

2.2.2. Automatic Single Laser Pulse Evaluation

A further possibility to increase the experimental precision of the CD-REMPI-MS technique is an improvement of the statistics by establishing a new automatic single laser pulse evaluation. As already mentioned in section 1.4, an anisotropy factor calculation consisted usually of 200 left-circular followed by 200 right-circular polarized laser pulses. Each of these 200 laser pulse packages is separately averaged for the ion yield values I_L and I_R, which results in one g-value due to equation [13]. With the help of a simultaneously measured achiral reference molecule and equation [14] this provides one reference corrected g-value. This measurement is then repeated about 100 times leading to 100 g-values (with or without reference correction) that can be averaged to one overall anisotropy factor. This overall g-value has depending on the standard deviation σ of the averaged g-values a standard error of $\frac{\sigma}{\sqrt{N}}$ (here: $N = 100$; amount of g-value measurements), which represents the value range around the overall g-value in which the real g-value can be expected. For a more precise approximation of the real g-value the standard error can be reduced by increasing the amount of g-value measurements or by decreasing the standard deviation by more precise measurements with reduced spreading of the separately calculated averaged g-values. For example, the latter can be carried out by establishing an advanced experimental technique, such as the twin-peak method, for reduced laser fluctuation influences in supersonic beam CD measurements (see previous section).

2.2. Experimental and Data Analyzing Improvements

An increase of the amount of g-value measurements can be enabled by simply increasing the measurement time, which is not a useful option for a technique that should be used for fast in situ analysis of chiral molecules as products of a dynamical changing asymmetric catalytic reaction. Another possibility is the increase of the repetition rate of the used laser system by e.g. utilizing pico- or femtosecond lasers and thus increasing the amount of measurable g-values within the same measurement time (see section 2.1.2). However, those laser systems have disadvantages as a higher spectral linewidth (see footnote [4]).

Therefore, an idea to improve the g-value statistics without changing the laser system or an increase of the measurement time is the establishment of a single laser pulse evaluation instead of the previous 200 laser pulse averaging method. Technically this was realized with a modified LabVIEW program (see appendix C.2.2) by saving sequences out of 200 single oscilloscope records representing the ion yield of one laser pulse each. Thus, one laser pulse gives one mass spectrum and can be used for one g-value calculation, if it is combined with one mass spectrum recorded for the opposing circular polarization. This increases the amount of measured g-values by a factor of 200 for CD measurements without twin-peak method. Obviously the standard deviation of those single laser pulse g-values is increased, while the resulting standard error is nearly unchanged. However, the recording of mass spectra from single laser pulses enables new possibilities to observe the experimental conditions for each mass spectrum and to handle the post processing and data evaluation based on those conditions with new LabVIEW programs (see appendix C.2.3 and C.2.4).

On the one hand, the mass spectra can be filtered depending on the recorded ion yields for the mass peaks of interest. If a mass spectrum for example has a vanishing (below noise level) ion yield for the analyte or the reference molecule mass peak, this mass spectrum can be erased from the data list and thus does not contribute to the g-value calculation. On the other hand, simultaneous to the mass spectra the laser energy is recorded by a photodiode. This enables a filtering of mass spectra resulting from certain laser energies. If the laser energy is for example below a minimum level, the beam profile can become asymmetric and thus the overlap region of laser and molecular beam is not uniformly illuminated. If the laser energy is above a maximum level, the fragmentation of the sample molecule is more dominant and can limit the maximum ion yield similar to an occurring saturation effect. Therefore, mass spectra recorded for laser pulses with energies above or below a certain energy level are erased before the g-value calculation to reduce the influence of such extreme laser intensity conditions. With these two filtering criteria about 20% of the recorded mass spectra of single laser pulses are deleted and do not contribute to the g-value calculation.

A more significant advantage of the single laser pulse evaluation can be found in case of twin-peak measurements. Due to the fact that the twin-peak method provides all necessary

information to calculate one g-value out of a single mass spectrum (see section 1.4.2) a single laser pulse evaluation enables the full potential of this method. On the first view out of the 200 left- and 200 right-circular polarized laser pulses, which are repeated 100 times, an overall amount of 40000 mass spectra and thus 40000 g-values can be evaluated. However, as already mentioned in section 1.4.2 the twin-peak method adds two systematic error sources to the CD measurements. On the one hand, the intensity for the incident laser beam is higher than for the reflected laser beam. This is caused by loss of laser energy at each optical surface due to reflection at the chamber windows and lenses. On the other hand, the two laser beam paths are at different distances relative to the molecular beam inlet system and thus the molecular density is different at the two ionization spots. Both systematic error sources can be decreased by switching the circular polarization of the incident laser beam and averaging over two g-values (one with incident left-circular and one with incident right-circular polarized light; respectively g_{LR} and g_{RL}) as defined in equation [15] to get a twin-peak g-value g_{TP} with strongly reduced systematic errors. A full cancellation of the systematic errors is not possible, since they depend on the experimental conditions such as the incident laser energy and the overall molecular density delivered by the supersonic or effusive beam inlet system. For example, the supersonic beam generated by the general valve fluctuates from pulse to pulse. Therefore, pairing the g-values (g_{LR} and g_{RL}) from incident left- and right-circular polarized light together in the order as they were measured and thus randomly in sense of their experimental conditions does not allow for a good compensation of the systematic errors. Instead, the single laser pulse evaluation enables the possibility to previously sort the measured g_{LR} and g_{RL} data lists in order of increasing g-values for one and decreasing g-values for the other or vice versa. The reason for ordering the g-values is given by the dominance of the systematic error compared to the expected real g-value of the investigated sample molecule. Figure 9 shows as an example that even with an expected g-value of less than a percent for the investigated (R)-(+)-1-phenylethanol sample the ion yields for the incident and reflected laser beam can differ significantly more due to the systematic errors.[19] Therefore, sorting the measured g_{LR} in decreasing order represents an sorting in decreasing systematic error contribution and vice versa. Due to the switch of the circular polarization and thus opposing systematic error contributions in case of g_{RL}, the sorting for the g_{RL} values is performed in increasing order but still represents decreasing systematic error contribution. The sorted g-values of g_{LR} and g_{RL} can afterwards be paired together and the resulting standard deviation of g_{TP} is significantly lower than without previous sorting of the g-values and the influence of the systematic error is reduced to a minimum.

[19] This is just one exemplary time of flight spectrum but the signal difference between the ion yield generated by the incident and reflected laser beam is in general dominated by the systematic error sources with resulting g-values $> 10\%$.

This single laser pulse evaluation combined with the new inline supersonic beam for twin-peak measurements on single vibronic transitions of chiral molecules was first used for the CD investigations on (R)-(+)-1-phenylethanol shown in the second publication[66]. The reached experimental precision enables thereby about thirteen times smaller standard errors compared to the results on d_4-(R)-(+)-3-MCP with the previous experimental setup (see first publication[64]). This improvement is mentioned in section 2.3.2.

2.3. Chiroptical Inversion for Isolated Vibronic Transitions of Supersonic Beam-Cooled Molecules

The experimental setup for the CD-REMPI-MS measurements on single vibronic transitions of (R)-(+)-1-phenylethanol presented in this publication[66], combined for the first time the twin-peak technique with supersonic beam-cooling and a single laser pulse evaluation. Therefore, especially the precision of the shown results is significantly improved compared to previous CD-REMPI-MS measurements.

2.3.1. Summary and Author Contribution

The first publication[64] presented in this thesis confirmed the huge influence of single vibronic excitations on the g-value of supersonic beam-cooled molecules on the example of d_4-(R)-(+)-3-MCP. However, due to the previously known enhancing effect of the ring-twisting mode (ν_{18}) on the g-value of (R)-(+)-3-MCP only the anisotropy factor of the $18_0^4 25_0^1$ vibrational mode in the $n \rightarrow \pi^*$ transition of d_4-(R)-(+)-3-MCP has been investigated. Furthermore, ketones, like 3-MCP, in general possess high anisotropy factors of several percent even under effusive beam conditions, while chiral molecules without a carbonyl group have usually g-values of less than a percent.[72]

Therefore, the second publication[66] shows for the first time CD-REMPI-MS measurements of supersonic beam-cooled (R)-(+)-1-phenylethanol and thus of a common product of asymmetric catalysis.[57] Due to the expectable low molecular densities provided by the supersonic beam inlet and the sub-percent anisotropy factor of (R)-(+)-1-phenylethanol under effusive beam conditions, the previously mentioned significant improvements of the experimental precision were necessary for those measurements. For the (1+1)-REMPI investigations on the $\pi \rightarrow \pi^*$ transition of the phenyl ring of (R)-(+)-1-phenylethanol ($\lesssim 266\, nm$), a first supersonic beam spectrum was recorded to allow for an assignment of the isolated vibronic transitions with the help of literature[82]. Beside the 0_0^0-transition, ten different of those single vibronic transitions with an unique vibrational mode (two of them were ring-twisting modes) have been chosen for the CD measurements. Thus, the influence of different vibrational modes on the anisotropy factor of (R)-(+)-1-phenylethanol could be experimentally observed. In addition, effusive beam (1+1)-REMPI measurements have been done for seven wavelength of interest for a comparison with the supersonic beam results at nearly similar wavelength. This allowed for an investigation of the influence of hot bands and rotational broadening on the g-value. The latter effect leads to an overlap of various vibronic transitions under effusive beam conditions.

2.3. Chiroptical Inversion for Isolated Vibronic Transitions of Supersonic Beam-Cooled Molecules

The described measurements presented in this publication were performed by the author J. Lepelmeier with assistance by F. Mortaheb. The theoretical results were contributed by L. Alonso-Gómez.

Volume 19 | Number 32 | 28 August 2017 | Pages 21213–21906

PCCP

Physical Chemistry Chemical Physics
rsc.li/pccp

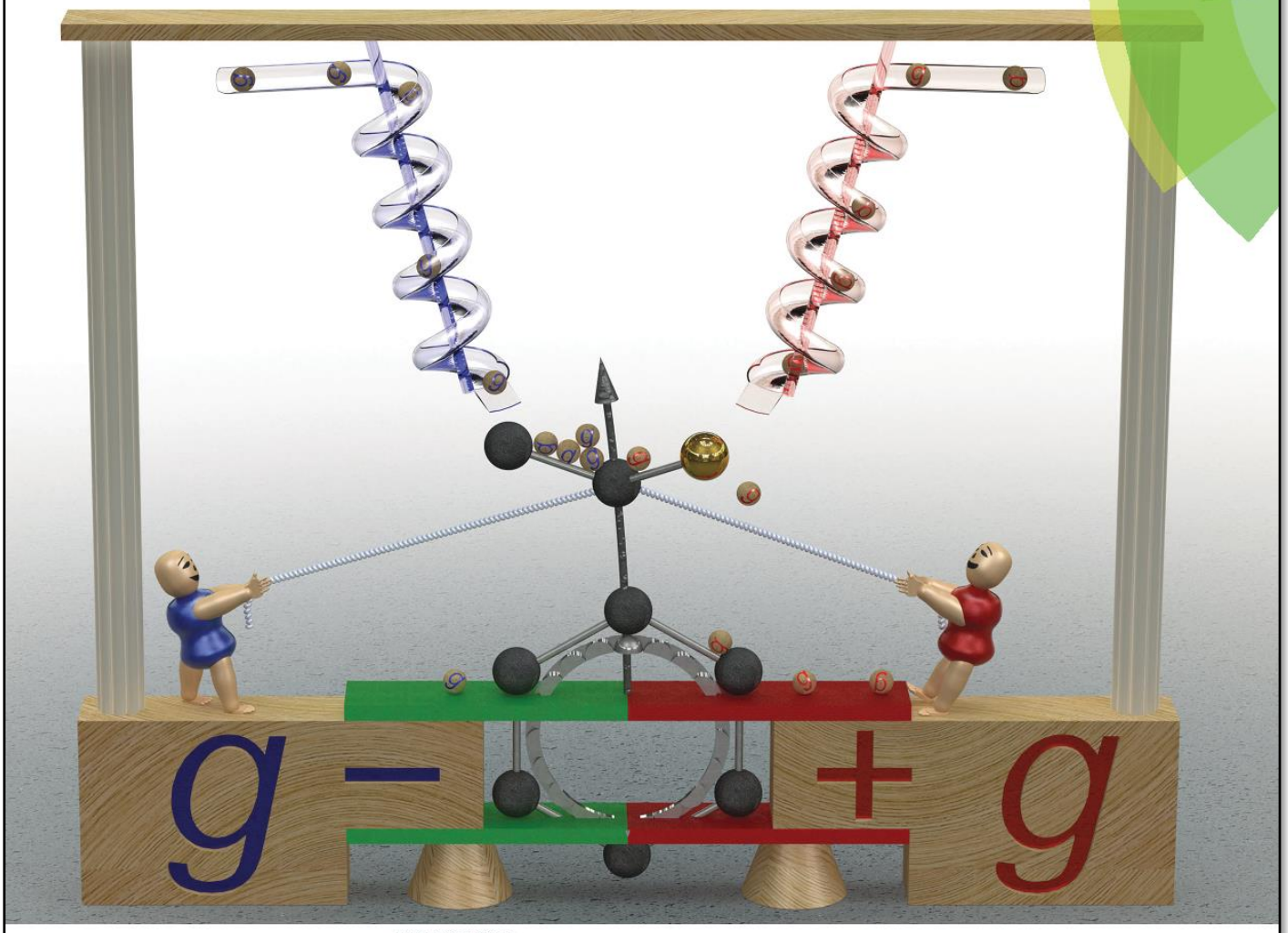

ISSN 1463-9076

ROYAL SOCIETY OF CHEMISTRY

PAPER
Aras Kartouzian *et al.*
Chiroptical inversion for isolated vibronic transitions of supersonic beam-cooled molecules

PCCP

PAPER

View Article Online
View Journal | View Issue

Cite this: *Phys. Chem. Chem. Phys.*, 2017, **19**, 21297

Chiroptical inversion for isolated vibronic transitions of supersonic beam-cooled molecules

Jörn Lepelmeier,[a] José Lorenzo Alonso-Gómez,[b] Farinaz Mortaheb,[a] Ulrich Boesl,[a] Ulrich Heiz[a] and Aras Kartouzian*[a]

Received 20th April 2017,
Accepted 19th June 2017

DOI: 10.1039/c7cp02596c

rsc.li/pccp

Circular dichroism-resonance-enhanced multiphoton ionization (CD-REMPI) was used for CD measurements on several single vibronic transitions of supersonic beam-cooled (*R*)-(+)-1-phenylethanol. Due to the low molecular densities within a supersonic beam and the expected small anisotropy factor of 1-phenylethanol in the permille region, the precision of the experimental method had to be significantly improved. Therefore, a single laser pulse evaluation combined with a twin-peak technique enabled within the used supersonic beam setup is presented. For the electronic transition $S_0 \rightarrow S_1$ of (*R*)-(+)-1-phenylethanol ($\pi \rightarrow \pi^*$ transition of the phenyl ring at 266 nm) ten different vibrational modes as well as the 0_0^0-transition were investigated with one-color (1 + 1) CD-REMPI. The results deliver new experimental insights on the influence of molecular vibrations on the anisotropy factor. TD-DFT theoretical predictions show how the angle between the electronic and magnetic transition dipole moments of the electronic transition can be modified by different vibrational modes, making even a flip of the sign of the anisotropy factor possible.

Introduction

Chirality plays an important role in a broad field of various industrial branches and aspects of life. Especially for pharmaceutical applications the enantiomers of a chiral molecule could lead to different cross reactions with the also chiral biochemical system of the human body.[1,2] Therefore, the quality of enantioselective synthesizing processes is crucial for this as well as other industries. Asymmetric catalysis provides one of those synthesizing methods for chiral molecules.[3–7] To monitor, and understand the enantioselectivity of such catalytic reactions, fast and sensitive analytical methods are necessary that allow for enantiomeric excess measurements of their products under divers conditions. The most common direct techniques for those purposes are based on circular dichroism (CD) as well as optical rotation dispersion (ORD).[8–10] The difference in absorption of left- and right-circularly polarized light for the enantiomers of a chiral molecule (CD effect), can be combined with various and special types of spectroscopy, as for instance with nonlinear two-photon spectroscopy[11,12] or angular-resolved photoelectron spectroscopy.[13,14] The circular dichroism resonance-enhanced multiphoton ionization mass spectrometry (CD-REMPI-MS)[15] presented here is a combination of enantioselective CD, wavelength selective REMPI[16–18] and mass selective MS.[11,12,19,20] Thus CD-REMPI-MS provides a three-dimensional highly selective analytical method for CD measurements of sample molecules even for undefined mixtures in the gas phase. Under vacuum conditions the spectroscopic selectivity of this technique can be further improved by cooling the sample molecules due to supersonic beam expansion.[21–23] This allows for resonant excitation and thus investigation of separated single vibronic transitions in electronic circular dichroism (ECD) studies. As predicted by theory,[24,25] these could have significantly different anisotropy factors compared to CD measurements under effusive beam (room temperature) or condensed-phase conditions as already experimentally proven for deuterated and non-deuterated 3-methylcyclopentanone in previous works of our group.[15,26] In the case of 3-methylcyclopentanone, even under effusive beam conditions the investigated $n \rightarrow \pi^*$ transition exhibits a high *g*-value of 27%[27] due to its carbonyl group that leads to a nearly electric dipole forbidden transition. For the same reason, other ketones have anisotropy factors of several percent, while chiral molecules in general usually possess *g*-values that are below one percent.[28]

The investigated sample molecule 1-phenylethanol is commonly obtained by enantioselective reduction of acetophenone and has an anisotropy factor of 0.63%[29] in effusive beam gas phase measurements (0.2%[30] in ethanol) for its electronic transition $S_0 \rightarrow S_1$ ($\pi \rightarrow \pi^*$ within the phenyl ring at 266 nm). Accordingly, for measuring the *g*-value of supersonic beam-cooled 1-phenylethanol the sensitivity and precision of the experiment had to be improved to allow the application of the CD-REMPI method. Therefore, a modified setup for utilizing the twin-peak[29,31] method was used and combined with a new single laser pulse evaluation for post processing data filtering and analysis.

[a] *Technical University of Munich, Lichtenbergstraße 4, 85748 Garching, Germany. E-mail: aras.kartouzian@tum.de*
[b] *University of Vigo, Lagoas-Marcosende, 36310 Vigo, Spain*

The anisotropy factor of the 0_0^0-transition and ten different vibrational modes of (*R*)-(+)-1-phenylethanol were investigated with (1 + 1)-REMPI. The results show the significant influence of molecular vibrations on the absolute *g*-value as well as its sign. Furthermore, an effusive beam wavelength scan and CD measurements for several different wavelengths were performed. For comparison between theoretical predictions and experimental results, TD-DFT calculations of the electronic and magnetic transition dipole moments and their relative angle have been performed for the 0_0^0-transition and three different vibronic transitions.

Experimental section

The experimental setup (see Fig. 1c) used for the CD-REMPI-MS measurements of (*R*)-(+)-1-phenylethanol (Sigma-Aldrich, enantiomeric excess >94.0% No. 07366-5G-F) presented here, is a modified version of the setup used in our previous works[15,26,32] in order to allow for utilizing the twin-peak technique in supersonic beam measurements. The pulsed general valve (with a 0.2 mm diameter nozzle) used as supersonic beam inlet was therefore mounted inside the vacuum chamber collinear to the ion source and Time-Of-Flight-Mass Spectrometer (TOF-MS). The latter followed the linear TOF-MS design of Wiley and McLaren[33] with a multi-channel plate as detector. The valve was pulsed synchronous with the dye laser system which had a repetition rate of 30 Hz. Argon with a backpressure of 2.8 bar was used as carrier gas for the supersonic beam expansion and led to a working pressure of 4×10^{-6} mbar within the vacuum chamber.

The repeller plate had an implemented effusive beam inlet to allow for additional effusive beam (room temperature) measurements of sample or reference molecules simultaneous to the supersonic beam measurements. The twin-peak method supplies thereby improved precision in both cases of effusive and supersonic beam measurements. The design (see Fig. 1b) consists of an inner cone (opening diameter from 7 mm to 9 mm in TOF direction) for the supersonic beam and two outer cones (with a diameter difference of 0.6 mm, closing from 15 mm to 10 mm in TOF direction) that generate a wrapping effusive beam. Thus, supersonic beam-cooled molecules are guided through the repeller plate nearly undisturbed and can be ionized and detected simultaneous to the surrounding effusive beam molecules. The collinear alignment of both molecular beams with the axis of ion source and TOF-MS is combined with a double laser beam overlap. This is achieved with the same laser pulse being reflected back into the overlap region by a nearly 0° mirror on the opposite side of the vacuum chamber. This leads to two ion clouds separated in space but still lying on the TOF-MS axis and thus gives rise to two ion signals for same masses (*e.g.* for the sample molecule ion) at different flight-times (twin-peak) as described in detail in previous work.[29,31] Furthermore, the circular rotation direction of circularly polarized light switches from left to right or right to left when the laser pulse is reflected. Therefore, molecules ionized with one laser pulse,

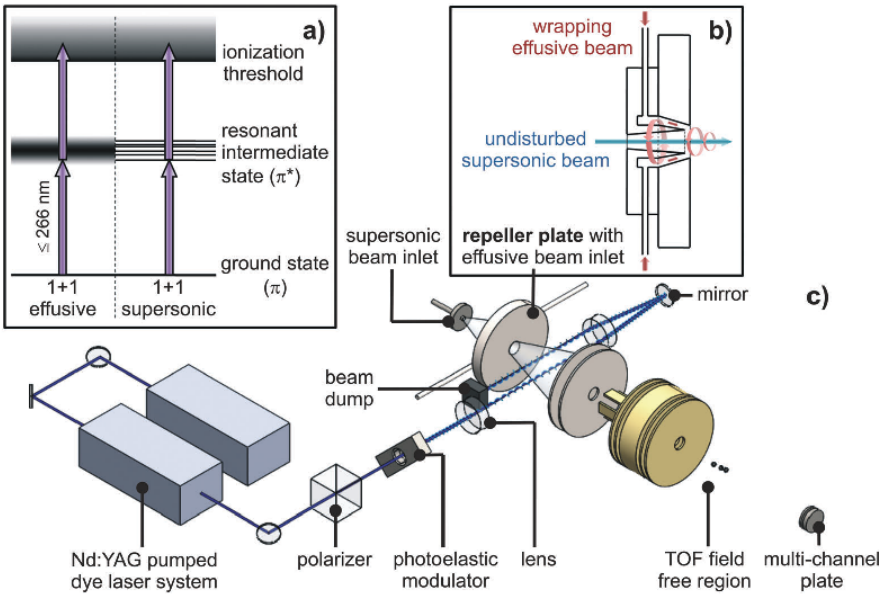

Fig. 1 (a) Ionization scheme of (*R*)-(+)-1-phenylethanol *via* resonant excitation of the π → π* transition in an effusive and supersonic beam for a (1 + 1)-REMPI process. (b) Schematic view of the repeller plate with an implemented effusive beam inlet for the simultaneous twin-peak measurement of supersonic beam-cooled together with effusive beam (room temperature) molecules. (c) Illustration of the experimental setup with the Nd:YAG pumped dye laser system for the resonant excitation and ionization of the sample molecules within the vacuum chamber under usage of the twin-peak method (reflection of the laser beam back into the vacuum chamber). The supersonic beam inlet as well as the effusive beam inlet, which is implemented in the repeller plate, are collinear to the ion optics and TOF-MS with a multi-channel plate as detector.

but excited at the two different spots with opposing circular polarization can be measured separately in one mass spectrum.

The laser system used for the resonant excitation and ionization of either supersonic beam-cooled or room temperature (effusive beam) (*R*)-(+)-1-phenylethanol in a (1 + 1)-REMPI process (see Fig. 1a) consists of a dye laser with a spectral linewidth of 0.04 cm^{-1} pumped by an Nd:YAG laser. The wavelength range of 259–266 nm suitable for the investigated transition $\pi \rightarrow \pi^*$ of (*R*)-(+)-1-phenylethanol was thereby generated by the frequency-doubled emission of Coumarin 153 dissolved in ethanol. The linear laser light was circularly polarized with a photoelastic modulator to allow for CD measurements of the sample molecules.

Results and discussion

All supersonic as well as effusive beam CD results of (*R*)-(+)-1-phenylethanol presented here have been measured with the twin-peak technique and post processed with a new single laser pulse data evaluation. As already mentioned, the twin-peak method allows for measurements of sample molecules excited and ionized by both circular polarizations of the light with one laser pulse. Thus, one laser pulse or respectively one mass spectrum provides all necessary information for the calculation of the anisotropy factor (*g*-value) that is defined for CD-REMPI measurements as follows[29]

$$g_{\text{CD-REMPI}} = 2\frac{I_L - I_R}{I_L + I_R} \quad (1)$$

with ion yields I_L and I_R obtained by the left- and right-circular polarized light. However, the conditions for the ion yields of the incoming and reflected laser pulse are not totally equal. On the one hand the laser intensity for the reflected compared to the incoming laser pulse is reduced due to losses at the vacuum chamber window and the reflection at the mirror itself. On the other hand, due to the different spatial positions of the incoming and reflected laser beam relative to the molecular beam inlet, the molecular densities are different within both overlap regions. Both sources of mismatch in ion yields maybe assumed as systematic errors because there is a constant percentage loss in laser intensity at each optical component and the ratio of the two molecular densities is constant for unchanged laser beam paths. Therefore, during experiments the circular rotation direction is switched after every 200 laser pulses to allow for correcting these additional systematic errors. Thus, the definition of the resulting anisotropy factor for CD-REMPI-MS measurements with twin-peak technique is[29]

$$g_{TP} = \frac{g_{LR} + g_{RL}}{2} = \frac{I_{L_1} - I_{R_1}}{I_{L_1} + I_{R_1}} + \frac{I_{L_2} - I_{R_2}}{I_{L_2} + I_{R_2}} \quad (2)$$

with ion yields I_{L_1} and I_{R_1} as produced by the incoming (left circular) and reflected (right circular) laser pulse, respectively, to measure g_{LR} and ion yields I_{R_2} and I_{L_2} as produced by the incoming (right circular) and reflected (left circular) laser pulse, respectively, to measure g_{RL}.

As already mentioned, instead of averaging over several mass spectra and thus partly losing the advantage of the twin-peak method with one separately calculable anisotropy factor per laser pulse (respective per mass spectrum) the post processing has been done with a new single laser pulse data evaluation. On one side, this allowed for filtering each laser pulse depending on its intensity as well as on the resulting ion yields. The intensities of the laser pulses were measured by a photodiode, and all laser pulses with intensities inside the 2σ range of the resulting Gaussian distribution were considered for the *g*-value calculations. Furthermore, all mass spectra with too low ion yield for one of the twin mass peaks in comparison to the noise level were deleted. About 80% of the measured mass spectra passed these two filtering processes. On the other side the single laser pulse evaluation allowed for sorting the listed g_{LR} and g_{RL} values before calculating g_{TP} in order to compensate for the previously mentioned systematic error of the experiment. It was thereby assumed that at similar experimental conditions (*e.g.* for similar incoming laser intensities and molecular densities) g_{LR} and g_{RL} should have the same value with only an opposite sign for the contribution of their systematic errors. For this reason, g_{LR} was sorted in order of decreasing values (decreasing systematic error contribution), while g_{RL} was sorted in the opposite way and thus also in decreasing systematic error contribution order. These presorted g_{LR} and g_{RL} values were then paired together for the g_{TP} calculation.

As basis for the CD investigations on the $\pi \rightarrow \pi^*$ transition of (*R*)-(+)-1-phenylethanol, an effusive as well as a supersonic (1 + 1)-REMPI spectrum have been recorded for 37 594–38 610 cm^{-1} (266–259 nm) (see Fig. 2 top). The spectrum for the supersonic beam-cooled molecules shows clearly separated narrow vibronic transitions. The assignment of these transitions, starting with the 0_0^0-transition at 37 612 cm^{-1} (265.873 nm), has been performed with the help of theoretical and experimental data from literature[34] (see Table 1). The weak resonance at 37 592 cm^{-1} and thus at lower energy than the predicted 0_0^0-transition can be assumed as a complex of (*R*)-(+)-1-phenylethanol with the used argon carrier gas.[34] For the supersonic beam CD measurements, beside the 0_0^0-transition ten different vibronic transitions have been chosen (marked with arrows) considering vibrational mode diversity (except two separate ring torsions) and measurability in sense of sufficient ion yields. In contrast to the supersonic beam spectrum, under effusive beam conditions a broad absorption band over the whole measured range is visible. This band is composed of overlapping broadened vibronic transitions and additional hot bands which are populated at room temperature. Thus, only one peak maximum around 38 138 cm^{-1} (262.206 nm) exists. Due to existence of hot bands and strong overlapping of vibronic transitions, a clear interpretation in terms of transition dependent anisotropy factors would not be possible under effusive beam conditions. Being aware of this fact, we have chosen seven wavelengths to be close but not identical to measured supersonic beam vibronic transitions, so that the dominance of the isolated transitions may be qualitatively observed. Furthermore, we included a measurement at 266 nm (4th harmonic of Nd:YAG) since this is present a commonly available wavelength across various research groups that are active in this field. It should be mentioned here, that although an anisotropy factor

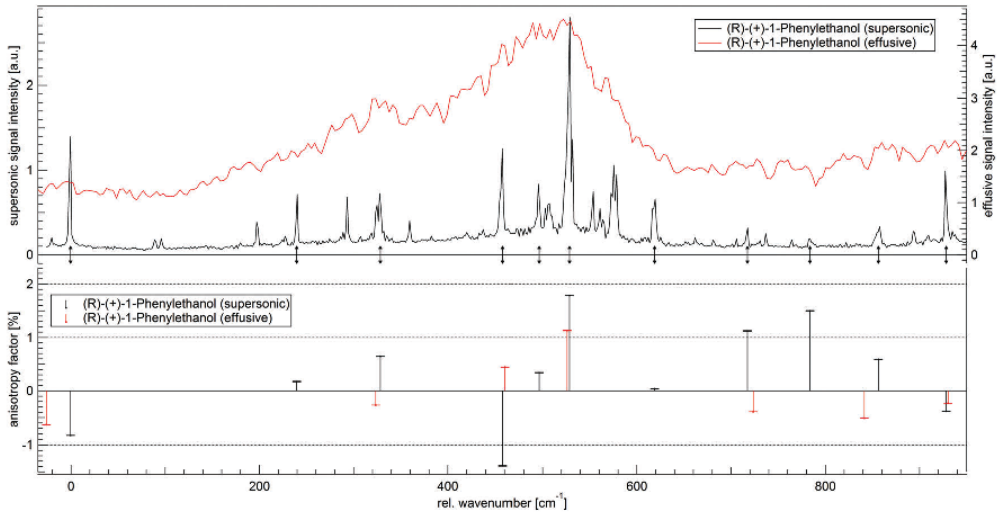

Fig. 2 Top: Supersonic beam (black, left scaling) and effusive beam (red, right scaling) spectrum of the electronic transition $\pi \rightarrow \pi^*$ of (*R*)-(+)-1-phenylethanol in wavenumbers relative to the 0_0^0-transition at 37 612 cm^{-1} (265.873 nm) measured with (1 + 1)-REMPI. The shown relative range in wavenumbers corresponds to 259–266 nm in wavelength. CD measurements were performed on the separated supersonic beam transitions that are marked with arrows (the 0_0^0-transition and ten different vibrational modes). Bottom: Anisotropy factors of (*R*)-(+)-1-phenylethanol for the measured supersonic beam transitions marked with an arrow (black, see Table 1) and seven different relative wavenumbers measured in effusive beam (red, see Table 2). In the shown scaling the calculated error bars are smaller than the measurement point symbols.

Table 1 Resulting *g*-values for the 0_0^0 and ten different single vibronic transitions measured in supersonic beam for the electronic transition $\pi \rightarrow \pi^*$ of (*R*)-(+)-1-phenylethanol with (1 + 1)-REMPI (see Fig. 2 bottom). The vibrational modes have been assigned with the help of literature[34] that provides theoretical ($\nu_{l,th}$) and experimental ($\nu_{l,exp}$) wavenumbers relative to the 0_0^0-transition. In comparison to the literature values, the measured supersonic beam values (ν_{rel}) from the presented spectrum (see Fig. 2 top) are shown

Vibrational mode	$\nu_{l,th}$[34]/cm^{-1}	$\nu_{l,exp}$[34]/cm^{-1}	ν_{rel}/cm^{-1}	*g*-Value/%
0_0^0-Transition	—	(37 618 ± 1)	(37 612 ± 1)	−0.829 ± 0.004
CH_3 torsion	248.0	242 ± 1	240 ± 1	0.174 ± 0.007
Ring CC def.	351.8	327 ± 1	328 ± 1	0.644 ± 0.003
CH_3 bending	459.5	462 ± 1	458 ± 1	−1.389 ± 0.007
H–O–C–H torsion	502.7	501 ± 1	496 ± 1	0.341 ± 0.005
Ring bending	526.8	532 ± 1	529 ± 1	1.785 ± 0.004
Ring CC bending	609.5	620 ± 1	619 ± 1	0.041 ± 0.003
Ring torsion	740.2	717 ± 1	718 ± 1	1.123 ± 0.008
C_b–C_g stretching	886.3	785 ± 1	783 ± 1	1.500 ± 0.006
Ring torsion	895.9	857 ± 1	858 ± 1	0.590 ± 0.004
Ring breathing	975.7	929 ± 1	927 ± 1	−0.381 ± 0.003

spectrum would be of great interest, it is currently practically not feasible in our lab, since measurement of the anisotropy factor at each single wavelength, as described below, takes more than three hours.

During the CD measurements, 200 laser pulses for g_{LR} were always followed by 200 laser pulses for g_{RL}. In general this process was repeated about 700 times over several days and leads to a total amount of 280.000 mass spectra. Due to filtering by laser intensities and ion yields, as previously described, about 220.000 mass spectra were considered for the *g*-value calculation. The resulting 110.000 g_{TP} values were finally averaged for the anisotropy factors presented here (see Fig. 1 bottom, Tables 1 and 2). At this point it should be mentioned, that because of the twin-peak method combination with the single laser pulse evaluation, the calculated absolute standard errors were $\leq$0.008% for all supersonic and $\leq$0.004% for all effusive beam results. Thus, in Fig. 2 (bottom) the error bars of the *g*-values are smaller than the measurement point symbols. At this point, it should be mentioned, that since the enantiomeric excess as claimed by the supplier may have an error on the order of 1%, the reported anisotropy factors cannot reflect absolute values but should be considered in relation to each other. The error in enantiomeric excess, however, does not influence the experimental error reported here, since throughout this work a single source of molecules has been used and thus although the exact enantiomeric excess is not known to us, this unknown value remains unchanged throughout the experiments presented here.

The supersonic beam results of (*R*)-(+)-1-phenylethanol (see Table 1) confirm the high influence of single vibronic excitations

Table 2 Resulting g-values for seven different wavelength (λ_{exp}) measured in effusive beam for the electronic transition $\pi \rightarrow \pi^*$ of (*R*)-(+)-1-phenylethanol with (1 + 1)-REMPI (see Fig. 2 bottom). In addition the wavenumbers (ν_{rel}) relative to the separated supersonic beam 0_0^0-transition at 37 612 cm^{-1} (265.873 nm) are shown

λ_{exp}/nm	ν_{rel}/cm^{-1}	g-Value/%
266.057	−26 ± 1	−0.635 ± 0.002
263.606	323 ± 1	−0.266 ± 0.001
262.656	461 ± 1	0.445 ± 0.002
262.206	526 ± 1	1.131 ± 0.004
260.855	723 ± 1	−0.389 ± 0.001
260.055	841 ± 1	−0.513 ± 0.002
259.455	930 ± 1	−0.231 ± 0.001

on the g-value as also observed for 3-methylcyclopentanone.[15,26] For instance the anisotropy factor of the ring CC bending mode with 0.041 ± 0.003% is the lowest of all investigated supersonic as well as effusive beam g-values. In comparison to that, the ring bending mode has a more than forty times higher anisotropy factor with 1.785 ± 0.004% and thus the overall highest recorded g-value for 1-phenylethanol (see Tables 1 and 2). Due to the exceptionally high anisotropy factors for the ring torsion (twisting) mode in d_4-(*R*)-(+)-3-methylcyclopentanone,[15,26] also two different ring torsion modes have been measured for (*R*)-(+)-1-phenylethanol, but both (at 718 cm^{-1} and 858 cm^{-1}) have only moderate anisotropy factors.

Another important aspect of the measured vibrational modes is the observable sign flip among the measured anisotropy factors. While for the 0_0^0-transition (−0.829 ± 0.004%), the CH_3 bending mode (−1.389 ± 0.007%) and ring breathing mode (−0.381 ± 0.003%) negative g-values occur, the other investigated single vibronic transitions have positive anisotropy factors. From the dependence

$$g = 4\frac{|\vec{m}||\vec{\mu}| \times \cos\theta}{|\vec{m}|^2 + |\vec{\mu}|^2} \quad (3)$$

of the anisotropy factor on the electric ($\vec{m}$) and magnetic ($\vec{\mu}$) transition dipole moments it is obvious that the sign of the g-value solely depends on the angle θ between $\vec{m}$ and $\vec{\mu}$. Our measurements demonstrate clearly that the angle θ changes its value from above 90° (resulting in negative g-values) to below 90° (resulting in positive g-values).

To explain this finding, TD-DFT calculations of the first 10 excited states at the m062x/6-31G(d) level of theory with the first electronic $\pi \rightarrow \pi^*$ transition at 219.80 nm (electric dipole forbidden) has been performed. It is known for conjugated systems that too short wavelengths may be predicted at this level of theory.[35] The theoretical results confirm a negative sign for the 0_0^0-transition with θ = 99.6° between the electric and magnetic transition dipole moments. This almost orthogonal alignment of $\vec{m}$ and $\vec{\mu}$ can lead to a sign flip of the g-value, if the angle becomes <90° because of small geometry distortions induced by certain vibrations. In order to support this hypothesis TD-DFT calculations at the same level of theory for geometries resulting from three representative vibrations have been performed. Two structures obtained for the two possible directions of the CH_3 bending at 483 cm^{-1} (experimentally: 458 cm^{-1}) lead to an angle of 99.1° and 123.8° and thus to the same sign for the anisotropy factor as experimentally observed. Calculations for the ring bending mode at 540 cm^{-1} (experimentally: 529 cm^{-1}) resulted in angles of 85.2° and 89.2° and for the ring torsion mode at 716 cm^{-1} (experimentally: 718 cm^{-1}) in angles of 72.6° and 89.9°, providing a sign flip for the corresponding g-values in agreement with the experimental observations.

In addition to the supersonic beam measurements, also g-values at seven different wavelengths have been investigated under effusive beam conditions (see Table 2). The resulting anisotropy factors show lower absolute values compared to the supersonic beam measurements on single vibronic transitions at nearly similar wavelength. In addition, the effusive beam results also show sign flips for the anisotropy factor within the investigated wavelength range which further indicates that the angle between the electric and magnetic transition dipole moments lies close to 90°. This general behavior of the effusive beam g-values confirms the assumption that g-values measured at room temperature represent the average of several overlapping vibronic transitions in agreement with previous works of our group.[15,26] However, a direct comparison between supersonic and effusive beam CD measurements has to be treated with caution due to the following two main reasons. On the one hand, not all vibrational modes, that are visible in the supersonic beam spectrum (see Fig. 2 top), could be investigated. On the other hand, under effusive beam conditions (at room temperature) the existence of hot bands, which are not populated and thus are not measurable for supersonic beam-cooled molecules, should be considered. It is therefore not surprising that simply averaging the measured g-values of several adjacent vibronic transitions in the supersonic beam do not match to g-values measured for the broadened transition in the effusive beam. This behavior can be clearly seen for effusive beam measurements performed at relative wavenumbers of 323 cm^{-1}, 723 cm^{-1}, and 841 cm^{-1} where even the sign of the anisotropy factor is different for supersonic and effusive beam measurements. Nevertheless, for the three dominant transitions in the supersonic beam spectrum (0_0^0, ring bending, and ring breathing), the respective effusive beam g-values −0.635 ± 0.002%, and −0.231 ± 0.001% have the same sign with a reduced absolute value. Therefore, the g-values of these dominant transitions can be expected to be also the dominant contributions to the averaged g-values in corresponding effusive beam measurements. In case of the g-value of 0.445 ± 0.002% at 461 cm^{-1}, it can be assumed that an overlap with the dominant ring bending transition at 529 cm^{-1} leads to the positive anisotropy factor compared to the negative sign of the CH_3 bending mode with an anisotropy factor of −1.389 ± 0.007% at 458 cm^{-1}. Such an overlap is reasonable since at room temperature the typical rotational envelope of vibronic bands of aromatic molecules is about 200 cm^{-1}.

Conclusion

The influence of isolated single vibronic transitions on the anisotropy factor has only be shown up to now for the carbonyl

3-methylcyclopentanone with its exceptionally large anisotropy factors.[15,26] The CD investigations of the $\pi \rightarrow \pi^*$ transition of supersonic beam-cooled (*R*)-(+)-1-phenylethanol with (1 + 1)-REMPI presented here prove that this influence is also found for types of molecules other than carbonyls. The results additionally show that the anisotropy factor can vary up to a factor of forty for different vibronic transitions. The highest *g*-value was observed for the ring bending vibration with 1.785 ± 0.004%, while the lowest *g*-value was observed for the ring CC bending with 0.041 ± 0.003%.

Furthermore, the comparison of the anisotropy factors for supersonic and effusive beam measurements reveals a strong enhancement of the *g*-values in the former case. The explanation is that under room temperature conditions rotational broadening and excitation of hot bands causes a considerable overlap of several vibrational modes. This leads to averaged and thus lower absolute *g*-values in comparison to the anisotropy factors of single vibronic transitions at similar wavelengths, which is in agreement with our previous findings.[15,26]

While the single vibronic excitation of the ring torsion mode of 3-methylcyclopentanone exhibits an extraordinary strong enhancement of the anisotropy factor,[15,26] no such effect is induced by excitation of ring torsion modes of (*R*)-(+)-1-phenylethanol. This is reasonable since the influence of a special vibrational mode on the molecular anisotropy depends on the molecular structure and the alignment of electric and magnetic transition dipole moments. In particular a change of the angle between both transition moments is of great interest.

A change of the angle from $>90^\circ$ to $<90^\circ$ has been observed experimentally for the $\pi \rightarrow \pi^*$ transition of (*R*)-(+)-1-phenylethanol upon excitation of various vibrational modes as manifested by a sign flip of the anisotropy factors. This behavior was confirmed by TD-DFT calculations at the m062x/6-31G(d) level of theory. This well-defined and theoretically predictable chiroptical inversion could be of interest in basic molecular research. On the one hand, this inversion induced by single vibrational modes may help to assign isolated vibronic bands to special vibrational motions and could therefore be of importance for molecular spectroscopy. On the other hand, this effect delivers additional information about the molecular geometry. This could be used to specify molecular structures more precisely or to distinguish between different conformers of a chiral substance.

It should be noted, that we do not believe that a vibrational mode dependent sign flip of the anisotropy factor is to be expected for all chiral molecules and transitions. This phenomenon depends on the initial angle between the electric and magnetic transition dipole moments of the involved electronic transition and the magnitude of its change due to the various vibrational modes. And since both the initial angle between transition dipole moments and the influence of various nuclear motions on it are generally independent from the nature of the transition (being allowed or forbidden), a general statement relating the nature of the transition and vibrational mode dependent sign flip of the anisotropy factor should be avoided.

The significantly improved precision of the CD-REMPI-MS technique with standard errors of ≤ 80 ppm due to a combination of the twin-peak method and single laser pulse data evaluation allows for the investigation of a broader range of different chiral molecules under supersonic beam conditions. In addition, the example of 1-phenylethanol demonstrates that now also chiral molecules with *g*-values in the permille region can be investigated with small errors. This is for instance advantageous for enantiomeric excess measurements on products of asymmetric catalytic reactions.

Acknowledgements

The authors greatly acknowledge the support by the German Research Foundation through the projects KA4166/2-1 and BO718/10, the European Research Council through an Advanced Research Grant 246645-ASC3, the Spanish Ministerio de Economia y Competitividad through CTQ2015-71924-REDT and CTQ2014-58629-R, and Xunta de Galicia through the research funding ED431F 2016/005. Furthermore, all authors are thankful to the Supercomputing Center of Galicia (CESGA) for generous allocation of computer time.

References

1 A. N. Collins, G. Sheldrake and J. Crosby, *Chirality in industry II: developments in the commercial manufacture and applications of optically active compounds*, John Wiley & Sons, 1997.
2 J. Patočka and A. Dvořák, *J. Appl. Biomed.*, 2004, **2**, 95–100.
3 W. Hao-Yang and G. Yin-Long, *Chiral Recognition in the Gas Phase*, CRC Press, 2010, pp. 167–179.
4 L. Ma, C. Abney and W. Lin, *Chem. Soc. Rev.*, 2009, **38**, 1248–1256.
5 M. S. Taylor and E. N. Jacobsen, *Angew. Chem., Int. Ed.*, 2006, **45**, 1520–1543.
6 M. T. Reetz, K. M. Kühling, H. Hinrichs and A. Deege, *Chirality*, 2000, **12**, 479–482.
7 R. Noyori, *Angew. Chem., Int. Ed.*, 2002, **41**, 2008–2022.
8 N. Sreerama and R. W. Woody, *Anal. Biochem.*, 2000, **287**, 252–260.
9 M. G. Finn, *Chirality*, 2002, **14**, 534–540.
10 L. Whitmore and B. A. Wallace, *Biopolymers*, 2008, **89**, 392–400.
11 U. Boesl, A. Bornschlegl, C. Logé and K. Titze, *Anal. Bioanal. Chem.*, 2013, **405**, 6913–6924.
12 R. Li, R. Sullivan, W. Al-Basheer, R. M. Pagni and R. N. Compton, *J. Chem. Phys.*, 2006, **125**, 144304.
13 C. Lux, M. Wollenhaupt, T. Bolze, Q. Liang, J. Koehler, C. Sarpe and T. Baumert, *Angew. Chem., Int. Ed.*, 2012, **51**, 5001–5005.
14 A. Kastner, C. Lux, T. Ring, S. Züllighoven, C. Sarpe, A. Senftleben and T. Baumert, *ChemPhysChem*, 2016, **17**, 1119–1122.
15 J. Lepelmeier, K. Titze, A. Kartouzian, U. Boesl and U. Heiz, *ChemPhysChem*, 2016, **17**, 4052–4058.
16 K. W. D. Ledingham and R. P. Singhal, *Int. J. Mass Spectrom. Ion Processes*, 1997, **163**, 149–168.
17 T. J. Cornish and T. Baer, *J. Am. Chem. Soc.*, 1987, **109**, 6915–6920.
18 T. J. Cornish and T. Baer, *J. Am. Chem. Soc.*, 1988, **110**, 3099–3106.

19 P. Horsch, G. Urbasch and K.-M. Weitzel, *Chirality*, 2012, **24**, 684–690.
20 C. Logé and U. Boesl, *ChemPhysChem*, 2012, **13**, 4218–4223.
21 G. B. Kistiakowsky and W. P. Slichter, *Rev. Sci. Instrum.*, 1951, **22**, 333–337.
22 A. Kantrowitz and J. Grey, *Rev. Sci. Instrum.*, 1951, **22**, 328–332.
23 A. Amirav, U. Even and J. Jortner, *Chem. Phys.*, 1980, **51**, 31–42.
24 N. Lin, Y. Luo, F. Santoro, X. Zhao and A. Rizzo, *Chem. Phys. Lett.*, 2008, **464**, 144–149.
25 N. Lin, F. Santoro, X. Zhao, A. Rizzo and V. Barone, *J. Phys. Chem. A*, 2008, **112**, 12401–12411.
26 K. Titze, T. Zollitsch, U. Heiz and U. Boesl, *ChemPhysChem*, 2014, **15**, 2762–2767.
27 C. Logé, A. Bornschlegl and U. Boesl, *Anal. Bioanal. Chem.*, 2009, **395**, 1631–1639.
28 F. Pulm, J. Schramm, J. Hormes, S. Grimme and S. D. Peyerimhoff, *Chem. Phys.*, 1997, **224**, 143–155.
29 C. Logé and U. Boesl, *ChemPhysChem*, 2011, **12**, 1940–1947.
30 S. T. Pickard and H. E. Smith, *J. Am. Chem. Soc.*, 1990, **112**, 5741–5747.
31 C. Logé, A. Bornschlegl and U. Boesl, *Int. J. Mass Spectrom.*, 2009, **281**, 134–139.
32 U. Boesl and A. Kartouzian, *Annu. Rev. Anal. Chem.*, 2016, **9**, 343–364.
33 W. C. Wiley and I. H. McLaren, *Rev. Sci. Instrum.*, 1955, **26**, 1150–1157.
34 A. Giardini Guidoni, S. Piccirillo, D. Scuderi, M. Satta, T. M. Di Palma and M. Speranza, *Phys. Chem. Chem. Phys.*, 2000, **2**, 4139–4142.
35 S. Castro-Fernández, M. M. Cid, C. S. López and J. L. Alonso-Gómez, *J. Phys. Chem. A*, 2015, **119**, 1747–1753.

2.3.2. Discussion and Conclusion

The chiral molecule 1-phenylethanol is a common product of an asymmetric catalytic reaction and has an expected anisotropy factor of less than a percent.[57] In comparison to the CD investigations on d_4-(R)-(+)-3-MCP in the first publication[64], the investigations on (R)-(+)-1-phenylethanol in the second publication[66] provide a better example for the majority of chiral molecules with g-values in the permille region. The combined supersonic beam-cooling and twin-peak technique allowed thereby for the first time for CD investigations on single vibronic transitions on (R)-(+)-1-phenylethanol and thus for another molecule than 3-MCP or d_4-3-MCP. The measured (1+1)-REMPI (one color; $\lesssim 266\,nm$) supersonic beam spectrum of the $\pi \rightarrow \pi^*$ transition of (R)-(+)-1-phenylethanol (see figure 2 of the second publication[66]) has been used for an assignment of the various vibrational modes with the help of literature.[82] In comparison to the supersonic beam spectrum, the effusive beam (room temperature) spectrum shows only a broad absorption band over the whole recorded wavelength range due to an overlap of the rotational broadened vibronic bands and additional hot bands similar to the previous observations on d_4-(R)-(+)-3-MCP.[64, 74]

On the first view the CD investigations on single vibronic transitions of supersonic beam-cooled (R)-(+)-1-phenylethanol show a similar behavior like the previous d_4-(R)-(+)-3-MCP results[64, 74]. Depending on the excited vibrational mode the anisotropy factor of the isolated vibronic transition can differ significantly by a factor of up to forty e.g. from a ring bend $+(1.785 \pm 0.004)\%$ to a ring CC bending $+(0.041 \pm 0.003)\%$ transition. The g-value of the ring bend vibrational mode was thereby the highest measured anisotropy factor for (R)-(+)-1-phenylethanol, while the two measured vibronic transitions with a ring torsion mode had only intermediate g-values ($+(1.123 \pm 0.008)\%$ and $+(0.590 \pm 0.004)\%$). Those ring torsion modes were expected from the previous (R)-(+)-3-MCP and d_4-(R)-(+)-3-MCP results[64, 74] to deliver maximum g-values. Due to the different molecular structure of (R)-(+)-1-phenylethanol, it is the ring bending mode which leads to a maximum anisotropy factor. A comparison of the standard errors of the highest g-value measured for d_4-(R)-(+)-3-MCP with $+(46.7 \pm 1.4)\%$ from the first publication[64] and the highest g-value for (R)-(+)-1-phenylethanol with $+(1.785 \pm 0.004)\%$ reveals the significant improvement of the experimental precision due to the inline twin-peak supersonic beam combination with single laser pulse evaluation. While the d_4-(R)-(+)-3-MCP measurement had a relative error of $\sim 3\%$, the error of the (R)-(+)-1-phenylethanol measurement is by a factor of about thirteen times smaller with a relative error of $\sim 0.22\%$. In general, all standard errors for the CD investigations on (R)-(+)-1-phenylethanol shown in the second publication are $\leq 80\,ppm$, which enables in the future CD measurements on various supersonic beam-cooled molecules with g-values in

the sub-percent region or ee measurements on such chiral molecules as probable asymmetric catalytic products.

Beside the CD measurements on single vibronic transitions under supersonic beam conditions, investigations of the anisotropy factor of (R)-(+)-1-phenylethanol under effusive beam conditions have been performed at seven different wavelength of interest in relation to the single vibronic transitions measured at similar wavelength. Those room temperature results confirm the idea of previous comparisons of supersonic and effusive beam measurements on 3-MCP and d_4-3-MCP that effusive beam g-values are an average value.[64, 74] Under effusive beam conditions the overlap of several rotational broadened vibronic transitions and additional hot bands leads to an averaged g-value out of all overlapping transitions. This results in a generally lower overall anisotropy factor for a certain wavelength than for a single vibronic transition measured at the same wavelength under supersonic beam conditions. That behavior becomes especially clear for the dominant[20] 0_0^0-, ring bend and ring breathing transition respectively at $37612\ cm^{-1}$, $38141\ cm^{-1}$ and $38539\ cm^{-1}$. This more or less direct relation between a single vibronic transition g-value and an effusive beam g-value which is just lowered by an averaging effect due to overlapping with other vibronic bands cannot be generalized. For less dominant single vibronic transitions even the sign of the anisotropy factor can switch for the averaged effusive beam g-value at the same wavelength due to a higher influence of additional hot bands or non-measured single vibronic transitions.

The most interesting and novel observation for the anisotropy factors of (R)-(+)-1-phenylethanol under supersonic beam conditions are the occurring sign switches of the g-value due to different single vibronic transition excitations. While the 0_0^0-transition has a negative g-value ($-(0.829 \pm 0.004)\%$) like the CH_3 bending and the ring breathing vibrational mode, the eight other single vibronic transitions have a positive anisotropy factor. From the definition of the g-value based on the electric and magnetic transition dipole moment (see equation [12])[25] it is clear that solely the angle θ between the two transition dipole moments can influence the sign of the resulting anisotropy factor. Due to the cosine an angle $< 90°$ leads thereby to a positive and an angle $> 90°$ to a negative g-value. Therefore, the excitation of certain vibrational modes has to result in an angle change from above to below $90°$ relative to the 0_0^0-transition, if the anisotropy factor of the single vibronic transition has a positive sign. This experimental assumption has been confirmed with the help of theoretical TD-DFT

[20] In sense of absorption efficiency (i.e. resulting ion yield; signal intensity) these three transitions dominate with respect to the surrounding vibronic transitions under supersonic beam conditions. Thus, it can be expected that their contribution to an averaged g-value at the same wavelength measured under effusive beam conditions is dominated by the g-value of these transitions even with additional hot bands.

calculations for the 0_0^0-transition and three different vibronic transitions (CH_3 bending, ring bending and one ring torsion vibrational mode). The occurrence of this sign switching effect due to excitation of different vibrational modes for the investigated $\pi \rightarrow \pi^*$ transition of (R)-(+)-1-phenylethanol can be explained by the theoretical calculation for the 0_0^0-transition with a resulting angle of $\theta = 99.6°$. This angle is already close to $90°$ and therefore a deformation of the molecular structure due to excitation of a vibrational mode can relatively easy result in an angle $< 90°$ and the respectively positive anisotropy factor.

This behavior is interesting for basic molecular research in case of molecular spectroscopy and geometry. On the one hand, the assignment of theoretically calculated vibronic transitions of chiral molecules to experimental data could be confirmed or corrected by comparison of the signs of the measured anisotropy factors of those vibronic transitions (if sign switches occur for the investigated electronic transition) or vice versa. On the other hand, the sign switch of the anisotropy factor due to different vibrational modes is directly related to the molecular geometry and thus delivers new insights on the molecular structure of the investigated chiral molecule. For example, this allows for a possibility to distinguish between different conformers of the supersonic beam-cooled molecule.

3. Outlook

The experimental modifications performed during this thesis improved the precision of the CD-REMPI-MS technique significantly. Due to the combination of supersonic beam-cooling with the twin-peak method and the new single laser pulse evaluation the relative error of CD measurements could be reduced by a factor of thirteen. This allowed the investigation of single vibronic transitions of 1-phenylethanol with an anisotropy factor of about one percent with an experimental precision of $\leq 80\,ppm$.[66] Those measurements show the possibilities of the modified CD-REMPI-MS technique for future CD investigations in the gas phase.[21]

On the one hand, the significant improved precision enables CD measurements of a broad class of chiral molecules with sub-percent g-values and also ee measurements of those chiral molecules. This increases the utility of the CD-REMPI-MS technique for its purpose as analyzing method for in situ ee investigations on chiral product molecules of asymmetric catalytic reactions in the gas phase. The presented results for (R)-(+)-1-phenyethanol as a common representative of an asymmetric catalytic reaction especially confirm the future purpose of the CD-REMPI-MS method. Therefore, a possibility to go one step further could be the use of CD-REMPI-MS for ee investigations on real asymmetric catalysis with 1-phenylethanol as product molecule in the gas phase. The non-constant experimental conditions with significantly higher molecular density fluctuations compared to the CD investigations on a relatively well defined effusive or supersonic beam could thereby be problematic. However, the CD-REMPI-MS technique fulfills all necessary requirements for such investigations even for less predictable sample conditions and mixtures of different chiral and achiral molecules.

On the other hand, the presented results of supersonic beam-cooled 1-phenylethanol revealed new possibilities to use CD-REMPI-MS investigations for basic molecular research. The anisotropy factor measurements of single vibronic transitions showed for the first time experimentally a sign switch of the g-value depending on the excited vibrational mode in ECD. This chiroptical inversion within the same electronic transition combined with the high precision of the measured g-values allows for a novel way to confirm the assignment of theoretically calculated vibronic transitions with the help of experimental observations. In the case of 1-phenylethanol this interaction between theory and experiment will be tested in the near future by theoretical predictions for the anisotropy factors of the isolated vibronic transitions of the investigated $\pi \rightarrow \pi^*$ transition.[83] The theoretical results will be compared with the experimental observations and might confirm or lead to a correction of the assumed vibronic assignments.

[21] At this point it should be considered that the high experimental precision in case of 1-phenylethanol measurements is also a result of the (1+1)-REMPI process with a strong resonant $\pi \rightarrow \pi^*$ transition.

Thereby, chiroptical inversion and thus the simpler comparison of g-value signs of certain single vibronic transitions just occurs and can be used in case of an already existing nearly $90°$ angle between the electric and magnetic transition dipole moment of the 0_0^0-transition. However, the high precision of the anisotropy factor measurements additionally allows for a comparison of theoretical and experimental absolute g-values. Beside the assignment of vibronic transitions within an electronically excited system, which is of interest in the field of molecular spectroscopy, new insights of the molecular structure and geometry of the investigated chiral molecule can be extracted. The assignment of energies as well as anisotropy factors to certain vibrational modes within the electronically excited state depends on the structure and thus the conformer of the chiral molecule in its ground and electronically excited state. Due to supersonic beam-cooling of the sample molecule the energetically most favored conformer can be assumed to persist as ground state structure of the investigated molecule, while a theoretical prediction of the molecular structure in the electronically excited state is more complicated. However, the molecular geometry of a chiral sample molecule in its electronically excited state can be revealed with the help of experimental CD investigations on different isolated vibronic transitions combined with theoretical calculations.

Furthermore, the modified experimental CD-REMPI-MS setup allows for CD investigations of laser desorbed non-volatile chiral molecules. This optional sample source has not been tested during this thesis but enables CD gas phase investigations on a much broader range of chiral molecules independent from their vapor pressure. Within the modified setup the laser desorption takes place in front of the pulsed valve that is used for the formation of the supersonic beam (see figure 7). With a laser pulse coming from an additional laser system a cloud of laser desorbed chiral molecules can be brought into the gas phase and is pushed by a coincident gas pulse from the general valve to the ion source of the TOF-MS. Matrix-assisted laser desorption ionization (MALDI)[84-85], that partly results in a direct ionization of the sample molecules, should thereby not be used due to the fact that at first neutral chiral molecules should be investigated with the CD-REMPI-MS technique. The CD-REMPI-MS method also allows investigations on molecular ions[73] but for first CD investigations on laser desorbed chiral molecules it is preferable to generate a mainly neutral cloud of non-fragmented sample molecules in the gas phase.

Those CD measurements of laser desorbed non-volatile chiral molecules enable anisotropy factor measurements in the gas phase which could differ significantly from g-values measured in liquid phase. Furthermore, such measurements deliver new insights on the desorption mechanism that is still quite unknown (even in the case of MALDI). The theoretical possibilities for the desorption mechanisms can be divided into two categories: thermal and non-thermal desorption.[86] In the first case, the energy of the laser pulse heats up (phonon creation) the

substrate and the sample till the temperature reaches the necessary minimum temperature for a vaporization of the sample molecules. This process is nearly independent from the wavelength of the used laser pulse due to the fact that no resonant absorption of the sample molecules is necessary.[87] Therefore, a thermal desorption of chiral molecules is not enantio sensitive and thus independent from the polarization of the laser pulse used for the desorption. However, in case of non-thermal desorption exist theoretical models like Desorption Induced by Electronic Transition (DIET) and Desorption Induced by Multiple Electronic Transitions (DIMET).[88-89] In both models the sample molecules resonantly absorb the photons of the laser pulse and thus overcome the energy barrier for their desorption from the surface (DIET: single photon absorption; DIMET: multi photon absorption). Laser desorption via DIET or DIMET process is therefore wavelength dependent and in addition polarization dependent, if the sample molecules are chiral. For example, an enantiopure sample could be easier desorbed by one handedness of circular polarized light than by the other dependent on the CD effect of the chiral molecules on the substrate. Either this difference in amount of desorbed molecules per laser pulse can be analyzed or another possibility is the investigation of the residual non-desorbed molecules. In the latter case, a racemic mixture of the chiral sample is illuminated and thus desorbed by a laser pulse of one circular polarization handedness. If one enantiomer compared to the other is preferable desorbed by the utilized circular polarization due to an enentio sensitive DIET or DIMET process, the residual sample on the substrate would not be racemic anymore after the desorption process.

With the modified CD-REMPI-MS setup, the anisotropy factor of the desorbed chiral molecule can be used as analyzing criterion for the desorption process. If the desorption process is non enantio sensitive (probably thermal), the desorption of a racemic mixture results in a racemic molecular cloud with a zero anisotropy factor in the gas phase. However, an enantio sensitive desorption process as DIET or DIMET should result in a measurable anisotropy factor of the desorbed molecule cloud with an ee depending on the percentage of thermal desorption compared to DIET or DIMET. Therefore, such laser desorption experiments with subsequent CD-REMPI-MS analysis of the created molecular cloud can deliver new insights of the fundamental desorption process.

B. Bibliography

1. Knapton, S. Meet Jeremy the lonely snail hoping to find a 'lefty'mate. http://www.telegraph.co.uk/science/2016/10/21/meet-jeremy-the-lonely-snail-hoping-to-find-a-leftymate/ (accessed 03.07.2017).

2. Kelvin, W. T. B., *The Molecular Tactics of a Crystal*. Clarendon Press: 1894.

3. Darwin, C., *On the Origin of Species by Means of Natural Selection, Or, The Preservation of Favoured Races in the Struggle for Life*. J. Murray: 1859.

4. Moss, G., Basic terminology of stereochemistry (IUPAC Recommendations 1996). *Pure Appl. Chem.* **1996,** *68* (12), 2193-2222.

5. Kelvin, W. T., *Baltimore lectures on molecular dynamics and the wave theory of light*. C.J. Clay and Sons: 1904.

6. Michal, G.; Schomburg, D., *Biochemical Pathways: An Atlas of Biochemistry and Molecular Biology*. Wiley: 2013.

7. Cronin, J. R.; Pizzarello, S., Enantiomeric Excesses in Meteoritic Amino Acids. *Science* **1997,** *275* (5302), 951-955.

8. McGuire, B. A.; Carroll, P. B.; Loomis, R. A.; Finneran, I. A.; Jewell, P. R.; Remijan, A. J.; Blake, G. A., Discovery of the interstellar chiral molecule propylene oxide (CH₃CHCH₂O). *Science* **2016,** *352* (6292), 1449-1452.

9. Julian, R. R.; Myung, S.; Clemmer, D. E., Do Homochiral Aggregates Have an Entropic Advantage? *The Journal of Physical Chemistry B* **2005,** *109* (1), 440-444.

10. Cordova, A.; Engqvist, M.; Ibrahem, I.; Casas, J.; Sunden, H., Plausible origins of homochirality in the amino acid catalyzed neogenesis of carbohydrates. *Chem. Commun.* **2005,** (15), 2047-2049.

11. Voet, D.; Voet, J. G.; Pratt, C. W., *Fundamentals of Biochemistry: Life at the Molecular Level*. Wiley: 2013.

12. Leitereg, T. J.; Guadagni, D. G.; Harris, J.; Mon, T. R.; Teranishi, R., Chemical and sensory data supporting the difference between the odors of the enantiomeric carvones. *J. Agric. Food. Chem.* **1971,** *19* (4), 785-787.

13. Flamm, W. G.; Lehman-McKeeman, L. D., The human relevance of the renal tumor-inducing potential of d-limonene in male rats: Implications for risk assessment. *Regul. Toxicol. Pharm.* **1991,** *13* (1), 70-86.

14. Nguyen, L. A.; He, H.; Pham-Huy, C., Chiral Drugs: An Overview. *International Journal of Biomedical Science : IJBS* **2006,** *2* (2), 85-100.

15. Abbott, A., Levodopa: the story so far. *Nature* **2010,** *466* (7310), S6-S7.

16. Schulz, M., Dark Remedy: The Impact of Thalidomide and its Revival as a Vital Medicine. *BMJ* **2001,** *322* (7302), 1608.

17. Silverman, W. A., The Schizophrenic Career of a “Monster Drug”. *Pediatrics* **2002,** *110* (2), 404-406.

18. Crawford, C. L., The Schizophrenic Career of a “Monster Drug”. *Pediatrics* **2003,** *111* (3), 712-712.

19. Eriksson, T.; Björkman, S.; Roth, B.; Höglund, P., Intravenous Formulations of the Enantiomers of Thalidomide: Pharmacokinetic and Initial Pharmacodynamic Characterization in Man. *J. Pharm. Pharmacol.* **2000,** *52* (7), 807-817.

20. Cintas, P., Tracing the Origins and Evolution of Chirality and Handedness in Chemical Language. *Angew. Chem. Int. Ed.* **2007,** *46* (22), 4016-4024.

21. Eyring, H.; Liu, H.-C.; Caldwell, D., Optical rotatory dispersion and circular dichroism. *Chem. Rev.* **1968,** *68* (5), 525-540.

22. Dalgliesh, C. E., 756. The optical resolution of aromatic amino-acids on paper chromatograms. *Journal of the Chemical Society (Resumed)* **1952,** (0), 3940-3942.

23. Bicchi, C.; D'Amato, A.; Rubiolo, P., Cyclodextrin derivatives as chiral selectors for direct gas chromatographic separation of enantiomers in the essential oil, aroma and flavour fields. *J. Chromatogr. A* **1999,** *843* (1), 99-121.

24. Karger, B. L., HPLC: Early and Recent Perspectives. *J. Chem. Educ.* **1997,** *74* (1), 45.

25. Berova, N.; Nakanishi, K., *Circular dichroism: principles and applications*. John Wiley & Sons: 2000.

26. Finn, M. G., Emerging methods for the rapid determination of enantiomeric excess. *Chirality* **2002,** *14* (7), 534-540.

27. Einstein, A., Über die Entwicklung unserer Anschauungen über das Wesen und die Konstitution der Strahlung. *Physik Journal* **1969,** *25* (9), 386-391.

28. Mehra, J.; Rechenberg, H., *The Historical Development of Quantum Theory*. Springer New York: 2000.

29. The Nobel Prize in Physics 1921. http://www.nobelprize.org/nobel_prizes/physics/laureates/1921/ (accessed 13.07.2017).

30. Oerter, R., *The Theory of Almost Everything: The Standard Model, the Unsung Triumph of Modern Physics*. Penguin Publishing Group: 2006.

31. Raman, C. V.; Bhagavantam, S., Experimental proof of the spin of the photon. *Indian J. Phys.* **1931,** *6*, 353-366.

32. Tipler, P. A.; Mosca, G., *Physik für Wissenschaftler und Ingenieure*. Spektrum Akademischer Verlag: 2009.

33. Maxwell, J. C., *A dynamical theory of the electromagnetic field [microform] / by J. Clerk Maxwell ; read December 8, 1864*. The Society: [London, 1865.

34. Degl'Innocenti, M. L.; Landolfi, M., *Polarization in Spectral Lines*. Springer Netherlands: 2004.

35. PEM Principles of Operation. http://www.hindsinstruments.com/knowledge-center/technology-primer/pem-100photoelastic-modulation/principles-of-operation/ (accessed 19.07.2017).

36. Bergmann, L.; Raith, W.; Schaefer, C., *Elektromagnetismus*. de Gruyter: 2006.

37. Carey, F. A.; Sundberg, R. J., *Advanced Organic Chemistry: Part A: Structure and Mechanisms*. Kluwer Academic/Plenum Pub.: 2000.

38. Hecht, E., *Optics*. Addison-Wesley: 2002.

39. Rodger, A.; Nordén, B., *Circular Dichroism and Linear Dichroism*. Oxford University Press: 1997.

40. Drake, A. F., Polarisation modulation-the measurement of linear and circular dichroism. *J. Phys. E: Sci. Instrum.* **1986,** *19* (3), 170.

41. Azzam, R. M. A.; Bashara, N. M., *Ellipsometry and polarized light*. North-Holland: 1987.

42. Berova, N.; Di Bari, L.; Pescitelli, G., Application of electronic circular dichroism in configurational and conformational analysis of organic compounds. *Chem. Soc. Rev.* **2007,** *36* (6), 914-931.

43. Keiderling, T. A., Vibrational Circular Dichroism. *Applied Spectroscopy Reviews* **1981,** *17* (2), 189-226.

44. Logé, C.; Bornschlegl, A.; Boesl, U., Progress in circular dichroism laser mass spectrometry. *Anal. Bioanal. Chem.* **2009,** *395* (6), 1631-1639.

45. Logé, C.; Boesl, U., Multiphoton ionization and circular dichroism: new experimental approach and application to natural products. *ChemPhysChem* **2011,** *12* (10), 1940-1947.

46. Wiley, W. C.; McLaren, I. H., Time - of - Flight Mass Spectrometer with Improved Resolution. *Rev. Sci. Instrum.* **1955,** *26* (12), 1150-1157.

47. Lux, C.; Wollenhaupt, M.; Bolze, T.; Liang, Q.; Koehler, J.; Sarpe, C.; Baumert, T., Circular Dichroism in the Photoelectron Angular Distributions of Camphor and Fenchone from Multiphoton Ionization with Femtosecond Laser Pulses. *Angewandte Chemie-International Edition* **2012,** *51* (20), 5001-5005.

48. Lux, C.; Wollenhaupt, M.; Sarpe, C.; Baumert, T., Photoelectron Circular Dichroism of Bicyclic Ketones from Multiphoton Ionization with Femtosecond Laser Pulses. *ChemPhysChem* **2015,** *16* (1), 115-137.

49. Ritchie, B., Theory of the angular distribution of photoelectrons ejected from optically active molecules and molecular negative ions. *Physical Review A* **1976,** *13* (4), 1411-1415.

50. Böwering, N.; Lischke, T.; Schmidtke, B.; Müller, N.; Khalil, T.; Heinzmann, U., Asymmetry in Photoelectron Emission from Chiral Molecules Induced by Circularly Polarized Light. *Phys. Rev. Lett.* **2001,** *86* (7), 1187-1190.

51. Kastner, A.; Lux, C.; Ring, T.; Züllighoven, S.; Sarpe, C.; Senftleben, A.; Baumert, T., Enantiomeric Excess Sensitivity to Below One Percent by Using Femtosecond Photoelectron Circular Dichroism. *ChemPhysChem* **2016,** *17* (8), 1119-1122.

52. Herwig, P.; Zawatzky, K.; Schwalm, D.; Grieser, M.; Heber, O.; Jordon-Thaden, B.; Krantz, C.; Novotný, O.; Repnow, R.; Schurig, V.; Vager, Z.; Wolf, A.; Trapp, O.; Kreckel, H., Determination of the absolute configuration of a chiral epoxide using foil induced Coulomb explosion imaging. *Journal of Physics: Conference Series* **2015,** *635* (1), 012014.

53. Pitzer, M.; Kastirke, G.; Kunitski, M.; Jahnke, T.; Bauer, T.; Goihl, C.; Trinter, F.; Schober, C.; Henrichs, K.; Becht, J.; Zeller, S.; Gassert, H.; Waitz, M.; Kuhlins, A.; Sann, H.; Sturm, F.; Wiegandt, F.; Wallauer, R.; Schmidt, L. P. H.; Johnson, A. S.; Mazenauer, M.; Spenger, B.; Marquardt, S.; Marquardt, S.; Schmidt-Böcking, H.; Stohner, J.; Dörner, R.; Schöffler, M.; Berger, R., Absolute Configuration from Different Multifragmentation Pathways in Light-Induced Coulomb Explosion Imaging. *ChemPhysChem* **2016,** *17* (16), 2450-2450.

54. Patterson, D.; Schnell, M.; Doyle, J. M., Enantiomer-specific detection of chiral molecules via microwave spectroscopy. *Nature* **2013,** *497* (7450), 475-477.

55. Shubert, V. A.; Schmitz, D.; Patterson, D.; Doyle, J. M.; Schnell, M., Identifying Enantiomers in Mixtures of Chiral Molecules with Broadband Microwave Spectroscopy. *Angew. Chem. Int. Ed.* **2014,** *53* (4), 1152-1155.

56. Kaltenböck, K., *Chromatographie für Einsteiger*. Wiley-VCH-Verlag: 2008.

57. Reetz, M. T.; Kühling, K. M.; Hinrichs, H.; Deege, A., Circular dichroism as a detection method in the screening of enantioselective catalysts. *Chirality* **2000,** *12* (5-6), 479-482.

58. Koskinen, A. M. P., *Asymmetric Synthesis of Natural Products*. Wiley: 2012.

59. Krutmeijer, E. The Nobel Prize in Chemistry 2001. http://www.nobelprize.org/nobel_prizes/chemistry/laureates/2001/press.html (accessed 02.08.2017).

60. Noyori, R., Asymmetric Catalysis: Science and Opportunities (Nobel Lecture). *Angew. Chem. Int. Ed.* **2002,** *41* (12), 2008-2022.

61. Heitbaum, M.; Glorius, F.; Escher, I., Asymmetric Heterogeneous Catalysis. *Angew. Chem. Int. Ed.* **2006,** *45* (29), 4732-4762.

62. Lemaire, M., Heterogeneous asymmetric catalysis. In *Pure Appl. Chem.*, 2004; Vol. 76, p 679.

63. Huo, H.; Shen, X.; Wang, C.; Zhang, L.; Rose, P.; Chen, L.-A.; Harms, K.; Marsch, M.; Hilt, G.; Meggers, E., Asymmetric photoredox transition-metal catalysis activated by visible light. *Nature* **2014,** *515* (7525), 100-103.

64. Lepelmeier, J.; Titze, K.; Kartouzian, A.; Boesl, U.; Heiz, U., Mass-Selected Circular Dichroism of Supersonic-Beam-Cooled [D4]-(R)-(+)-3-Methylcyclopentanone. *ChemPhysChem* **2016,** *17* (24), 4052-4058.

65. Bornschlegl, A.; Logé, C.; Boesl, U., Investigation of CD effects in the multi photon ionisation of R-(+)-3-methylcyclopentanone. *Chem. Phys. Lett.* **2007,** *447* (4), 187-191.

66. Lepelmeier, J.; Alonso-Gomez, J. L.; Mortaheb, F.; Boesl, U.; Heiz, U.; Kartouzian, A., Chiroptical inversion for isolated vibronic transitions of supersonic beam-cooled molecules. *PCCP* **2017,** *19* (32), 21297-21303.

67. Boesl von Grafenstein, U.; Bornschlegl, A., Circular Dichroism Laser Mass Spectrometry: Differentiation of 3-Methylcyclopentanone Enantiomers. *ChemPhysChem* **2006,** *7* (10), 2085-2087.

68. Loge, C.; Boesl, U., Laser mass spectrometry with circularly polarized light: two-photon circular dichroism. *PCCP* **2012,** *14* (34), 11981-11989.

69. Placzek, G.; Teller, E., Die Rotationsstruktur der Ramanbanden mehratomiger Moleküle. *Zeitschrift für Physik* **1933,** *81* (3), 209-258.

70. McClain, W. M., Two-photon molecular spectroscopy. *Acc. Chem. Res.* **1974,** *7* (5), 129-135.

71. Boesl, U.; Neusser, H. J.; Schlag, E. W., Two-photon spectroscopy in the gas phase: first excited state of naphthalene, 1B3u. *Chem. Phys.* **1976,** *15* (2), 167-178.

72. Pulm, F.; Schramm, J.; Hormes, J.; Grimme, S.; Peyerimhoff, S. D., Theoretical and experimental investigations of the electronic circular dichroism and absorption spectra of bicyclic ketones. *Chem. Phys.* **1997,** *224* (2), 143-155.

73. Logé, C.; Boesl, U., Laser Mass Spectrometry with Circularly Polarized Light: Circular Dichroism of Molecular Ions. *ChemPhysChem* **2012,** *13* (18), 4218-4223.

74. Titze, K.; Zollitsch, T.; Heiz, U.; Boesl, U., Laser Mass Spectrometry with Circularly Polarized Light: Circular Dichroism of Cold Molecules in a Supersonic Gas Beam. *ChemPhysChem* **2014,** *15* (13), 2762-2767.

75. Logé, C.; Bornschlegl, A.; Boesl, U., Twin mass peak ion source for comparative mass spectrometry: Application to circular dichroism laser MS. *Int. J. Mass spectrom.* **2009,** *281* (3), 134-139.

76. Boesl, U.; Bornschlegl, A.; Logé, C.; Titze, K., Resonance-enhanced multiphoton ionization with circularly polarized light: chiral carbonyls. *Anal. Bioanal. Chem.* **2013,** *405* (22), 6913-6924.

77. Al-Basheer, W.; Pagni, R. M.; Compton, R. N., Spectroscopic and Theoretical Investigation of (R)-3-Methylcyclopentanone. The Effect of Solvent and Temperature on the Distribution of Conformers. *J. Phys. Chem. A* **2007,** *111* (12), 2293-2298.

78. Amirav, A.; Even, U.; Jortner, J., Cooling of large and heavy molecules in seeded supersonic beams. *Chem. Phys.* **1980,** *51* (1), 31-42.

79. Boesl, U.; Kartouzian, A., Mass-Selective Chiral Analysis. *Annu. Rev. Anal. Chem.* **2016,** *9* (1), 343-364.

80. Unique Features of the Photoelastic Modulator. http://www.hindsinstruments.com/knowledge-center/technology-primer/pem-100photoelastic-modulation/unique-features/ (accessed 22.08.2017).

81. Archard, J. F.; Taylor, A. M., Improved Glan-Foucault Prism. *Journal of Scientific Instruments* **1948,** *25* (12), 407.

82. Giardini Guidoni, A.; Piccirillo, S.; Scuderi, D.; Satta, M.; Di Palma, T. M.; Speranza, M., Chirality and intermolecular forces: studies using R2PI experiments in supersonic beams. *PCCP* **2000,** *2* (18), 4139-4142.

83. Santoro, F.; Mortaheb, F.; Lepelmeier, J.; Boesl, U.; Heiz, U.; Kartouzian, A., High-Resolution Absorption and Electronic Circular Dichroism Spectra of (R)-(+)-1-Phenylethanol. Confident Interpretation Based on the Synergy between Experiments and Computations. *ChemPhysChem*, n/a-n/a.

84. Hillenkamp, F.; Karas, M.; Beavis, R. C.; Chait, B. T., Matrix-Assisted Laser Desorption/Ionization Mass Spectrometry of Biopolymers. *Anal. Chem.* **1991,** *63* (24), 1193A-1203A.

85. Karas, M.; Bachmann, D.; Bahr, U.; Hillenkamp, F., Matrix-assisted ultraviolet laser desorption of non-volatile compounds. *Int. J. Mass Spectrom. Ion Processes* **1987,** *78*, 53-68.

86. Budde, F.; Hamza, A. V.; Ferm, P. M.; Ertl, G.; Weide, D.; Andresen, P.; Freund, H. J., Photodesorption of NO from Ni(100)-O. *Phys. Rev. Lett.* **1988,** *60* (15), 1518-1521.

87. Li, Y.; Jr., R. T. M.; Hemminger, J. C., Experimental determination of thermal and nonthermal mechanisms for laser desorption from thin metal films. *J. Chem. Phys.* **1990,** *93* (7), 4719-4723.

88. Ageev, V. N., Desorption induced by electronic transitions. *Prog. Surf. Sci.* **1994,** *47* (1), 55-203.

89. Misewich, J. A.; Heinz, T. F.; Newns, D. M., Desorption induced by multiple electronic transitions. *Phys. Rev. Lett.* **1992,** *68* (25), 3737-3740.

C. Appendix

C.1. Acronyms

CD	-	circular dichroism
CP	-	cyclopentanone
DNA	-	deoxyribonucleic acid
DIET	-	desorption induced by electron transition
DIMET	-	desorption induced by multiple electron transition
ECD	-	electronic circular dichroism
ee	-	enantiomeric excess
GC	-	gas chromatography
HPLC	-	high-performance liquid chromatography
LC	-	liquid chromatography
MALDI	-	matrix-assisted laser desorption ionization
MCP	-	methylcyclopentanone
MS	-	mass spectrometry
PECD	-	photoelectron circular dichroism
PMT	-	photomultiplier tube
REMPI	-	resonance-enhanced multiphoton ionization
TOF	-	time of flight
UV-Vis	-	ultraviolet-visible
VCD	-	vibrational circular dichroism

C.2. LabVIEW Programs

In the following sections all LabVIEW programs (LabVIEW versions 2013 and 2015) written for the CD-REMPI-MS data post processing and especially for the new single laser pulse evaluation are explained in short notes. Some of the programs are thereby totally new while others are based on old LabVIEW VIs of previous PhD students at the CD-REMPI-MS setup, as mentioned for the programs respectively. In general, all programs are just explained in sense of a standard data evaluation usage and not in their full functionality[22] or their basic programming structure. The basic program structure and function of SubVIs are therefore commented directly in the programs for a deeper understanding of the background processes.

C.2.1a PEM test measurement with two photodiodes (with LeCroy Waverunner 610Zi).vi

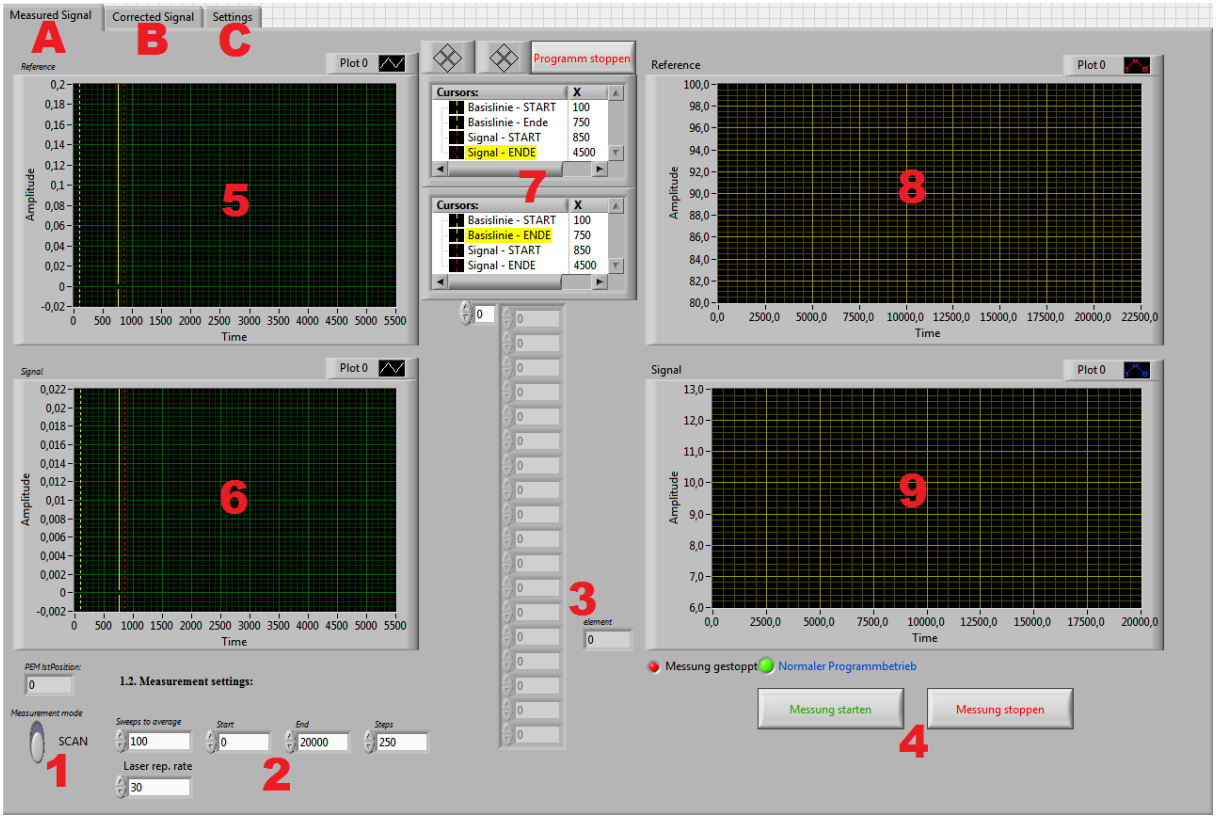

This program was used for the calibration of the PEM with the help of two photodiode signals as explained in detail in section A.1.4.3. The fundamental program structure is based on a program by Dragan Jelisavac.

[22] Some of the programs have extra functions for different tests around other ways of data evaluation which were proven during this thesis but decided to not being useful for the final standard post processing procedure.

C. Appendix

A) Program notes:

0) The LabVIEW program can be directly set to “run”.
1) First before starting a measurement the user should use this switch to choose between “SCAN” and “SEQUENCE” mode. The “SCAN” mode (standard mode) allows for a stepwise measurement at different subsequent delay times of the PEM till a full period of the PEM is fulfilled and the measurement stops. The “SEQUENCE” mode (for test measurements) allows measurements at fixed and chosen delays of the PEM in an endless sequence (see step 3).
2) Measurement parameter like repetition rate of the laser, amount of averages per measurements, etc. for the “SCAN” or “SEQUENCE” mode.
3) Delay time list for the “SEQUENCE” mode. The program measures subsequently at the listed delay times and starts from the beginning after reaching the end of the list. For example, if only one delay time is set in the program, it measures infinite times at the same delay time.
4) Buttons to start/stop the measurement. For the first run, the program should be directly started and stopped after the first measurement point to enable a correct adjustment of the integral starting and ending positions for the baseline and signal.
5) Averaged signal of the “reference photodiode” (see figure 4 in section A.1.4.3) with integral border lines for the baseline correction and the “reference” intensity measurement.
6) Averaged signal of the “signal photodiode” (see figure 4 in section A.1.4.3) with integral border lines for the baseline correction and the “signal” intensity measurement.
7) Lists of the integral borders set in graph 5 and 6.
8) “Reference” integral value of the “reference photodiode” for all already measured delay times.
9) “Signal” integral value of the “signal photodiode” for all already measured delay times.

→ These data and graphs of sheet A can be seen as raw data, while the reference corrected signal intensity is found in sheet B of the program.

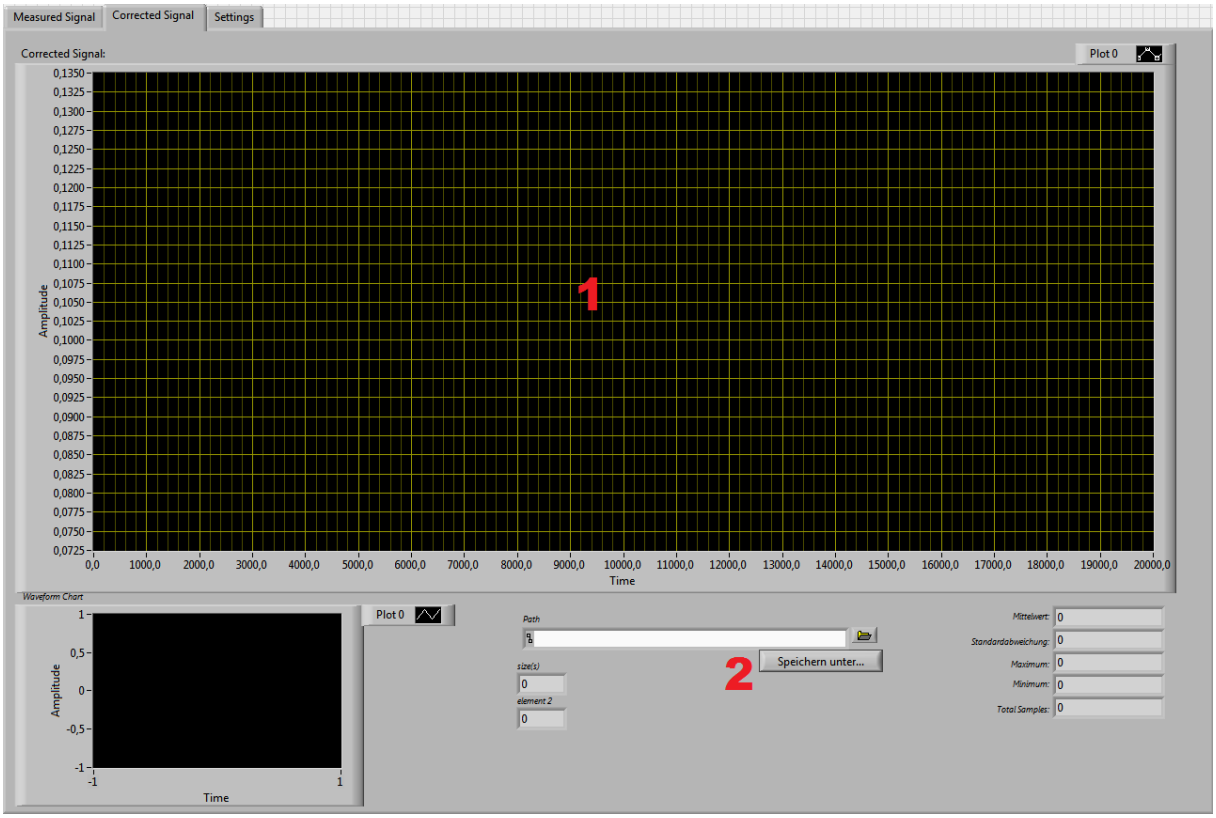

B) Program notes:

1) The reference corrected signal intensity of the already measured PEM delays (“signal” integral value divided by the “reference” integral value). The here shown graph can be used for the determination of the PEM delays which circular polarize the incident linear polarized laser pulse (see figure 5 in section A.1.4.3).
2) The shown graph 1 can be saved via this panel but also simply by right clicking and exporting the (copy – paste) the graph data as a list of data points in an excel sheet or text file.

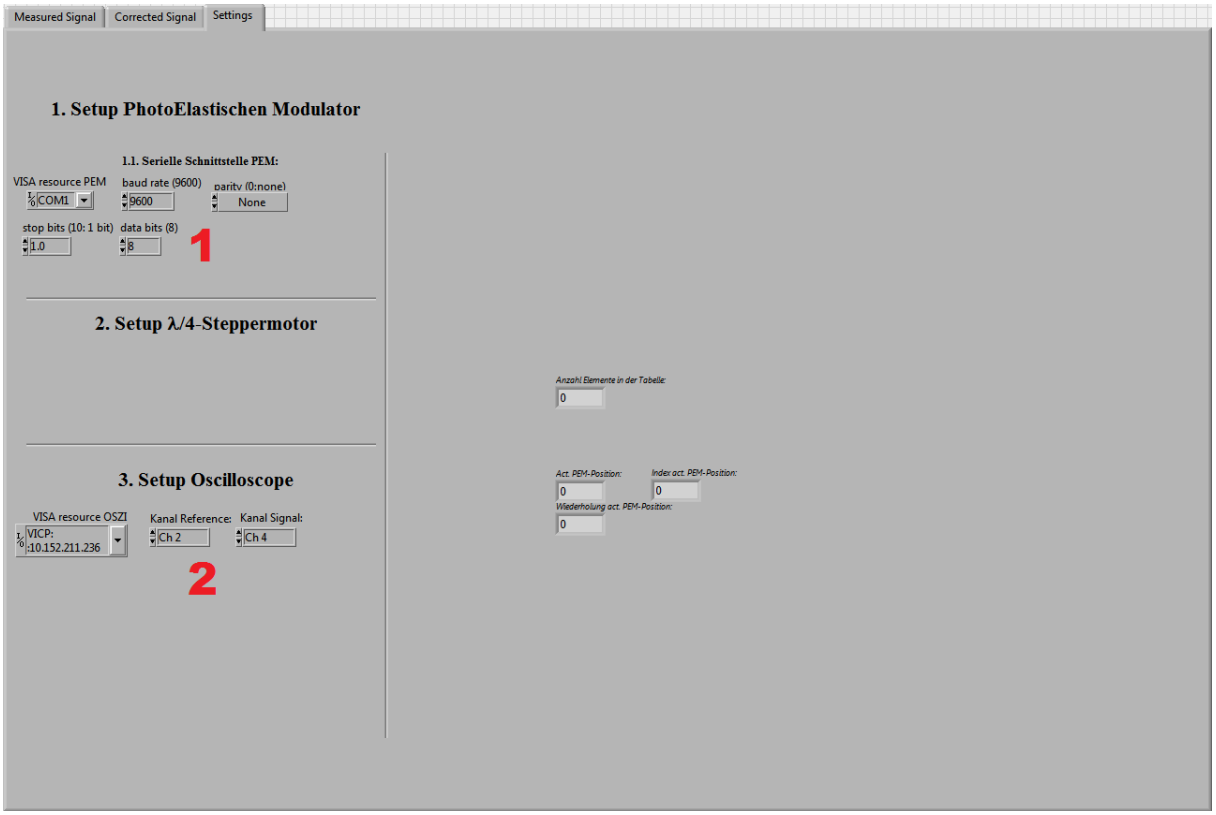

C) Program notes:

1) General setup parameter for the photoelastic modulator with VISA resource, baud rate, etc.
2) General setup parameter for the oscilloscope with VISA resource and used channels for the reference and signal photodiode.

C.2.1b QW test measurement with two photodiodes (with LeCroy Waverunner 610Zi).vi

This program can be used for the calibration of the quarter-wave plate with the help of two photodiode signals as explained in detail in section A.1.4.3. The fundamental program structure is based on a program by Dragan Jelisavac and has the exact same functions as the previously explained program for the PEM (see section C.2.1a). The only difference between the two programs are the usage of stepper motor positions instead of delay times (sheet A) and thus the general setup parameter (sheet C). Beside those two differences the programs are similar and deliver the same output (sheet B).

C.2.2. CD with l4 or PEM (with LeCroy Waverunner 610Zi).vi

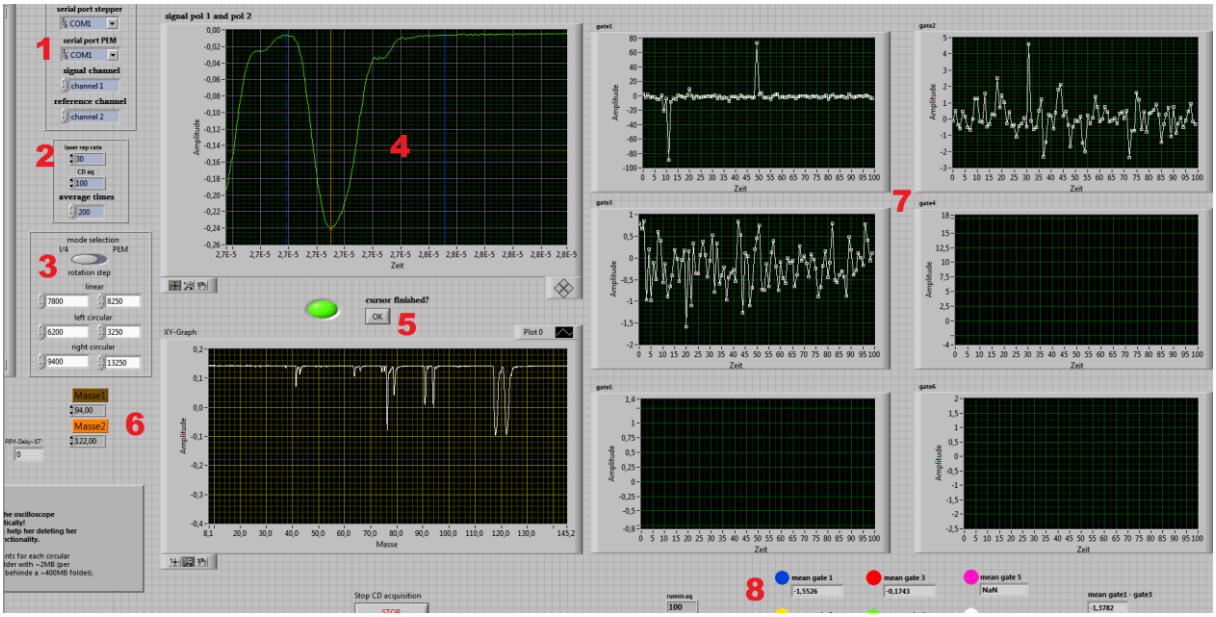

This program was used for CD measurements (“normal” as well as “twin-peak”) with a quarter-wave plate or a PEM with the LeCroy Waverunner 610Zi as explained in general in section A.1.4.3 and also for the new automatic single laser pulse evaluation, as explained in section A.2.2.2. The fundamental program structure is based on a program by Katharina Titze but had to be significantly modified to allow for binary data acquisition and thus later for single laser pulse evaluation with the other post processing programs in the following sections.

Program notes:

0) Before running this LabVIEW program first clarify if the parameter for the measurement (steps 1, 2 and 3) are all correct due to the fact that directly a first test measurements starts when the program is started.
1) Ports and channels of the used photoelastic modulator or quarter-wave plate and the oscilloscope.
2) General parameter for the data acquisition as the repetition rate of the laser, the averaging times per CD measurement (e.g. 100 means 100 left-circular laser pulses followed by 100 right-circular laser pulses) and the amount of CD measurements before the program stops (i.e. 100 means 100 repetitions of the 100 left- and 100 right-circular polarized laser pulsed = 20000 laser pulses overall).
3) Depending on usage of a PEM or a quarter-wave plate the slider and all delay times or stepper motor positions should be set here correctly before starting a measurement. The delays/positions can be identified with the help of the program explained in the previous sections C.2.1.

4) Run now the LabVIEW program to get a first averaged time of flight spectrum and set in here the integral boarders for all mass peaks of interest for the CD measurement (in general the blue boarders for the chiral molecular ion of interest and the red boarders, third integral, for the achiral reference molecular ion). Furthermore, two cursors (orange and brown) can be set here to enable a direct mass calibration which can also be used to identify within the spectrum the peaks of interest (especially in the more complicated twin-peak time of flight spectra).
5) If all cursors are set in graph 4, the measurement can be started by clicking on “ok”.
6) Masses for the already mentioned orange and brown cursor in graph 4 to enable a direct mass spectrum (to the right) out of the time of flight spectrum. This “mass calibration” is optional and has no relevance for the g-value calculation.
7) Directly calculated anisotropy factors (without twin-peak or single laser pulse evaluation) out of the averaged signal intensities within the set boarders in graph 4.
8) The averaged g-value for the measured g-values shown in the graphs 7. To the right a reference corrected (averaged value of the first graph minus averaged value of the third graph) is shown.

→ Important: The g-values shown in the program are “old-school” g-values without recognition of twin-peak, any filtering (not even baseline correction) and especially no single laser pulse evaluation advantages!

→ The really important part of the program occurs in the background unseen by the user because overall this program is mainly used to generate binary files out of single laser pulse mass spectra packed together as sequences on the oscilloscope. Those binary files are first saved on the oscilloscope. Therefore, take care on the hard disc space of the oscilloscope and empty it after several weeks of measurements. After finishing the whole measurement all sequences are copied to the PC connected to the oscilloscope in a special named folder with subfolders that should not be renamed or relocated to allow for a correct functionality of the binary analyzing and evaluation programs explained in the following sections.

C.2.3. Waverunner 610Zi Binary Sequence File Analyser.vi

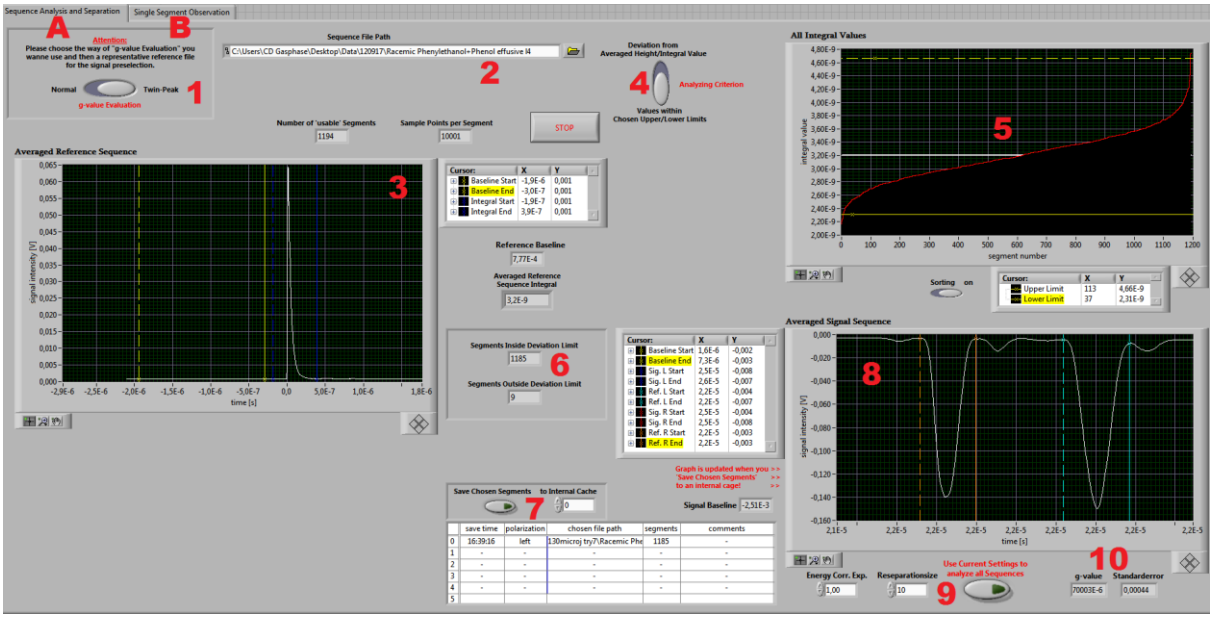

This program was used for g-value calculations (“normal” as well as “twin-peak”) out of recorded binary files of sequences with single laser pulse mass spectra as explained in section A.2.2.2. The program is totally new and needs as input binary files recorded with the program “CD with I4 or PEM (with LeCroy Waverunner 610Zi).vi” mentioned before. Those binary data should not be renamed or relocated due to the fact several procedures in this VI are based on the correct naming of the binary files and their relative location to each other.

A) Program notes:

1) Before running the program, the slider should be set to “Normal” or “Twin-Peak” depending on the measurement principle behind the recorded binary data that should be analyzed.
2) Run the program and it will directly ask for a binary file as first input. Choose one binary file (independent if it holds a sequence measured with left- or right-circular polarized light) to start the analyzing procedure. After analyzing one file completely the user can choose here directly a new binary file (of another measurement) and continue with a second analyzing process. However, the program has some problems with the high amount of binary files that are continuously opened and closed during the analyzing process. This leads often after two analyzing processes to a “memory error” that can be easily avoided by just stopping and then running the program again instead of continuing with a second set of binary files during the same “run” of the LabVIEW program.
3) The program automatically averages over several sequences (each 15th within the chosen subfolder) of photodiode signals (“reference” binary files) that are used as laser

energy measurement during the CD measurements and shows them in this graph. Here the integral boarders for the baseline correction (yellow cursors) and the photodiode signal (blue cursors) can be set.

4) This slider can be used to choose between two energy filtering methods. Either mass spectra are filtered out if they deviate by a certain percentage from the average energy value or manually an upper/lower limit for the energy of used laser pulses can be set. The latter variant can be seen as standard and was used during all data analyzing and evaluation processes of this thesis due to the fact that it allows for a view on the integrated photodiode signal intensities (laser energies) in graph 5.
5) This graph shows all integrated photodiode signal intensities that led to the averaged signal form in graph 3. As already said, the program choses each 15th binary file and thus gives a good overview of the laser energies during the whole measurement. During the thesis it was also tried to use really each sequence for the analyzing process but the huge amount of segments resulted in a memory overload. With the slider below the graph the measured energies can be sorted depending on their value. The white line shows the average value and the horizontal yellow cursors can be used to set the upper/lower limit for the laser energies that are used for the g-value calculation (see section A.2.2.2).
6) These values show the amount of segments within and outside the chosen upper/lower energy boarders to give the user a feeling of how many mass spectra will be filtered out and not used later on for the g-value calculation.
7) After setting the correct upper/lower energy limits the user has to accept his choice by a click here to save the energy limits and thus chosen segments that will be used for the analyzing process. Furthermore, the here shown cache was used as intermediate storage for the functions on sheet B (see below).
8) This graph shows the averaged time of flight spectra of all segments that were selected as useful in sense of their laser energy within graph 6 and by the click on button 7 (the graph refreshes if the button 7 is clicked again). Within this graph the time of flight peaks of interest for the analyzing process can be chosen with the help of several integral boarders that are listed to the left. Beside the cursors for the baseline correction (yellow), for a twin-peak analyzing process obviously two cursors can be set for the chiral molecular ion peaks of interest (blue for the incident and red for the reflected laser beam ions) and two cursors can be set for the achiral reference peaks (teal for the incident and orange for the reflected laser beam ions). The integral values for all four peaks (without twin-peak only two peaks) that are calculated out of this averaged time of flight spectrum are used as second filtering method beside the energy level filtering process mentioned before (see section A.2.2.2). If within any analyzed

segment the integral value of one of the four peaks deviates from this average value by more than 75%, the segment is filtered out and not used for the g-value calculation.

9) Here an exponent for a direct energy correction (integral values divided by the related photodiode signal integral with the chosen exponent) can be set before starting the analyzing and filtering process for all measured segments. The “Reseparationsize” function was for testing the effect of averaging over a certain amount of laser shots but it was not used for any g-value calculation in this thesis. A click on the button starts the energy and time of flight peak integral filtering process for all segments within the whole measurement. A SubVI (either for “twin-peak” or “normal” measurements) compares all segments one by one with the chosen upper/lower energy limits and average time of flight peak integral values. All segments that are within the chosen limits are listed together (one left-circular and one right-circular per row) and saved in a spreadsheet with 36 different columns (see section C.2.4a). About half of the columns stands for information/values (e.g. sequence and segment number, laser pulse energy, integral values for up to four different time of flight peaks and those values also energy corrected by the measured laser pulse energy with the chosen exponent) of the incident left-circular polarized laser pulses and the other half stands for the incident right-circular polarized laser pulses. In addition, the program directly calculates g-values out of the measured and energy corrected integral values. In case of twin-peak measurements one g-value is calculated per segment while for normal CD measurements each left-circular polarized segment is paired together with one right-circular polarized segment to calculate one g-value. At the very end of each column at first a mean value for the whole column is calculated, followed by the standard deviation of this mean and then the standard error of it (standard deviation divided by the square root of the amount of averaged values). Overall the created spreadsheet contains all interesting information and values that can be extracted from the recorded binary files and can be readout with the help of the programs explained in the next sections. However, a trustable reference and energy corrected g-value averaged over all calculated g-values is shown with its standard error directly to the right of the execute button (extracted from the final spreadsheet at the very bottom of column 29).

B) This sheet (not shown here) was used during the first tests around the single laser pulse evaluation for clarification of the functionality of all usable options on sheet A. For example, the sheet allows for a one by one view on the single laser pulse mass spectra that were out of the set energy ranges or within them etc. Due to the fact that at the end of the thesis these options were no more relevant later versions of the program were not proven in case of the functionality of the options on sheet B. Therefore, this program part might be buggy but with some fixes could be used again for a view on single laser pulse mass spectra.

C.2.4a Spreadsheet readout (single column).vi

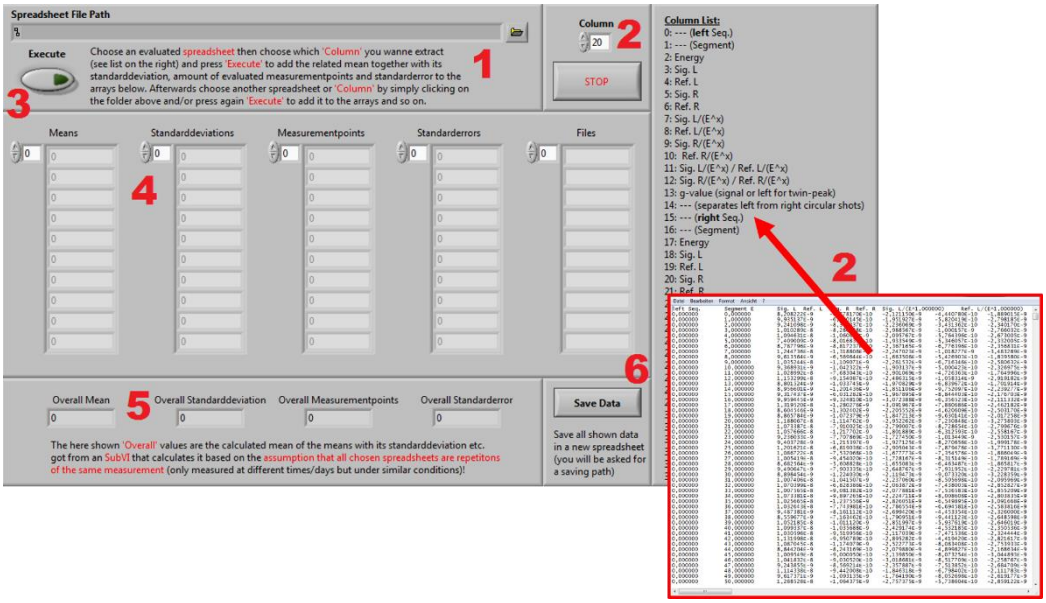

This program was used for the spreadsheet readout to extract the calculated g-values or other values of interest out of the spreadsheet. It is also possible to “manually” readout the values of interest from the spreadsheet by simply opening it with Notepad, Excel, Igor, Origin, etc., but the huge amount of columns and especially rows (around 10.000) makes this option very time consuming. Therefore, this program as well as other quite similar once are totally new programmed and need as input a spreadsheet that has been created with the program “Waverunner 610Zi Binary Sequence File Analyser.vi” mentioned before.

Program notes:

1) Run the LabVIEW program and it will directly ask for a spreadsheet file to readout. After reading out the first file, it is possible to choose here the direction of the next spreadsheet and so on. Thus, for example several g-values of different measurements can be averaged together to a final “overall g-value”.
2) In this version of the spreadsheet readout program the user has full control of the column of interest that he wants to be extracted from the chosen spreadsheets. As already mentioned before for the previous program, each column of the spreadsheet has its own information about the evaluated measurement. Usually the most interesting column is number 29 (take care that the numbering starts with 0) with the averaged final g-value (therefore other programs are written to solely extract this value without a possibility to choose another column). However, especially during tests of new programs this function to choose different columns has huge advantages in case of flexibility for the user.

3) After choosing the column of interest the execute button can be pressed to directly extract the value of interest and its error etc.
4) The value of interest is listed here with its mean, standard deviation, amount of measurement points and standard error. Furthermore, an abbreviation of the file name the values were extracted from is shown in the last column. With each usage of button 3 a new entry is added to the arrays. Therefore, press only once the execute button, then change the file directory, press the button again and continue this procedure for all measurements under similar conditions that should be averaged together for an "overall value" (e.g. for an "overall g-value").
5) These values are the "overall values" of mean, standard deviation, measurement points and standard error calculated out of all already extracted values shown in the arrays 4. The overall averaging and error calculation is thereby solely correct under the assumption that all chosen measurements are recorded under similar experimental conditions and should result in the same "real" mean value.
6) The shown arrays 4 as well as the overall calculated values can all be saved together with this button to a new spreadsheet that can afterwards simply be opened with Notepad, Excel, Igor, Origin, etc.

→ As already mentioned, several slightly different versions of this program exist to directly readout a special value from the spreadsheet without previously choosing a certain column. Usually the name of the program directly shows which value it extracts from the spreadsheet.

C.2.4b Spreadsheet Twin-Peak g-value Combinator (sorted).vi

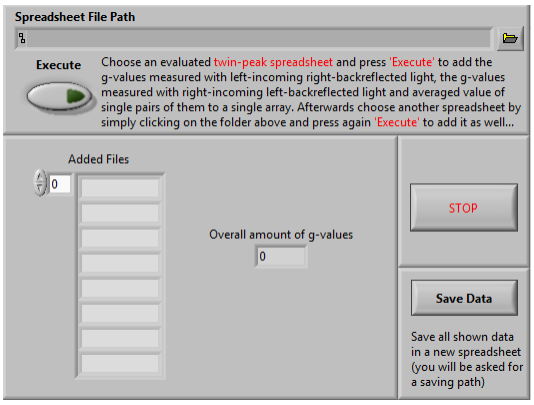

This program was also used for the spreadsheet readout to combine the calculated g-values of several spreadsheets related to separate twin-peak measurement together in one array. Therefore, this program is also totally new programmed and needs as input a spreadsheet that has been created with the program "Waverunner 610Zi Binary Sequence File Analyser.vi" out of a recorded twin-peak measurement. The fundamental principle (run the program, choose a

spreadsheet, press execute, choose another spreadsheet and continue) is similar to the preciously explained program. However, instead of extracting a single value it adds the whole column of incident left-circular polarized g-values of several measurements together and does the same for the incident right-circular polarized g-values. In addition, this version of the program sorts the extracted g-value arrays one in increasing and the other in decreasing order, and calculates out of each g-value pair an averaged g-value to get g-values without a systematic error and a really low standard deviation (see section A.2.2.2). The sorting of the g-values is thereby separate for each chosen measurement (the g-values of different measurements are not mixed together) and any new chosen measurement is added up in the array after the previous measurements. Thus, an overall array of several separately sorted twin-peak g-value measurements can be finally saved as a new spreadsheet with three columns (third column shows the paired g-values without systematic error).

Acknowledgement:

First, I want to thank Prof. Dr. U. Boesl von Grafenstein and Prof. Dr. U. Heiz for giving me the opportunity to work at their chair on my PhD thesis about this interesting topic, which I had no knowledge about before I started. Especially in the several discussions I had with U. Boesl I learned a lot not only about chirality, laser spectroscopy or mass spectrometry but also about scientific work in general. Even after his retirement, he had always an open ear and some advices for me. At this point, I want to thank Dr. A. Kartouzian who undertook somehow the position of U. Boesl and thus the task to guide his last existing PhD student (me) through the second half of his thesis. This guidance led finally to some more fruitful results than I expected. However, as common in modern science those results as well as my whole thesis would not have been possible without the group work of several wonderful minds. Therefore, I want to thank my closest colleagues E. Alonso-Gil, F. Mortaheb and K. Wienhold but also the other Master and PhD students of the physical chemistry chair.

Obviously, a PhD thesis is more than just scientific work. It is also quite a long and defining phase in a man's life with private ups and downs in addition to the scientific ride on an emotional rollercoaster. Thereby, beside my already mentioned closest colleagues I have to thank my parents, brother and friends for their love independent from any successes or defeats on my way through those years. Such love is not easy to find even if you are seeking for it. On my own quest for more of it, I had to find out that not only snails have problems with their chirality but in case of humans the signs of handedness are less obvious and investigations on it can be complicated and painful. However, as science teaches us also fails can lead to new knowledge and thus I even have to thank the wrong wound snails for my grown wisdom. Finally, I want to emphasize that it seems to exist also for me a wonderful person with similar chirality. Therefore, I want to thank C. Letzel for her support and love during the last year that healed my soul.